REPORT DOCUMENTATION PAGE

AFRL-SR-BL-TR-98-

0123

1. AGENCY USE ONLY (Leave Blank)	2. REPORT DATE	3. REPORT TYPE AND DATES COVERED
	15 Apr 97	Final (15 Feb 94 – 14 Feb 97)

4. TITLE AND SUBTITLE	5. FUNDING NUMBERS
Semiconductor Laser Dynamics	F49620-94-1-0144
6. AUTHORS	
Professor J. Moloney	
7. PERFORMING ORGANIZATION NAME(S) AND ADDRESS(ES)	8. PERFORMING ORGANIZATION REPORT NUMBER
University of Arizona Tucson, AZ 85721	
9. SPONSORING/MONITORING AGENCY NAME(S) AND ADDRESS(ES)	10. SPONSORING/MONITORING AGENCY REPORT NUMBER
AFOSR/NM 110 Duncan Avenue, Room B-115 Bolling Air Force Base, DC 20332-8080	
11. SUPPLEMENTARY NOTES	
12a. DISTRIBUTION AVAILABILITY STATEMENT Approved for Public Release	12b. DISTRIBUTION CODE

13. ABSTRACT *(Maximum 200 words)*

Significant progress has been made in constructing a mathematical model of wide aperture semi-conductor lasers which simultaneously resolves multi-longitudinal mode and transverse filamentation instabilities in high brightness lasers. The original working model discussed under project "Simulations of Broad Area Flared Amplifiers and Lasers" utilized a nonlinear gain/index model but ignored gain and index dispersion. Gain and index spectra computed microscopically for specific laser structures and including the contributions of barrier states, are fed as rational functions approximations into the laser simulation code. Using this model, we have been able, for the first time, to simulate the full space-time evolution of all the relevant optical fields and carrier density in the state-of –the-art commercial MOPA high brightness source. Our simulations, suggesting a redesign of this device for improved stability, has attracted the attention of Opto Power Corporation laser design engineers.

14. SUBJECT TERMS	15. NUMBER OF PAGES
lasers, simulation, gain/index model	
	16. PRICE CODE

17. SECURITY CLASSIFICATION OF REPORT	18. SECURITY CLASSIFICATION OF THIS PAGE	19. SECURITY CLASSIFICATION OF ABSTRACT	20. LIMITATION OF ABSTRACT
Unclassified	Unclassified	Unclassified	UL

ARIZONA CENTER FOR MATHEMATICAL SCIENCES

Sponsored by the Air Force Office of Scientific Research
under Contract No. AFOSR-F49620-94-1-0144DEF

SEMICONDUCTOR LASER DYNAMICS

FINAL REPORT FOR THE PERIOD
February 1994 - February 1997

April 15, 1997

University of Arizona
Tucson, Arizona 85721

I. OVERVIEW

A. SUMMARY

The Arizona Center for Mathematical Sciences (ACMS) was formed in 1986 with an initial three-year grant from the Air Force Office of Scientific Research under the University Research Initiative Program. Offices and computer facilities for ACMS personnel, originally located on the eighth floor of the Gould-Simpson Building, were moved last summer to a larger space in the Economics Building. Close ties are maintained with faculty in the Departments of Mathematics, Physics, Aerospace and Mechanical Engineering, Optical Sciences and the Applied Mathematics Program at the University of Arizona.

The ongoing and primary goal of current research is the pursuit of understanding of nonlinear processes in natural phenomena arising in optics. Optics, a fertile area of research in nonlinear science, provides a vital underpinning for new technology and also serves as a useful paradigm for gaining an increased understanding in other fields. For example, turbulence in optics, the study of the complex space-time filaments, patterns and defects which appear in wide aperture high-power lasers and counterpropagating beams, may be more analytically tractable than in other branches of continuum mechanics.

This report details research progress made under AFOSR contract AFOSR-F49620-94-1-0144DEF, "Semiconductor Laser Dynamics" during the period of the contract. As specified in the original proposal, our overall goal was to establish a close synergism between sophisticated mathematical analysis, fundamental physics and high performance computing with interactive graphical visualization. An interdisciplinary team of researchers from mathematics, optical sciences and physics has been assembled locally at the University of Arizona, close collaborative ties are being maintained with Air Force Scientists at the Phillips Laboratory, Kirtland AFB and with experts at outside institutions. We have recently established a direct working link with Opto Power Corporation, a semiconductor laser company that moved to Tucson in 1996. Dissemination of research results is facilitated through regular ACMS Workshops, national and international conference invited and contributed papers, regular laboratory visits, email, fax and telephone communications.

B. COLLABORATIONS

A unique strength of ACMS activity, is the degree to which collaboration is fostered between local researchers at the University of Arizona, with research scientists at the Air Force laboratories and through international links to the European Community. Regular visits are made to the Phillips Laboratory, Kirtland AFB, Albuquerque for the express purpose of disseminating research results and obtaining direct feedback from Air Force scientists on our work. Our direct contacts at the Laboratory, Dr. D. Depatie, Drs. D. Bossert and M.M. Wright, are in regular contact by phone, fax and email. One of the ACMS graduate students, Mr. J.K. White spent a summer period workiing closely with D. Bossert on the study of filamentation instabilities in broad area high-power semiconductor lasers. A number of joint papers with this group have been published or recently submitted.

The Center has acted as the host for annual AFOSR contract review workshops which bring together groups funded directly by AFOSR to meet and interact with Air Force scientists. The last such meeting "AFOSR/ACMS Nonlinear Optics Workshop" was held from October 10-12. 1996.

A direct industrial link with Opto Power Corporation, a manufacturer of high power semiconductor laser sources was established in May 1996. We have been working with this company to design high brightness sources using our laser simulation capability.

Our activity on the international front offers a unique window on relevant European science and technology. Two years ago, an international workshop on "Singularities in Patterns and Collapse: Applications to Semiconductor Lasers and Critical Focusing of Ultra-Short Optical Pulses", was co-organized by the present PI and by Professor J.G. McInerney, Professor of Physics at University College Cork, Ireland and a

collaborator on the present contract. This workshop, sponsored mainly by EOARD (London), was a resounding success, drawing together Air Force scientists and leading academic and industrial experts from Europe and the U.S. The leading European scientists attending the meeting were participants in two European Union semiconductor laser network contracts. A follow-on EOARD-sponsored Workshop entitled "Fundamentals and Modeling of Lasers and Ultrashort Pulse Interactions", will be held from July 20 - 26, 1997.

C. RESEARCH PROGRAM

The overall research program is succinctly summarized in the block diagrams of Figs. 1 and 2. These list the research methodology (Fig. 1) and individual research projects (Fig. 2). Developing robust mathematical and physical models to describe semiconductor amplifiers and lasers, requires detailed knowledge of the microscopic many-body physics of the interaction of light with a semiconductor material. At the same time one needs an understanding of the methodology used in the reduction of realistic complex mathematical models of a physical problem to more manageable universal order parameter equation descriptions. Thus our pooled expertise simultaneously brings to bear fundamental solid state theoretical physics with asymptotic and singular perturbation methods in mathematics. Computation links these two diverse disciplines and is carried out on all levels, ranging from pre- and post- processing on high performance graphics workstations through to intermediate size in-house supercomputing and on to remote supercomputing on vector and massively parallel machines (CM-5 at AHRPC (Minnesota), SP-2 (Maui) and Cray C-90 (WES). Our recent acquisition of a Silicon Graphics Power Challenge L 4-processor compute engine, an Indigo-2 and 4 Indy graphics workstations under the recent DURIP program has greatly enhanced our in-house computing capability.

The diversity of our overall research program reflects the committment made in the original research proposal to unify fundamental physics and mathematics in order to establish a hierarchy of robust mathematical models capable of addressing the important application area of high power semiconductor laser sources. The following itemized summaries offer a global picture of our research program and indicate how the individual parts contribute to achieving the specific long term goal.

- Femtosecond Pulse Propagation in Semiconductor Amplifiers and Lasers

  The study of femtosecond pulse propagation in semiconductor amplifiers (narrow stripe and broad area) is allowing us to establish the fundamental physics responsible for limiting the actual modulation bandwidth achievable in semiconductor lasers or amplifiers. Dynamic bandgap renormalization, spectral hole burning, Coulomb screening, plasma cooling and non-Markoffian dynamics all significantly influence the details of pulse propagation in semiconductor amplifiers.

- Microscopically Computed Quantum Well Gain Spectra

  An important open question from the outset, has been how to effect a closure of the infinite hierarchy of many-body equations describing the semiconductor optical response. A significant breakthrough was made by us recently in resolving the significant discrepancy between experimentally measured and theoretically computed Quantum Well gain spectra. Although excellent agreement had been achieved with bulk gain spectra, it was found necessary to include the full nondiagonal scattering terms in the Quantum Boltzmann equation to achieve quantitative agreement with Quantum Well structures.

- Universal Order Parameter Equation Description of Laser Patterns

  The ambitious goal of deriving a robust rate equation description of wide aperture semiconductor lasers offers a huge payoff in terms of modeling of real structures. The current state of the art

modeling of wide aperture lasers and amplifiers uses the Beam Propagation Method (BPM) and does not account for time-dependent behavior. On the other hand, the full Maxwell-Semiconductor Bloch many-body laser equations are well beyond the capabilities of the most powerful massively parallel or vector supercomputers available today or in the foreseeable future. By working with simpler prototypical laser models, such as the two-level laser Maxwell-Bloch equations, we can evaluate the robustness of the order parameter equation description against the original physical model. This experience is essential as a precursor to tackling the full semiconductor laser equations. We have recently derived a Semiconductor Laser Complex Swift-Hohenberg equation description which has been verified against a full scale nonlinear pde model.

- Controlling Optical Turbulence

  Our work under the project "Universal Order Parameter Equation Description of Laser Patterns" provided the impetus for extending the complex order parameter equation description to both single longitudinal and two longitudinal mode wide aperture semiconductor lasers. The "finite support quasi-plane traveling wave" solutions of the Complex Swift Hohenberg equations were shown to be ubiquitous for all classes of wide aperture lasers. This motivated us to implement a feedback control scheme which simultaneously filters spatially and spectrally the weakly turbulent output of a broad area laser. The scheme has been demonstrated to be extremely robust, stabilizing and steering the laser output.

- Modeling Spatio-Temporal Dynamics of Broad Area/Flared Semiconductor Laser Amplifiers

  This project has a direct bearing on the applications areas of direct interest to the Phillips Laboratory scientists and the commercial needs of Opto Power Corporation. A rate equation approach incorporating the microscopic many-body physics through a look-up table for the gain and refractive index functions, allows in principle, for a full study of the spatiotemporal evolution of filaments in broad area/flared amplifiers and lasers. Simulations of laser switch-on dynamics, filamentation instabilities in broad area lasers and flared MOPA structures, feedback instabilities of MOPA's as a function of feedback level and eventually, nonlinear stabilization and control methods for such structures are all within the capabilities of this level of modeling. Problems with spurious high-transverse wavenumber instabilities were taken care of by adding an artificial diffusion term to the nonlinear pde's describing the laser. A significant improvement on this model is discussed next.

- Full Space-Time Simulation of High Brightness Semiconductor Lasers

  Significant progress has been made in constructing a mathematical model of wide aperture semiconductor lasers which simultaneously resolves multi-longitudinal mode and transverse filamentation instabilities in high brightness lasers. The original working model discussed under project "Simulations of Broad Area Flared Amplifiers and Lasers" utilized a nonlinear gain/index model but ignored gain and index dispersion. Gain and index spectra computed microscopically for specific laser structures and including the contributions of barrier states, are fed as rational functions approximations into the laser simulation code. Using this model, we have been able, for the first time, to simulate the full space-time evolution of all the relevant optical fields and carrier density in the state-of-the-art commercial MOPA high brightness source. Our simulations, suggesting a redesign of this device for improved stability, has attracted the attention of Opto Power Corporation laser design engineers.

- Plasma and Lattice Heating Effects in Quantum Well Lasers and VCSELs

  We have recently shown that discrimination between plasma and lattice heating is important in explaining the switch-off of VCSELs under increased pumping and we have predicted a temperature dependent hysteresis effect in these lasers which has been recently observed experimentally. The

model starts from the microscopic many-body theory and builds in, in an incremental manner, the relevant microscopic effects once their contribution becomes evident. This approach lies midway in the hierarchical chain alluded to above.

- Polarization Patterns in Wide Aperture 3-Level and Semiconductor Lasers

  The vector character of the laser output field has been ignored in the study of wide aperture lasers and amplifiers. It is well known experimentally that wide VCSEL structures show polarization discrimination in the transverse plane. Our approach is to develop the vector order parameter equation description for basic 3- and 4- level laser models with the latter approximating the band structure of semiconductor lasers. The additional polarization degree of freedom considerably extends the available range of experimentally observable behaviors. The combination of spatial patterns and polarization domains offers exciting opportunities for nonlinear polarization switching and control of patterns in spatially extended lasers.

- 1D - 3D Vector Maxwell Solvers

  Ultrashort intense light pulses propagating through wavelength scale inhomogeneous structures such as periodic index gratings, sharp subwavelength dimensional interfaces, Quantum Well stacks, Quantum wire structures, semiconductor micro-cavites etc all require a full resolution of the full optical carrier wave. Possible nonlinear effects associated with such propagation include carrier and envelope shocking of intense femtosecond optical pulses, novel nonlinear localization phenomena, backscattering from nonlinearly induced index inhomogeneities etc. Many of the 1D solvers can be optimized to run in real time on our new Power Challenge machine offering a nonlinear optical CAD-like environment. The goal of this project is to develop interactive graphical tools which maximize efficiency in transitioning new nonlinear optical effects to technology applications.

- Dynamic Nonlinear Optical Skin Effect

  This project utilized the vector Maxwell solvers to study a novel nonlinear reflection phenomenon at an interface. Our prediction is that an intense femtosecond optical pulse, incident on a nonlinear interface, can induce a moving sub-wavelength absorption front which acts as a curved reflector. Direct experimental evidence for this phenomenon has recently been provided by our colleagues at the Optical Sciences Center.

- Large Scale Computational Nonlinear Optics

  Our group has been taking the lead in promoting this emerging field of computational science. The recent DURIP award of an SGI Power Challenge L plus 5 Indigo graphics workstations has considerably enhanced our intermediate scale supercomputing and real time graphical visualization capabilities. Our two main large scale computational projects involve:

  (1) developing a 3D + time vector Maxwell solver on the CM5 at AHPCRC, Minnesota, for nonlinear optics problems of relevance to the present project and to a companion AFOSR contract No. F49620-94-1-0051 "3D Collapse Phenomena in Dispersive Nonlinear Media: A Critique of Envelope Models."

  and

  (2) developing a Maxwell-Semiconductor Bloch code incorporating full many-body interactions on the SP2 machine on Maui

  The former code is highly parallel and takes advantage of these features on the CM5 whereas the course-grained parallelism of the latter is ideally suited for the SP2.

- Relaxation Processes in Semiconductor Light Amplifiers

  This project extends the description of the nonequilibrium ultrafast relaxation and thermalization of carriers beyond the basic quantum Boltzmann description. The idea is to include higher order correlations neglected in the Kadanoff-Baym theory. As semiconductor lasers are examples of systems which deviate considerably from equilibrium, the role of higher order correlations needs to be evaluated in this context. The work combines the method of nonlinear optical susceptibility with the multiple scales method in order to compute the next order correction term to the quantum Boltzmann equation.

- Multimode Laser Dynamics

  Edge emitting semiconductor lasers typically accommodate 20-30 longitudinal modes under the gain bandwidth. Multi-longitudinal mode oscillations are also observed in broad area semiconductor lasers immediately beyond lasing threshold. This project explores multi-longitudinal mode oscillations in a simpler 2-level laser with and without external mirror feedback. The goal is to use our experience gained from this simpler system to build a realistic multi-longitudinal mode wide aperture semiconductor laser model. The rate equation approach described above also shows multi-longitudinal mode oscillations in a broad area laser but suffers from the fact that we must include an artificial diffusion. The present approach includes the fast polarization dynamics and the problem is extremely stiff mathematically.

- Circularly Symmetric Distributed Feedback Semiconductor Lasers

  New generations of circularly symmetric distributed feedback lasers (CSDFB) are being investigated at a preliminary stage using a standard beam propagation algorithm. These lasers offer the advantages of circularly symmetric output, low-divergence output beam and the ability to phase-lock a 2D array.

D. RESEARCH FACULTY AND GRADUATE STUDENTS

Principal Investigator:

Jerome V. Moloney, Professor, Department of Mathematics.

Center Faculty

Jerome V. Moloney, Professor, Mathematics and Director ACMS
Alan C. Newell, Professor of Mathematics
Nick Ercolani, Professor, Mathematics
Rob Indik, Adjunct Assistant Professor, Mathematics
Ewan Wright, Associate Professor, Optical Sciences and Physics
Rolf Binder, Assistant Professor,Optical Sciences

External Faculty Who Spend Regular, Extended Periods at the Center

William Firth, University of Strathclyde, Glasgow
John McInerney, University College Cork, Ireland
Andreas Knorr, Phillips University Marburg, Germany
Stephen Hughes, Phillips University Marburg, Germany
Stephan Koch, Phillips University Marburg, Germany
Joceline Lega, Universite de Nice, France
Maxi San Miguel, Universitat de les Illes Balears, Spain

Center Staff

Robert Condon, Coordinator for Academic and Research Computing
Susan Dzik, Administrative Assistant
Zora Mlejnkova, Graphics Specialist
Rex Allison, Systems Manager

Postdoctoral Fellows

Randy Flesch, Ph.D, University of Southern California
C.Z. Ning, Ph.D., Stuttgart, Germany
W. Forysiak, Ph.D., Heriot-Watt University, Edinburgh
Q.Y. Feng, Ph.D., Bayreuth, Germany
S.A. Glasgow, Ph.D., University of Arizona
A. Egan, Ph.D., Trinity College, Dublin

Graduate Students

J.K. White
C. Bowman
Y. Lvov
D. Hochheiser
N. Komarova
M. Mlejnek
J. Riordan

E. TECHNICAL REPORTS

Femtosecond Pulse Propagation in Semiconductor Amplifiers and Lasers

We have performed a variety of computations studying the behavior of femtosecond pulses in semiconductor amplifiers. We employ a many-body theory describing the interaction of light with a bulk semiconductor material. The behavior of an optical pulse with full width at half maximum (FWHM) of the order 100 - 500 femtoseconds, propagating over a long distance in a semiconductor amplifier has been studied in both strongly confined and broad area planar geometries. The role of the various physically important interactions on the pulse evolution along the amplifier have been investigated.

Our initial studies reported on here are confined to a strong femtosecond optical pulse interacting with a highly excited bulk GaAs semiconductor. In this regime the equations used to model the interaction describe the evolution of the electric field envelope E in the traveling frame of reference $\xi = z - tc/n$

$$\frac{\partial E}{\partial \xi} - \frac{1}{2ik_0}\nabla_\perp E = \frac{i\mu_0\omega_0^2}{k_0 V}\int_q P_q\, dq \tag{1}$$

the momentum resolved polarization P_q and electron/hole distribution functions, which evolve as

$$\frac{\partial P_q}{\partial t} = -i\left(\Delta_q - \omega_0\right)P_q - i\Omega_q(n_q^e + n_q^h - 1) + \left.\frac{\partial P_q}{\partial t}\right|_{\text{coll}} \tag{2}$$

$$\frac{\partial n_q^{e/h}}{\partial t} = iP_q^\star\Omega_q - iP_q\Omega_q^\star + + \left.\frac{\partial n_q^{e/h}}{\partial t}\right|_{\text{coll}} \tag{3}$$

with the renormalized Rabi frequency $\Omega_q = \frac{\Omega}{2} + \frac{1}{\hbar}\sum_{q'} V_{q-q'}P_{q'}$. Here $n_{q'}^{e/h}$ and $\Delta_q = \varepsilon_q - \frac{1}{\hbar}\sum_{q'} V_{q-q'}(n_{q'}^e + n_{q'}^h)$ denote the distribution functions for electrons or holes and the energy dispersion including the band gap renormalization, respectively. The Coulomb potential, V_q, is treated in a quasi-statical screening model. The Rabi frequency $\Omega = d_{cv}\cdot E/\hbar$ is determined by the dipole matrix element d_{cv} and the amplitude of the external electrical field $\tilde{E} = E(t,\xi)e^{-i\omega_0 t + ik_0 z}$.

We are considering a broad area semiconductor device. The lateral "y" direction has strong confinement due to the layered structure of the amplifier. This has the effect of multiplying the right hand side of equation 1 by the confinement factor Γ, and replacing the Rabi frequency Ω by $\Gamma\Omega$. If the wave is also strongly guided in the transverse direction, a correspondingly smaller confinement factor must be used, and the diffraction term $\nabla_\perp E$ may be ignored, it just produces an effective shift in ω_0.

Anomalous absorption

R. Indik, A. Knorr, R. Binder, J.V. Moloney, S.W. Koch and W.W. Chow

Before we can use our model equations, we must choose some specific form for the collision terms. To start with we approximate the collision terms using a rate equation (no memory) with uniform time constants $\gamma_q^{e/h} = (60\text{ fs})^{-1}$

$$\frac{\partial P_q}{\partial t}|_{\text{coll}} = -\frac{\gamma_q^e + \gamma_q^h}{2}P_q \tag{4}$$

$$\frac{\partial n_q^{e/h}}{\partial t}|_{\text{coll}} = -\gamma_q^{e/h}\left(n_q^{e/h} - f_q(\mu^{e/h}, T)\right) \tag{5}$$

The terms $f_q^{e/h}(\mu^{e/h}, T)$, are Fermi distributions with chemical potentials $\mu^{e/h}$ and temperature T chosen so that they produce the same carrier densities $N^{e/h} = \int_q n_q^{e/h}\, dq$ and total kinetic energy as the distributions $n_q^{e/h}$. This form for the collision term corresponds to considering carrier-carrier collisions, all of which

preserve total kinetic energy and the numbers of electrons and of holes. The Fermi distributions are assumed to have a common temperature, and individual chemical potentials. In all of our computations, we assume the polarizations and the densities are isotropic in the momenta q.

One of the more surprising predictions of the MSB equations is that if one increases the intensity of the light pulse sufficiently, the amplifier will become an absorber. [1]. This is different from the behavior of a simple two level system, where one can saturate the gain, but can never convert it into absorption. The source of the anomalous absorption is the coupling of the light field with the electrons in higher momentum states. For higher momenta, the material is not inverted, i.e. light at corresponding (higher) frequencies would be absorbed. Even light at the lower frequencies is absorbed slightly. Ordinarily, that absorption is more than counterbalanced by the gain that the lower frequency light experiences as a result of its interaction with the inverted lower momentum states that are resonantly coupled. However, when the intensity of the light is sufficient to saturate the gain, the absorptive coupling to the higher momentum states may be revealed.

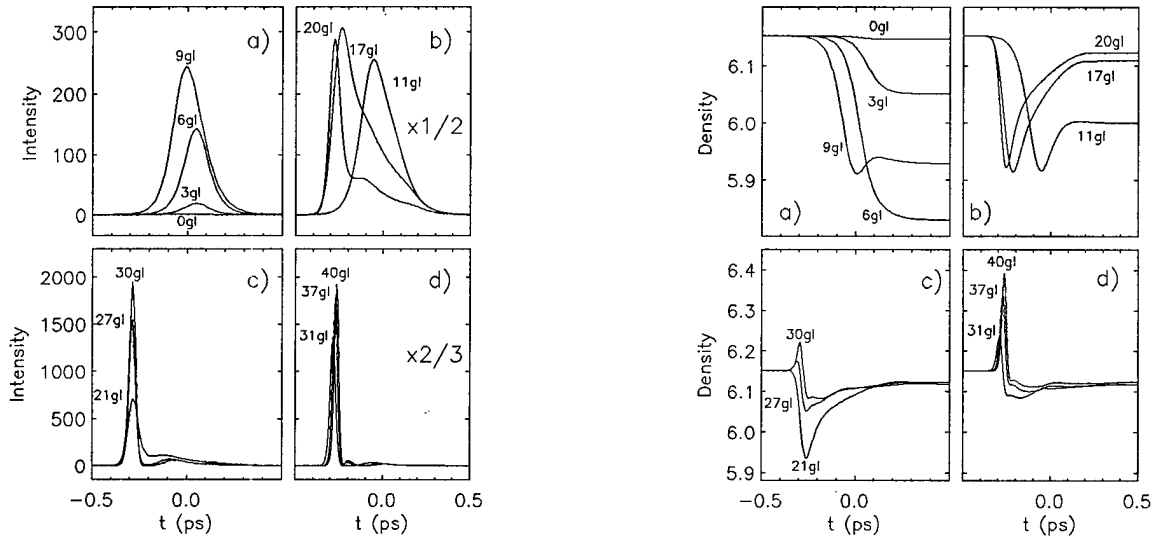

Figure 1: *Evolution of intensity (left) and density (right) during propagation.*

If one assumes for simplicity that the pulse doesn't change its shape as it propagates, we see that this model predicts that there is an intensity I_0 such that whatever the initial intensity, after sufficient propagation the intensity will return to I_0. I_0 is the intensity value for at which the semiconductor response switches from a net gain $I < I_0$ to a net absorption if $I > I_0$. Thus it is natural to ask: what is the long term behavior of a pulse that propagates in a semiconductor amplifier? We considered this question [2] and found yet another surprising prediction of this model. Figure 1 shows the result of propagating a relatively weak pulse in such an amplifier over a long distance. Initially the pulse is amplified linearly, and we can see slight effects of gain dispersion and group velocity dispersion in the reshaping of the pulse and its spectrum. This continues until the amplifier is saturated. This saturation is a consequence of plasma heating, spectral hole burning and total carrier density depletion. Carrier-carrier collisions "refill" the spectral hole, but the model in equations 11 and 12 have no way for the plasma to cool, except through stimulated emission and absorption. Once the plasma is heated, the carriers are distributed across more momentum states, and fewer of those states are inverted. Plasma heating is the dominant source of gain saturation. As is nearly always the case with a saturable amplifier, the leading portion of the pulse steepens, and the peak of the pulse actually moves faster than the speed of light in the material. In addition, the refractive index dispersion is such that the redder frequencies travel faster than the blue. Thus these frequencies end up closer to the leading edge of the pulse, and experience more gain. Thus we see the center of the spectrum

of the pulse shifting below the peak of the gain spectrum. Self-phase modulation also contributes to this effect. The reshaping of the pulse, its splitting into a very short very intense leading portion and much weaker and broader tail is harder to understand. We can see by comparing the shape of the intensity of the light pulse with the total carrier density, that we have entered a regime of adiabatic following. Observation of the q resolved density and polarization shows that much of that adiabatic following is due to coupling to very high momentum states. The robustness of this phenomenon was checked by varying the amplitude, shape and frequency of the initial pulse. Without exception, if we propagated far enough, the pulse entered a regime of adiabatic following. This observation was intriguing as we felt that the presence of a very short intense pulse that forms spontaneously and robustly could be useful in applications.

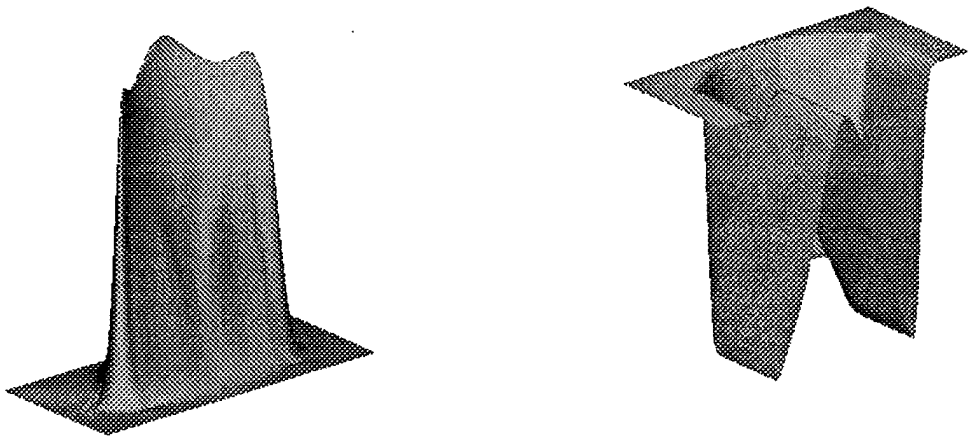

Figure 2: *Intensity (left) and Density (right) as functions of t and x.*

The transverse confinement was then removed to study the propagation of pulse with a Gaussian transverse cross-section over a distance of 1mm (length leading to a linear gain for the intensity of e^{10}). It is now observed that the pulse produces its own transverse waveguide. The intense central portion depletes the carrier density. This lower carrier density induces a higher refractive index, and therefore a focusing effect. Figure 2 shows the amplitude and the carrier density as a function of time and the transverse dimension after the beam has propagated 1mm. Figure 3 shows a comparison of the amplitude in the center of the beam with transverse structure and the amplitude of a beam with strong transverse guiding.

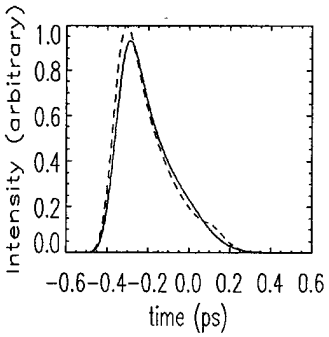

Figure 3:*Comparison of intensity of planewave (solid) and center value of intensity for a Gaussian-beam after propagating 1 mm.*

We have also explored the behavior of the amplifier when two strong pulses at different frequencies are compete for gain [3]. In that case we see the effects of plasma heating, four wave mixing and spectral hole burning. Figure 4 shows the evolution of the spectra of such interacting pulses.

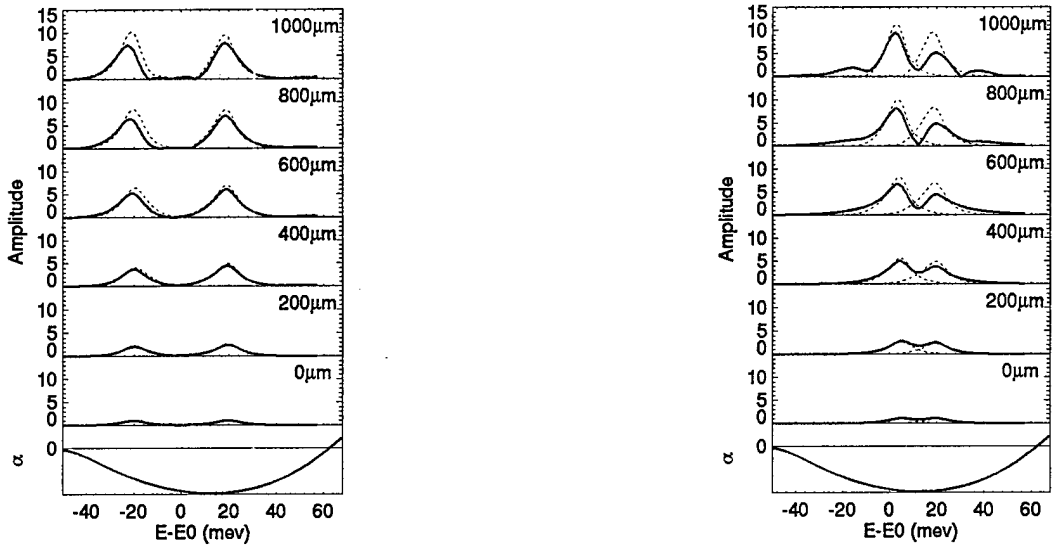

Figure 4: *Evolution of the spectrum for pairs of coincident pulses with different frequencies. Dashed lines show evolution of individual pulses.*

Plasma cooling
R. Indik, R. Binder, M. Mlejnek and J.V. Moloney

One of the more important features governing the evolution of the propagating pulse above is that the plasma cannot cool other than through interaction with the light field itself. On the whole, the interaction with the light field would tend to heat the plasma, since the absorption tends to be into high momentum states, (creating fast carriers), and the emission removes low momentum carriers. The collision terms, however, should include terms we initially neglected that tend to cool the plasma. The carriers collide not only with each other, but also with optical phonons. The optical phonons can take energy from the carriers and couple it to the lattice. This process is slower than carrier-carrier scattering, but is still fairly rapid. By using a quasi-equilibrium assumption one can estimate the cooling rate for the carriers. Once again, we add this term to our equation using a rate equation approximation.

$$\frac{\partial P_q}{\partial t}|_{\text{coll}} = -\frac{\gamma_q^e + \gamma_q^h}{2} P_q - \frac{\gamma_q^{eo} + \gamma_q^{ho}}{2} P_q \tag{6}$$

$$\frac{\partial n_q^{e/h}}{\partial t}|_{\text{coll}} = -\gamma_q^{e/h}\left(n_q^{e/h} - f(\mu^{e/h}, T)_q\right) - \gamma_q^{eo/ho}\left(n_q^{e/h} - f(\mu^{eo/ho}, T_L)_q\right) \tag{7}$$

Here we have introduced two new rates $\gamma_q^{eo/ho}$ and two new Fermi distributions. The new Fermi distributions $f(\mu^{eo/ho}, T_L)$ are chosen to preserve the total carrier density, but have a fixed lattice temperature T_L. On much longer time scales, one must consider that the lattice itself will be heated, and thus dynamics for T_L could become important [4]. This much slower thermal process is not relevant to our study. As expected, the effect of including the cooling of the plasma is to make the saturation of the gain more difficult. As the plasma cools, carriers move from high momentum states to lower ones and once again become available for stimulated emission. In thin slabs, when the pulses are short enough, there is little effect. Table 1 shows how the intensity (presented in terms of the corresponding Rabi frequency Ω_0) at which the gain is saturated varies with pulse length with and without cooling.

Pulse length (FWHM)	Ω_0 (no cooling)	Ω_0 (with cooling)
100 fs	21.89 mev	22.85 mev
200 fs	16.39 mev	18.81 mev
400 fs	12.03 mev	16.49 mev
800 fs	8.67 mev	15.78 mev
1600 fs	6.18 mev	17.78 mev

Table 1: Ω_0 with and without cooling as a function of the pulse length.

For longer propagation lengths, we see that cooling has a dramatic effect even for pulses that are initially very short. Where previously the gain was depleted by the leading portion of the pulse, we now see that the cooled carriers produce additional gain on the trailing portion of the pulse. The leading edge of the pulse is not greatly changed (at least qualitatively), but now the vast bulk of the energy in the pulse is on the trailing portion. To take advantage of the very sharp leading portion of the pulse, it would have to be separated from its much larger tail. Figure 5 shows the time resolved intensity of the pulse after propagation roughly 2mm. Figure 6 shows the transverse structure formed by a 150 femtosecond pulse with a transverse Gaussian profile after propagating 1mm. Note that the self guiding is still quite pronounced. We have also looked at the effect of varying the shape of the initial pulse on the output of the long amplifier. In contrast to the case without optical phonon collisions, we find that the shape of the output varies with the shape of the input. The "wiggles" that follow the sharp initial peak in the output are more pronounced for initial shapes that fall off more quickly.

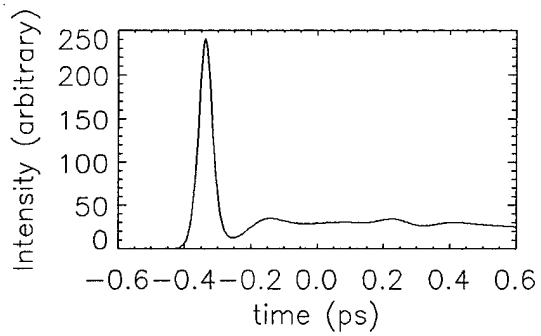

Figure 5: *Intensity of pulse after propagating 2mm. Cooling effects have been included.*

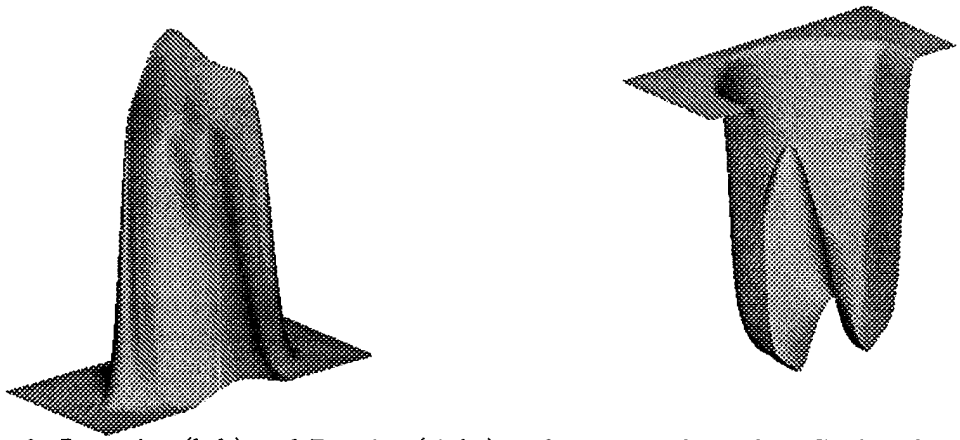

Figure 6: *Intensity (left) and Density (right) as functions of t and x. Cooling has been included.*

Memory effects

R. Indik, R. Binder, J.V. Moloney, A. Knorr, S.W. Koch

The rate equation form that we choose for the collision term in the decay of the polarization is a result of making a simplifying assumption about carrier-carrier scattering. Namely, we assume that the collision process has no memory. There is significant experimental evidence to suggest the contrary. In the low density case, it is known that the absorption falls of exponentially with detuning below the exciton frequency. This "Urbach" tail has been modeled using a Gaussian or a sech lineshape rather than the Lorentzian profile consistent with a fixed polarization damping rate. Even at higher densities, we suspect that the Lorentzian line shape (corresponding to no memory) must be incorrect. Below the (renormalized) bandgap, there is very little absorption. However, in a bulk semiconductor, use of a Lorentzian lineshape leads to a gain spectrum with an absorptive tail that extends well below the bandgap. If a sech lineshape is used, this feature disappears. If we examine the argument that indicates how the high momentum states together with the quadratic density of states cumulatively produce significant absorption for frequencies that ordinarily would see net gain, we can see that we need only assume that the lineshape falls off faster than $1/\delta^2$ to remove the tails. Thus a decrease like $1/\delta^4$ is enough to greatly diminish the influence of the high momentum states. There is some literature, proceeding from first principles using quantum Boltzmann equations, that calculates lineshapes with asymptotics as described above. Such models are quite significantly more complex than those we have been using, and we have captured the essential features (i.e. the aymptotics) using a phenomenological approach.

It turns out that if we take for the collision term of the polarization

$$\left.\frac{\partial P_q}{\partial t}\right|_{\text{coll}} = \int_0^t g_q(t-t')P_q(t') \tag{8}$$

where

$$g_q(t) = \gamma_{2q} e^{-(\gamma_{1q}+\gamma_{2q})t} e^{i\omega_q t}.$$

the lineshape will have the desired quartic fall off with detuning, and that if we restrict to such simple diagonal memory terms this is essentially unique. We call this a two pole model, as in Fourier space the response function corresponding to the diagonal linear terms in the P_q can be written as a rational function with two poles in the complex upper half plane. One very convenient feature of such a form, is that it is easily converted back into a system of coupled ODEs. We replace the P equation with a pair of equations,

$$\dot{P}_q = i\omega_q P_q - \gamma_{1q} Q_q + i\Omega_q(n_q^e + n_q^h - 1) \tag{9}$$

$$\dot{Q}_q = (-\gamma_{1q} - \gamma_{2q} + i\omega_q)Q_q + \gamma_{2q} P_q \tag{10}$$

Assuming a two pole form for the response, is equivalent to replacing the Markovian assumption that leads to the Lorentzian line shape with a two-stage Markovian assumption.

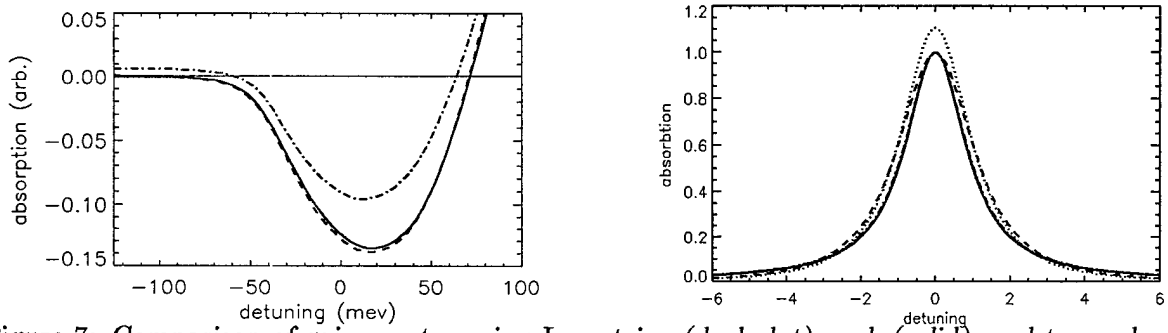

Figure 7: *Comparison of gain spectra using Lorentzian (dash-dot), sech (solid), and two pole (dashed) models (left), and lineshapes (right)*

Figure 7 (right) shows a comparison of the gain computed using the Lorentzian, several choices of parameter values of the 2-pole model, and a sech lineshape. Our preferred set of parameters is chosen to make the 2-pole lineshape approximate the sech lineshape. The Lorentzian tail is removed by both the sech and the 2 pole models. In fact there is little to distinguish them when looking at the gain, though both differ significantly from the Lorentzian. Figure 8 (left) compares the response of the total density to a very strong pulse. Cooling effects have not been included as they are not important for such short pulses in a thin slab. We see that the anomalous absorption is absent. This should be understood in terms of the decreased absorptive coupling to the high momentum states. Instead we see a new feature. The density seems to follow the field intensity up and down, temporarily increasing over its initial value, while the strong pulse is present. This behavior can be understood from the behavior of the real part of the susceptibility $\chi'(\omega)$. By construction, the imaginary part of the susceptibility decays rapidly with detuning, but applying Kramers-Kronig shows us that the real part still decays like the inverse of the detuning. This is the coupling that leads to adiabatic following. This is just as strong as before, but now the absorptive coupling is much weaker, and the adiabatic following is dominant. If we increase the intensity of the pulse a great deal, we can once again see anomalous absorption, however, the intensities are now quite huge, and the adiabatic following is now very pronounced (Figure 8 right). We have also calculated the result of propagation without cooling, but using the 2-pole model. It is interesting that these memory effects, even without cooling, provide gain behind the leading edge of the pulse. Figure 9 shows the corresponding results for propagation in a broad area amplifier using the 2-pole model with cooling included. The similarity to the plane wave propagation due to the presence of the self trapping is still quite marked.

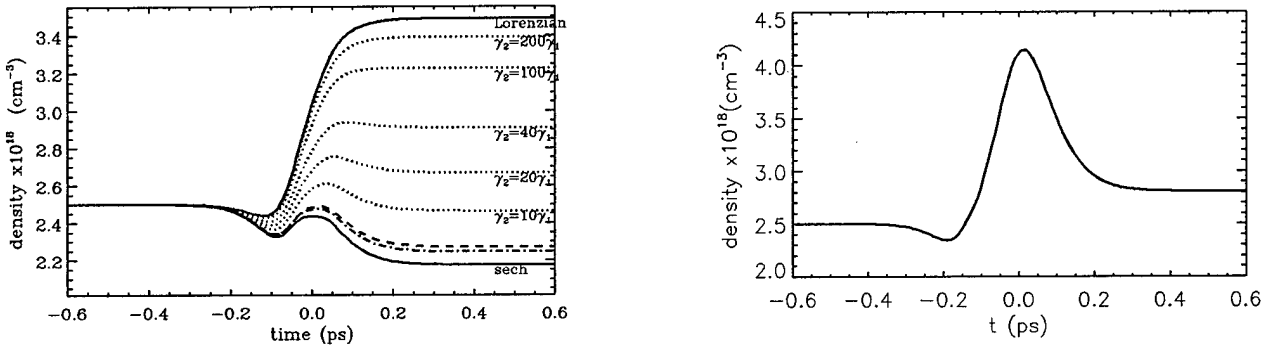

Figure 8: *(left) Comparison of response of the total density to a very strong using Lorentzian (upper solid), sech (lower solid), and and various two pole models (dashed). (right) response of the two pole model to a pulse 9 times as intense.*

Conclusions

Our preliminary studies of femtosecond pulse propagation in a bulk semiconductor amplifier have revealed a subtle and complex interplay between various physical mechanisms which can be ascribed to many-body effects. The significant contribution of these phenomena for femtosecond probes even stretches the bounds of the many-body theory as currently developed and it is highly unlikely that simple parameterized rate equation models can provide any significant insight. In particular, we have studied systematically the role of carrier-carrier scattering, carrier-phonon scattering and memory effects on femtosecond pulse propagation in narrow stripe and broad area lasers. Plasma cooling and memory effects are shown to lead to a pronounced amplification of the trailing edge of the pulse and hence severe pulse distortion both in single stripe and broad area structures. In addition these effects accentuate the self-induced transient index guide formed in a broad area structure.

It is expected that these many-body ingredients will allow us to evaluate the ultimate modulation response

of mode-locked semiconductor lasers and unearth the source of the observed strong frequency chirp in these devices. Computationally, this class of problem poses significant challenges especially in modeling broad area amplifier structures or lasers. On the other hand, it will allow us to build more manageable and realistic semi-phenomenological amplifier and laser models based on the insight gained from the more comprehensive many-body approach.

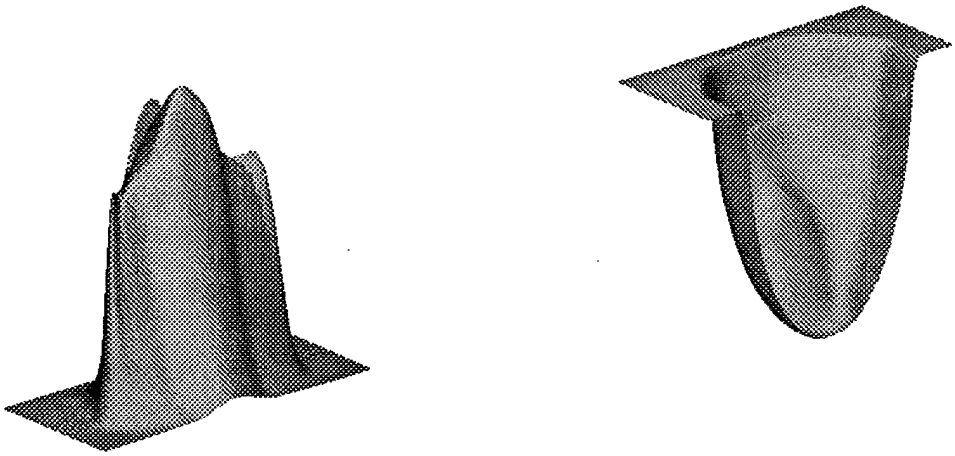

Figure 9: *Transverse structure of intensity (left) and density (right) after 1mm when cooling and memory effects are included.*

References

[1] A. Knorr, R. Binder, E.M. Wright, and S.W. Koch, "Amplification, absorption, and lossless propagation of femtosecond pulses in semiconductor amplifiers", Opt.Lett., **18**, 1538 (1993); also: Optics and Photonic News (December 1993)

[2] R. Indik, A. Knorr, R. Binder, S. Koch and J. Moloney, "Propagation-induced adiabatic following in a semiconductor amplifier", Opt. Lett., **19**, (13), 966-968, (1994).

[3] W.W. Chow, R. Indik, A. Knorr, S.W. Koch and J.V. Moloney,"Time-Resolved Nondegenerate Four-Wave Mixing in a Semiconductor Amplifier", Phys. Rev. A, **52**, (3), 2479-2482, (1995).

[4] C.Z. Ning, R. Indik, and J.V. Moloney,"A Self-Consistent Approach to Thermal Effect in Vertical-Cavity-Surface-Emitting Lasers", JOSAB, **12**, (10), 1993, (1995); C.Z. Ning and J.V. Moloney, "Plasma-Heating Induced Intensity-Dependent Gain in Semiconductor Lasers", Appl. Phys. Lett., **66**, 559, (1995); C.Z. Ning, R. Indik, J.V. Moloney and S.W. Koch, "Effects of Plasma and Lattice Heating in VCSELs", SPIE-Physics and simulation of optoelectronic devices III, 6-9 Feb, 1995, San Jose, SPIE-Proceedings **2399**, 617-628, (1995), Eds. W. Chow and M. Osinski

[5] R. Indik, R. Binder, W.W. Chow, A. Knorr, J.V. Moloney, and S.W. Koch "Many-body effects in the propagation of short pulses in a semiconductor amplifier", SPIE-Physics and simulation of optoelectronic devices III, 6-9 Feb, 1995, San Jose, SPIE-Proceedings 2399, Eds. W. Chow and M. Osinski

Conferences:

AFOSR Meeting for Contractors and Grantees in Computational and Physical Mathematics, June 1-3 Kirtland AFB. R. Indik, J.V. Moloney, S.W. Koch, R. Binder, A. Knorr OSA Annual Meeting, Dallas, Oct. 2-7 (1994)

SPIE-Physics and simulation of optoelectronic devices III, 6-9 Feb, 1995, San Jose.

Microscopically Computed Quantum Well Gain Spectra

S. Hughes, A. Girndt, C.Z. Ning, S.W. Koch, R. Indik, R. Binder and J.V. Moloney

An open question that remains in the study of many-body interactions in semiconductor media is how to effect a closure of the infinite hierarchy of equations describing the nonlinear optical response. A significant discrepancy existed between experimentally measured and microscopically computed quantum well gain spectra until a few months ago. We have recently identified this discrepancy with an inconsistent treatment of carrier collision effects, at the level of quantum kinetic theory in the Markovian limit. Earlier comparisons between bulk spectra where the collison terms in the Semiconductor Bloch equations (SBE) were treated in a rate equation approximation, and experiment proved to be excellent. An important conclusion to be drawn from this study is that *femtosecond carrier-carrier and carrier-phonon scattering events*, profoundly affect the shape of the CW semiconductor optical response function.

In the microscopic treatment of the semiconductor optical response, the momentum resolved polarization P_k and electron/hole distribution functions, evolve as

$$\frac{\partial P_k}{\partial t} = -i\left(\Delta_k - \omega_0\right) P_k - i\Omega_k(n_k^e + n_k^h - 1) + \left.\frac{\partial P_k}{\partial t}\right|_{\text{coll}} \tag{11}$$

$$\frac{\partial n_k^{e/h}}{\partial t} = iP_k^{\star}\Omega_k - iP_k\Omega_k^{\star} + + \left.\frac{\partial n_k^{e/h}}{\partial t}\right|_{\text{coll}} \tag{12}$$

with the renormalized Rabi frequency $\Omega_k = \frac{\Omega}{2} + \frac{1}{\hbar}\sum_{k'} V_{k-k'}P_{k'}$. Here $n_{k'}^{e/h}$ and $\Delta_k = \varepsilon_k - \frac{1}{\hbar}\sum_{k'} V_{k-k'}(n_{k'}^e + n_{k'}^h)$ denote the distribution functions for electrons or holes and the energy dispersion including the band gap renormalization, respectively. The Coulomb potential, V_k, is treated in a quasi-statical screening model. The Rabi frequency $\Omega = d_{cv}\cdot E/\hbar$ is determined by the dipole matrix element d_{cv} and the amplitude of the external electrical field $\tilde{E} = E(t,\xi)e^{-i\omega_0 t + ik_0 z}$.

The issues of anomalous absorption, memory effects etc, discussed above can be traced to how one computes the collision terms in the polarization equation. When calculating semiconductor gain spectra, one often approximates collision effects with a constant effective dephasing rate, which leads to anomalous absorption below the renormalized bandgap. Moreover, experimentally measured quantum-well gain spectra look bulk-like whereas computed gain spectra show a sharp rise near the band edge[1]. A more extended treatment of collision effects involves extending the screened Hartree-Fock treatment to include contributions from the next higher order correlations involving the Coulomb potential[2, 3]. The resulting equation for the microscopic polarization due to an electron-hole pair, p_k, has the form

$$\frac{\partial}{\partial t}p_k = -i\omega_k p_k - i\Omega_k(n_{e,k} + n_{h,k} - 1) - \Gamma_k p_k + \sum_q \Gamma_{k,q}p_{k+q}. \tag{13}$$

The first two terms on the right hand side describe the oscillation of the polarization at the transition frequency, ω_k, and the stimulated emission and absorption processes. The screened Hartree-Fock contributions lead to a bandgap renormalization, resulting in the above transition energy and the renormalized Rabi frequency above. Carrier-carrier collisions give rise to the last two terms. The third term is a diagonal contribution, with

$$\Gamma_k = \sum_{a=e,h}\sum_{b=e,h}\sum_q\sum_k \frac{2\pi}{\hbar}V_{s,q}^2\,\delta(\epsilon_{a,k}+\epsilon_{b,k}-\epsilon_{a,k+q}-\epsilon_{b,k-q})\times[n_{a,k+q}(1-n_{b,k})n_{b,k-q}+(1-n_{a,k+q})n_{b,k}(1-n_{b,k-q})] \tag{14}$$

The fourth term is a nondiagonal contribution, $\sum_q \Gamma_{k,q}p_{k+q}$, which couples the polarizations with different k's. For this contribution,

$$\Gamma_{k,q} = \sum_{a=e,h} \sum_{b=e,h} \sum_{k} \frac{2\pi}{\hbar} V_{s,q}^2 \delta(\epsilon_{a,k} + \epsilon_{b,k} - \epsilon_{a,k+q} - \epsilon_{b,k-q}) \times [(1-n_{a,k})(1-n_{b,k}) n_{b,k-q} + n_{a,k} n_{b,k} (1-n_{b,k-q})] \quad (15)$$

The dramatic modification of the quantum well gain spectrum when the constant dephasing assumption is removed, is illustrated in Figure 1(a) where the gain spectra with (dashed) and without (solid) this assumption are compared for three values of the total carrier density. Note that the sharp rise on the negative detuning side is removed and the peak gain values are significantly larger. Figure 1(b) is a comparison of the new gain spectra with experimental measurements of D. Bossert at PL/LIDA. The solid squares are experimental measurements and the agreement is seen to be excellent. This latter picture is reproduced in Color Plate I below.

The computation of the full gain spectra requires supercomputing resources but the payoff is huge. Now, for the first time, we have confidence that we can design a laser structure from the bottom up and predict its performance prior to fabrication. The gain spectra have recently been computed for other QW structures and verified experimentally by a different group[4].

References

[1] W.W. Chow, S.W. Koch and M. Sargent III, Semiconductor Laser Physics, (Springer Verlag) 1994.

[2] S. Hughes, A. Knorr, S.W. Koch, R. Indik, and J.V. Moloney, Solid State Comm., **100**, 555 (1996).

[3] A. Girndt, F. Jahnke, A. Knorr, S.W. Koch, and W.W. Chow, "Multi-band Bloch Equation and Gain Spectra of Highly Excited II-IV Semiconductor Quantum Wells", (preprint attached).

[4] W.W. Chow, P.M. Smowton, P. Blood, A. Girndt, F. Jahnke and S.W. Koch, Comparison of Experimental and Theoretical GaInP Quantum Well Gain Spectra, (preprint).

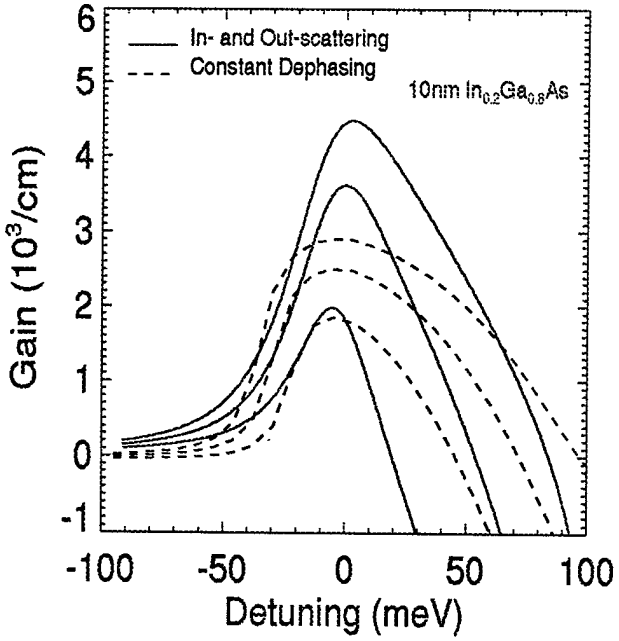

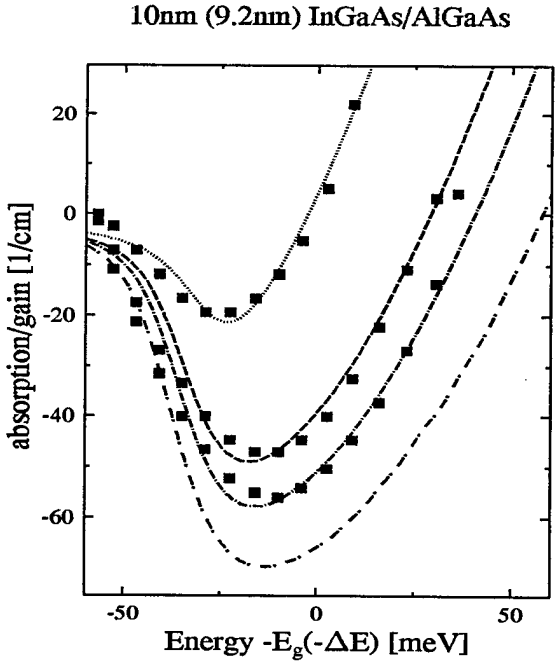

Universal order parameter equation description of laser patterns

J. Lega, Q. Feng, J.V. Moloney and A.C. Newell

This project derives the complex order parameter equations for a laser starting with the physical laser equations. A goal is to evaluate the robustness of the order parameter equation model relative to the original physical model as a precursor to deriving an order parameter equation description for a broad area semiconductor laser. The latter would start from the full many-body Maxwell-Semiconductor Bloch equations and some preliminary progress has been made on this as noted below. Our prototypical models have been the 2-level homogeneously, inhomogenously broadened and Raman (3-level) lasers. These systems separately mirror a particular physical manifestation of the known behavior of the semiconductor laser at a less complicated level. The latter is assumed to have a 2-band structure and is inhomogeneously broadened in electron momentum space. In a semiconductor, the carrier density dependent detuning dynamically alters the bandgap (bandgap renormalization), while a Raman laser exhibits an intensity dependent detuning (A.C. Stark effect). By studying the role of the constituent parts in simpler mathematical settings we hope to glean the influence of analogous physics in the much more complicated many-body semiconductor problem.

We have derived the complex Ginzburg-Landau (CGL)(negative detuning), and coupled complex Newell-Whitehead-Segel (CNWS) (positive detuning) amplitude equations for both the 2-level and Raman lasers [1]. Very recently, we derived a complex Swift-Hohenberg (CSHE) description[3] which, although strictly valid near the peak gain of the laser, proves to be very robust. The CSH model agrees with the numerically computed instability curves for the 2-level laser well beyond lasing threshold. The CSH has been extended to derive a "generalized rate equation" for a mathematically stiff laser which would represent a lowest order approximation to a realistic semiconductor laser model. This extended system is given by:

$$\begin{aligned} \psi_t &= (\mu + i\Omega)\psi + ia\nabla^2\psi - \frac{\sigma}{\sigma+1}(\Omega - a\nabla^2)^2\psi - \sigma n \\ n_t &= -bn + |\psi|^2 \end{aligned}$$

This coupled system has an obvious physical interpretation. The linear growth rate (gain) is represented by μ, the Hopf bifurcation frequency (frequency pulling) by Ω , the diffraction parameter is a , σ is the cavity loss, and b is the normalized inversion decay rate. The diffusion term (third term on the right) acts as a gain discrimination, favoring the emission of an off-axis far-field output at critical transfer wavenumber $k_c = \sqrt{\frac{\Omega}{a}}$, by damping modes at either side of this wavennumber. Without this term, spurious high wavenumber modes sees growth and look like numerical grid oscillations[1].

The mean flow term given by the second equation is important in contributing to the robustness of the model. With this equation appended, we find that the various phase and amplitude instability boundaries of this "rate equation" agree quantitatively with the full Maxwell-Bloch 2-level laser equations up to two to three times threshold[4]. It is easy to demonstrate in fact that the single CSHE is insensitive to the stiffness of the system (parameter b) and that the additional equation is therefore essential. We have also shown that the usual amplitude equations derived in [2] for negative (complex Ginzburg-Landau (CGL)) and positive (complex Newell-Whitehead-Segel (CNWS)) detuning from peak gain are in precise agreement with those derived directly from the above coupled CSHE model.

An important conclusion from this study is that the stiffness inherent in semiconductor lasers causes the Busse balloon (stable lasing emission domain) to disappear, implying that the laser is intrinsically unstable even at lasing threshold. This is consistent with experimental observations showing strong uncontrolled filamentation in semiconductor lasers. Mathematically, this instability can be ascribed to a strong perturbation by the eigenvalue of the linearization, associated with the mean flow (n), of the complex eigenvalues associated with the order parameter ψ. Although this eigenvalue can be damped at $k = 0$, its real part can become positive at finite k.

We have also investigated the influence of highly absorbing boundaries on pattern selection in these large aspect ratio lasers. One finds that the boundary forces a selected wavenumber on the pattern in the bulk[5]. A quantitative understanding of these issues is vital to understanding how to control or usefully manipulate filamentation instabilities in broad area and flared high-power semiconductor lasers. In addition we know that these lasers run on multi-longitudinal modes even just above threshold. The *state of the art* of semiconductor laser modeling in the general research community is still based on the *Beam Propagation Method* which ignores time dependence entirely. Simply extending this method by adding time dependence will lead to the spurious oscillations mentioned above.
This work is provides a vital input to our modeling of realistic wide aperture semiconductor lasers as described below. Proof of principle methodology can be developed within the present framework utilizing a mix of analytical and computational approaches. Extending the current model to include multi-longitudinal modes is a high priority.

References

[1] P.K. Jakobsen, J.V. Moloney, A.C. Newell and R. Indik, Phys. Rev. A, **45**, 8129 (1992).

[2] P.K. Jakobsen, J. Lega,Q. Feng, M. Staley, J.V. Moloney and A.C. Newell, Phys. Rev. A **49**, 4189-4200 (1994); J. Lega, P.K. Jakobsen, J.V. Moloney and A.C. Newell, Phys. Rev. A, **49**, 4201-4212 (1994).

[3] J. Lega, J.V. Moloney and A.C. Newell, Phys. Rev. Lett., **73**, 2978 (1994); J. Lega, J.V. Moloney and A.C. Newell, "Universal Description of Laser Dynamics near Threshold", Physica D, **83**, 478, (1995).

[4] Q. Feng, J.V. Moloney and A.C. Newell, Phys. Rev. Lett., **71**, 1705 (1993).

[5] I. Aranson, D. Hochheiser and J.V. Moloney, Phys. Rev. A, **55**, 3173 (1997).

Conference Invited Papers

- Gordon Research Conference on Nonlinear Optics and Lasers, Aug. 1-6, (1993), Wolfeboro, NH.
- FSU-USA Conference on Chaos, Woods Hole, Massachussetts, July 19-23, (1993).
- Nonlinear Optics and Guided Waves, A Study Center of the European Science Foundation, Aug. 1-20, 1994.
- Workshop on "Singularities in Patterns and Collapse: Applications to Semiconductor Lasers and Critical Focusing of Ultrashort Optical Pulses", University College Cork, Ireland, Aug. 21-27, 1994.
- AFOSR/ACMS Nonlinear Optics Workshop, University of Arizona, Oct. 9-11, 1994.
- Dynamics Days 14-th Annual International Workshop, Houston, Jan. 4-7, (1995).
- Third SIAM Conference on the Applications of Dynamical Systems, Snowbird, Utah, May 21-24, (1995).

Controlling Optical Turbulence

D. Hochheiser, J.V. Moloney and J. Lega

This project presents a robust global control strategy for a class of partial differential equations exhibiting spatio-temporal disorder[1]. The control, implemented as a spatial filter with delayed feedback, is shown to stabilize and steer the weakly turbulent output of a spatially-extended system. The latter is described by a generalized complex Swift-Hohenberg equation [2] which is used as a generic model for pattern formation in the transverse section of semiconductor lasers.

The technique we propose takes advantage of the fact that the spatio-temporal spectrum of the turbulent output often satisfies, to a good approximation, the dispersion relation of the system. Control is then achieved by filtering this spectral output about a desired plane wave and feeding back the corresponding delayed signal into the system, together with a contribution proportional to the retarded field. This method is likely to be applicable to any partial differential equation which sustains traveling waves and is particularly suited for optical systems. In the latter, the farfield output is indeed a natural spatial Fourier transform of the complex envelope of the electromagnetic field and applying a temporal Fourier transform to successive readings of the farfield yields the desired spatio-temporal spectrum.

The control scheme has been illustrated on the example of a generalized laser Swift-Hohenberg equation [2], which phenomenologically describes the dynamics of wide aperture semiconductor lasers. The Swift-Hohenberg equation is a well-known generic model of pattern formation in extended systems, and it was shown in [2] that when coupled to an equation for the population inversion, a complex SH equation gives a good description of 2-level, class B lasers. Particular effects can then be included in this model to reproduce filamentation, a typical feature of wide aperture semiconductor lasers. The latter are interesting physical manifestations of spatially extended systems showing persistent weakly turbulent behavior. In contrast to wide aperture two-level lasers, they display strong dynamic filamentation instabilities immediately at threshold. Moreover, their large gain leads to strongly amplified spontaneous emission along the laser axis and hence, to a persistent noisy background behavior.

Ideally, a robust control strategy for an infinite dimensional nonlinear dynamical system should require no a priori knowledge of the solution to be stabilized and should take into account the fact that the system may have no stable attracting state. The method we propose here not only stabilizes unstable traveling waves in the turbulent regime but allows one to select and angle tune (steer) the system output starting from initial noise or a turbulent state.

The most important distinction between the semiconductor and other laser systems is the marked asymmetry of its gain and refractive index spectra. This causes a very strong nonlinear amplitude-phase coupling in the field which leads to uncontrolled dynamical filamentation in the laser intensity at and beyond threshold. This effect is modeled by a nonlinear coupling between the electric field and the carrier density through a coefficient known as the α- factor. By introducing a similar term in the 2-level laser complex Swift-Hohenberg (CSH) equation, we obtain the following system:

$$\begin{aligned}(\sigma+1)\frac{\partial\psi}{\partial t} &= \sigma(r(x)-1)\psi + ia\nabla^2\psi - i\sigma\Omega\psi \\ &\quad -\frac{\sigma}{(1+\sigma)^2}(\Omega + a\nabla^2)^2\psi - \sigma(1+i\alpha)n\psi \qquad (1)\\ \frac{\partial n}{\partial t} &= -bn + |\psi|^2,\end{aligned}$$

where α is negative for semiconductor lasers.

The complex order parameter ψ is the scaled envelope of the electric field and n is a scaled relative carrier density. The latter acts as a mean-flow and has a profound influence in destabilizing the system, leading to a very complicated linear growth behavior of the traveling wave solutions. Here σ is the scaled

cavity loss coefficient, a is proportional to the inverse of the Fresnel number of the laser and measures the characteristic length scale in the transverse dimension relative to the wavelength of light, Ω is the dimensionless detuning of the laser frequency from the gain peak, ∇^2 is generally the two dimensional Laplacian although we restrict our study here to one transverse dimension x, and b is the dimensionless ratio of the carrier recombination to polarization dephasing times in the Semiconductor Bloch equations. The external pump parameter $r(x)$ is the scaled external current applied to the laser and the x-dependence is explicitly displayed in order to emphasize that the pumping is only applied over a finite transverse section of the laser. Outside the pumped region, the passive semiconductor acts as a very strong absorber. In the discussion below we first assume that the pump is infinitely extended in x, in order to take advantage of the known properties of solutions to the CSH equation. We then show explicitly that many of the properties of this idealized system carry over to the realistic finitely pumped cross-section.

Equation (1) admits traveling wave solutions of the form $\psi = Re^{i(k\cdot x-\omega t)}, n = R^2/b$ where $R^2 = b(r-1-(\frac{\Omega-ak^2}{1+\sigma})^2)$. The frequency of the traveling wave of wavenumber k is given by $(1+\sigma)\omega = -[ak^2 + \Omega\sigma + \alpha\sigma[r-1-(\frac{\Omega-ak^2}{1+\sigma})^2]]$. This latter expression shows that the nonlinear amplitude-phase coupling makes the frequency dependent on the distance above threshold for lasing.

Optically, as the nonlinear dispersion curve (or $k-\omega$ spectrum) is an experimentally accessible quantity, it is natural to introduce an optical feedback scheme which filters, in k and ω, the desired traveling wave lying on the actual dispersion curve (attractor). The idea is then to introduce a delayed feedback with a spatial filter (consisting of a lens and aperture at the focal point of the lens). Ideally the delay (proportional to ω^{-1}) should be chosen to locate the desired coordinate on the $k-\omega$ plot. If this scheme works, we simultaneously have achieved stabilization and a beam steering capability by simply tuning the filter along the experimental dispersion curve. Our control technique is then the following: we add a feedback term of the form $-\gamma(\psi(x,t)-\tilde{\psi}(x,t-\tau))$ to the above equation where

$$\tilde{\psi}(x,t-\tau) = \mathcal{F}^{-1}\left(F(k-k_0)\,\mathcal{F}\left(\psi(x,t-\tau)\right)\right),$$

$\mathcal{F}$ is the Fourier transform operator and F is a suitable aperture. This represents a time-delayed, spatially filtered feedback of the original complex field $\psi(x,t)$ at the output facet.

With this technique, the unstable region, which for $\alpha < 0$ corresponds to the whole domain of existence of traveling waves, can be stabilized over the full range of pump strengths and angular tuning (k-axis). Figure 1 presents a succinct overview of the control achieved for different steering angles (proportional to k) of the idealized and ramped pump systems respectively. For these plots, the external pump is twice the lasing threshold value, the feedback strength $\gamma = 0.25$, and the feedback delay time τ is chosen to match the selected angle (k-value) on the analytic dispersion curve. Note that the controlled far-field spectra are extremely sharp in k and ω for the infinitely wide pump. For the ramped pump case in (b), there is some spectral broadening in k and ω, indicating a modulated finite support traveling wave (Fig. 2.) rather than an infinitely extended constant amplitude signal. Besides, the controlled state is no longer a traveling wave of the isolated system but instead is a solution of the full partial differential equation with delay. Its wavenumber (angle tuning) is precise but the frequency is off. The traveling wave emanates on one side from a defect (source) and is absorbed on the other (a sink), as shown in Fig. 2 for $r = 2$ and $k = 4$. In this case the wave travels from right to left (since the corresponding ω is positive). The situation is reversed if control is established at $-k$: the wave then travels from left to right. Also shown on this picture is beam steering from $k = 4$ to $k = 7$. When control is switched from one wavenumber to the other (around t=0.27), the traveling wave at $k = 4$ is first damped out since it is no longer stabilized by the feedback term. Then the mode at $k = 7$ starts growing and is stabilized around $t = 6.8$ (arbitrary units). Our observations indicate that the spatial filter is the critical component in enabling effective control. The time delay, while less critical, proves most effective when matched to the relevant frequency on the nonlinear dispersion curve. In the unramped case, we have seen locking to an intermediate controlled state

which is stable but not the desired one when there is a significant frequency mismatch between the delay and the desired frequency on the dispersion curve. This resembles the asymptotic state of the ramped system.

The control scheme has been extended to a two-longitudinal mode model, described by a coupled set of CSH equations[3]. This study shows that the time delay (frequency filter) becomes more important for successful control and a restriction is placed on the feedback control strength.

References

[1] D. Hochheiser, J.V. Moloney and J. Lega, Phys. Rev. A (Rapid Comm.), in press (June 1997).

[2] J. Lega, J.V. Moloney and A.C. Newell, Phys.Rev. Lett., **73**, 2978 (1994); ibid Physica D, **83**, 478 (1995).

[3] M.E. Bleich, D. Hochheiser, J.V. Moloney, and J.E.S. Socolar, Phys. Rev. E, **55**, 2119 (1997).

Conferences:

AFOSR/ACMS Nonlinear Optics Workshop, Tucson, Arizona, October 10-12, 1996.

D. Hochheiser, Controlling Optical Turbulence in High Brightness Semiconductor Lasers, SIAM Conference of the Applications of Dynamical Systems, Snowbird, Utah, May 18-22, 1997.

J. Moloney, AFOSR Annual Contractors Meeting on Dynamics and Control, Wright-Patterson AFB,Dayton, Ohio, May 21-23, 1997.

D. Hochheiser and J.V. Moloney, Controlling Optical Turbulence, Dynamics Days Arizona, Scottsdale, Arizona, January 9-10, 1997.

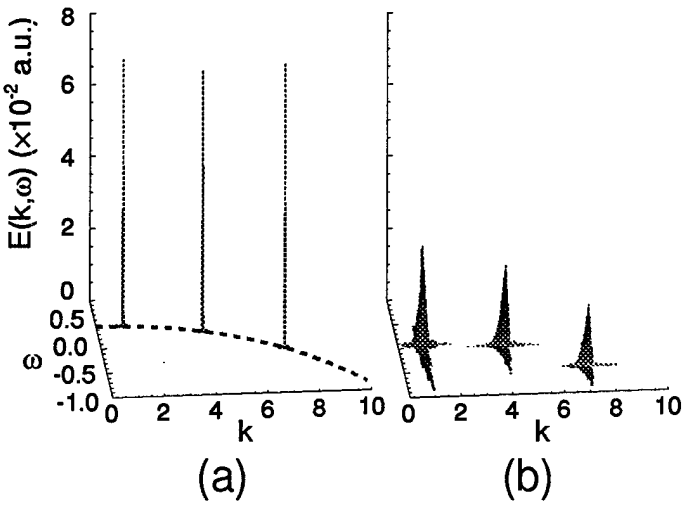

Figure 1: Left: A subset of controlled $k-\omega$ spectra superimposed on the analytic dispersion curve (dashed line) for the infinitely extended problem. Right: Similar $k-\omega$ spectra for the ramped pump.

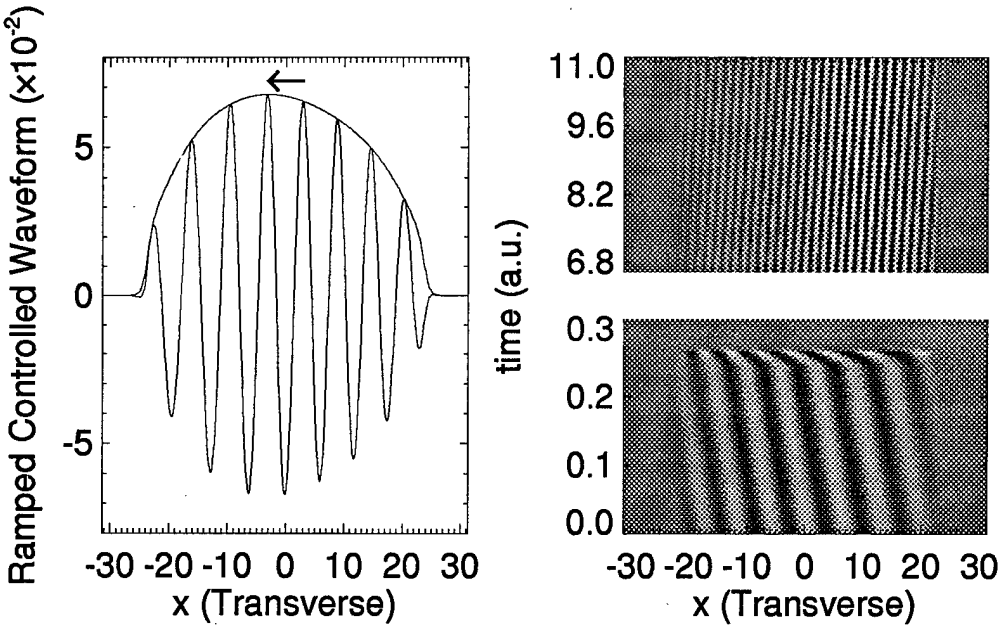

Figure 2: Left: Modulated traveling waveform and envelope for the controlled finite pump case with $r = 2, \alpha = -5$. All other parameter are the same. Right: Beam steering from an initial controlled signal at $k = 4$ to a stable signal at $k = 7$ at the same parameter values as in the left figure.

Modeling spatio-temporal dynamics of broad area/flared semiconductor laser amplifiers

J.K. White, J.G. McInerney, J.V. Moloney, S.W. Koch

Large aperture semiconductor laser amplifiers are extremely promising for applications combining pulsed and CW power levels $\sim 1 - 10$ W with high spatial coherence, as well as the usual advantages of semiconductor lasers. This project relates directly to modeling ongoing experiments by the LIDA group at the Phillips Laboratory, Kirtland AFB, Albuquerque. The model incorporates the complete spatiotemporal dynamics both transverse to and along the broad area/flared amplifier or laser axis. Existing models extensively used in the general literature employ the *Beam Propagation Method*, a time independent approach which in the specific context of lasers, can lead to ambiguity in the interpretation of results. The present approach utilizes a look-up table for the gain and refractive index functions, derived from the basic microscopic physics. We can investigate all intrinsically time dependent behaviors including switch-on of the laser, relaxation oscillations, uncontrollable filamentation, current modulation, injection-locking, mirror feedback and nonlinear control, arbitrary current injection profiles both transverse to and along the laser axis, amplification of pulse trains in a broad area/flared amplifier, and arbitrary index/gain guiding profiles as long as the characteristic time scales of the dynamics exceeds many picoseconds. Shorter time scale dynamics requires a more comprehensive description of the many-body microscopic physics of the interaction of light with semiconductor materials. In addition, some issues not satisfactorily dealt with within the current formulism are addressed under technical report *Plasma and Lattice Heating Effects in Quantum Well Lasers and VCSELs* and in [4].

The basis for the present model is the traveling wave amplifier laser rate equations:

$$\begin{aligned} \frac{n}{c}\frac{\partial E}{\partial t} + \frac{\partial E}{\partial z} &= \frac{i}{2k_0}\frac{\partial^2 E}{\partial x^2} + \Gamma[g(N,\omega_0) + ik_0\delta n(N,\omega_0)]E - \alpha E \\ \frac{\partial N}{\partial t} &= D_f\frac{\partial^2 N}{\partial x^2} + \frac{J(x,z)}{ed} - \gamma_{sp}N - \frac{\epsilon_0 cng(N,\omega_0)}{2\hbar\nu}|E|^2 \end{aligned} \tag{1}$$

where the symbols have their usual meanings. Details of a more comprehensive model for a broad area/flared laser which includes counterpropagating waves and boundary conditions have already been presented in [5]

The microscopic physics, including many-body effects like bandgap renormalization and interband carrier-carrier scattering, is included through the gain function $g(N,\omega_0)$ and change in refractive index $\delta n(N,\omega_0)$, both being determined by solving the semiconductor Bloch equations in the quasi-equilibrium approximation for the polarization P:

$$\left[i\frac{\partial}{\partial t} - (e_{e,k} + e_{h,k})\right] P_k = (f_{e,k} + f_{h,k} - 1)\left[d_{cv,k}\frac{E_0(t)}{2\hbar} + \sum_{q\neq k}\frac{V_{|k-q|}}{\hbar}P_q\right] \tag{2}$$

The Hopscotch method has been employed to solve the model equations. The method divides the computational domain into a checkerboard of alternating even/odd points. At each time step the odd/even points are advanced explicitly in time while the even/odd points are then advanced implicitly. The next time step the order is reversed. This method has the advantage of properly handling the beam diffraction through the implicit step while using an explicit Lax-Wendrof scheme to correctly propagate the beam in the longitudinal direction. Alternative pseudo-spectral methds are also being implemented on this model. When the polarization is adiabatically eliminated from the Maxwell-Bloch equations, one of the eigenvalues goes marginally unstable for large values of the transverse wave vector k[1]. This appears as a large

oscillation at the gridscale of the computational domain. By adding a small, artificial diffusion, the high-k oscillations can be damped out. Care must be given that the diffusion is not so large it begins to dampen real features of the device. A more physically and mathematically consistent approach would derive the appropriate order parameter equations from the full Maxwell-Semiconductor Bloch laser equations, a formidable approach currently being undertaken as part of the present contract.

In the broad area/flared amplifier case, interaction of an input Gaussian beam with the sharp edges of the current stripe leads to the formation of "bat ears", or sharply peaked side lobes. This implies that the sudden drop in carrier density at the edge of the current stripe is responsible. By smoothing this edge the "bat ears" can be reduced (see attached figure). A linear transverse analysis shows that a perturbation related to the first and second derivatives of the current stripe seeds nonlinear growth of the "bat ears".

Currently we are investigating multilongitudinal modes and their associated dispersion curves in broad area semiconductor lasers. In earlier work we predicted the existence of parabolic nonlinear dispersion curves (k vs ω) for a free-running broad area laser undergoing uncontrolled filamentation. Such dispersion curves were recenly observed experimentally by Dave Bossert at the Phillips Lab/LIDA. Our current goal is to correlate our theoretical prediction with his experimental observation. Eventually we hope to explore strategies for nonlinear control of the turbulent output of these devices. Work is in progress on a joint publication combining theory and experiment.

Modeling the spatiotemporal dynamics of semiconductor laser amplifiers presents many challenges. By using look-up tables to incorporate the many-body physics and artificial diffusion to eliminate the high-k instability we have created a model that captures most of the relevant physics in these devices. Already we have shown that the formation of "bat ears", one of the limiting factors of power in the central lobe, is a result of the input pattern's interaction with the edges of the current stripe

Areas of future study include:

- Filamentation dynamics
- Stability under pulsed operation
- Derivation of complex order parameter equations for the semiconductor problem (see J. Lega, J.V. Moloney, and A.C. Newell, "Universal Description of Laser Dynamics Near Threshold", Physica D.)
- Developement of a mean field code to be run in "real time" on a Silicon Graphics "Power Challenge" machine.

References

[1] J.K. White, J.G. McInerney, J.V. Moloney, "Effects of the injection current profile shape on side lobes in large aperture semiconductor laser amplifiers", Optics Lett., **20**, (6), 593-595, (1995).

[2] J.K. White, J.G. McInerney, J.V. Moloney, "Formation of sharply peaked side lobes in large aperture single pass semiconductor laser amplifiers", Electron. Lett., **31**, (1), 38-39, (1995).

[3] J.V. Moloney, R. Indik, J.K. White, P. Ru, S.W. Koch, W.W. Chow, "Modeling the nonlinear dynamics of wide aperture semiconductor lasers and amplifiers", SPIE conference proceedings, (1994).

[4] O. Hess, S.W. Koch, J.V. Moloney, "Filamentation and Beam Propagation in Broad Area Semiconductor Lasers", IEEE JQE, **31**, (1), (1995).

[5] P. Ru, J.V. Moloney and R. Indik, Phys. Rev. A., **50**, 831 (1994) and references therein.

Conferences:

J.K. White, J.G. McInerney, J.V.Moloney, "Modeling spatio-temporal dynamics of broad area/flared semiconductor laser amplifiers", AFOSR/ACMS Nonlinear Optics Workshop, University of Arizona, (1994).

J.K. White, J.V. Moloney, W.W. Chow, J.G. McInerney, "Issues of spatial and dynamical stabilities in the scaling of flared semiconductor laser amplifiers", OSA Annual Meeting, Dallas, (1994).
R.A. Indik, J.K. White, J.V. Moloney, S.W. Koch, W.W. Chow, J.G. McInerney, OSA Annual Meeting, Dallas, (1994).
J.K. White, J.G. McInerney, J.V. Moloney, Workshop on Singularities and Patterns in Collapse, University College, Cork, Ireland, (1994).
J.K. White, J.G. McInerney, J.V. Moloney, International Summer School in Nonlinear Optics, University of Edinburgh, Scotland (1994).

Full Space-Time Simulation of High Brightness Semiconductor Lasers

J.V. Moloney, C.Z. Ning, A. Egan, and R.A. Indik

This project involves direct collaborative links to Air Force Laboratory scientists (M.M. Wright and D. Bossert PL/LIDA) and to industry (R. Patel, S. Srinivasan Opto Power Corporation). The theoretical basis for this model involves building the full semiconductor optical response function from a microscopic basis and incorporating this in the laser simulation code. Color Plate I succinctly summarizes our approach.
Edge emitting wide aperture semiconductor lasers are intrinsically multi-moded in the longitudinal and transverse dimensions. Moreover, the carrier density and field intensities display large nonuniformities both along and transverse to the device. It is vital therefore to take account of the gain dispersion (for mode discrimination) and local (in space) dependence of the semiconductor optical response. A simulation model which takes full acount of the above features has recently been introduced and tested against the full microscopic many-body model for pulse propagation in a bulk GaAs amplifier[1]. We will discuss recent developements in the microscopic theory which, for the first time, allow quantitative comparison between experimentally measured and theoretically computed quantum well gain spectra. The essence of our model, discussed in detail in Ning *et al.*[1], is that the local gain and refractive index dispersion as a function of total carrier density (N), $\chi(N,\omega)$, extracted from the microscopic theory or experiment, are fitted with multiple Lorentzians:

$$\chi(N,\omega) \approx \chi_0(N) + \sum_l^M \frac{A_l(N)}{i\Gamma_l(N) + (\delta_0 + \omega - \delta_l(N))} \equiv \chi_0(N) + \sum_l^M \chi_l(\omega, N), \tag{1}$$

where $\chi_0(N)$ is a "background" contribution which is frequency independent. $\delta_0 = E_g/\hbar - \omega_c$ with ω_c being a reference frequency and E_g the bare bandgap energy. The number of Lorentzian oscillators required for an accurate fit will depend in general on the shape of the gain/index curves. For example, quantum well structures with closely spaced subbands may require more terms to account for the appearance of the higher subband peaks in the gain at high densities. The density dependence of the strength $A_l(N)$, the width $\Gamma_l(N)$ and the position $\delta_l(N)$ in the frequency domain of the individual Lorentzian oscillators allows the laser to respond on the fly to local changes in N along and across the structure as a function of time. It is important to stress that both semiconductor material dimensionality effects (3D, 2D), strain etc and the full many-body effects such as bandgap renormalization, Coulomb screening, etc. are all included in the microscopically computed gain and refractive index spectra $\chi(N,\omega)$.
From each oscillator $\chi_j(N,\omega)$, we can construct a corresponding polarization $\tilde{P}_j(\omega)$ through the relation

$$\tilde{P}_j(\omega) = \epsilon_0\epsilon_b\tilde{\chi}_j(N,\omega)\tilde{E}(\omega) = \frac{\epsilon_0\epsilon_b A_j(N)\tilde{E(\omega)}}{\Gamma_j(N) + i(\delta_0 + \omega - \delta_j(N)}, \quad (j = 0, 1, 2...) \tag{2}$$

where quantities with a ˜ represent their Fourier transforms. E is the laser field amplitude. Inverting the Fourier transform for $(j = 1, 2, ...)$, we obtain

$$\frac{dP_j(t)}{dt} = \{-\Gamma_j(N) + i[\delta_0 - \delta_j(N)]\}P_j(t) - i\epsilon_0\epsilon_b A_j(N)E(t), \tag{3}$$

while for $(j = 0)$ we simply have

$$P_0(N) = \epsilon_0\epsilon_b\chi_0(N)E(t), \tag{4}$$

because no frequency dependence of $\chi_0(N)$ is assumed. The assumption that the carrier density N is frozen on the time scale of the polarization dynamics is a good approximation for a laser.
Both the forward and backward field and carrier density equations must now be appropriately modified to couple to the locally linear oscillators.

$$\frac{\partial F}{\partial z} - \frac{i}{2K}\frac{\partial^2 F}{\partial x^2} + \frac{n_g}{c}\frac{\partial F}{\partial t} = \frac{iK}{2\epsilon_0\epsilon_b}(P_0 + P_1 + ...), \tag{5}$$

$$\frac{\partial B}{\partial z} - \frac{i}{2K}\frac{\partial^2 B}{\partial x^2} + \frac{n_g}{c}\frac{\partial B}{\partial t} = \frac{iK}{2\epsilon_0\epsilon_b}(P_0 + P_1 + ...), \tag{6}$$

$$\frac{dN}{dt} - D_N\frac{\partial^2 N}{\partial x^2} = -\gamma_1 N + \frac{\eta J}{ew} + \frac{i}{4\hbar}[(P_0 + P_1 + ...)^* E - (P_0 + P_1 + ...)E^*], \tag{7}$$

where n_g is the group index, and $K = \omega_c n_b/c$ is the wavevector in the medium of background index n_b. The η, J, e, w are respectively, the quantum efficiency, pumping current, electron charge, and active region width. Once a laser structure is specified, the corresponding gain and index spectra can be computed and incorporated into the counterpropagating field code.

As a test of this model we have carried out a full space-time simulation of the field and carrier density build-up from noise in a MOPA device. The device structure consists of two sections, a DBR laser Master Oscillator (MO) of total length 1.575 mm and a linearly expanding Power Amplifier (PA) of length 2 mm. The MO has a 750 μm pumped gain section, a 750 μm DBR end distributed reflector and a shorter 75 μm DBR reflector at the PA end. The PA has a separate electrical contact. The passive semiconductor under both DBR sections needs to be at least, partially bleached, before the forward and backward waves can see the gratings. This is reflected in the rather sharp turn-on of the device as the MO current is increased. Another important issue is the weak reflectivity from the PA output facet. This is known to be detrimental to the stable operation of the device. We have studied the spatiotemporal dynamics of the laser turn-on for a PA facet output reflectivity $R_F = 0\%$, 0.05% and 0.1%.

Surface plots of the carrier density and field intensity are shown above and below the device geometry in Color Plate II, for stable operation when when $R_F = 0.05\%$. Here the MO current is $I_{MO} = 100$ mA and the PA current is $I_{PA} = 1.5$ A. The forward field at the beginning of the PA does not follow the diffraction pattern predicted for a finite aperture of 4 μm as strong gain and index guiding provide a nonlinear modification. The lack of optical field between the intensely illuminated region and the straight edge of the PA leads to a pronounced concentration of unsaturated carriers in this region. These unsaturated carriers will be available for gain if there is any finite amplified back reflection in the PA. We also note that the MO output intensity is insufficient to saturate the carriers just beyond the entrance to the PA.

Turning on a finite facet reflectivity, one immediately sees evidence for an external resonator behavior [2]. The important new feature is the finite back-reflected field which becomes strongly amplified in the region of unsaturated carriers and leaks through the lossy 75 μm DBR into the MO. The backward field also displays some fine features in the section of MO close to the interface with the PA, which is a signature of the multimode behavior. As a result, the MOPA becomes unstable. The single mode integrity of the MO is now destroyed and one can observe multi-longitudinal mode oscillations associated with this section at frequencies typically in the range of $30 - 40$ GHz. We have also observed multi-longitudinal mode beats at around 16 GHz corresponding to the PA section. The transverse profile remains essentially unchanged in shape in this unstable regime. At much higher PA pumping currents we have observed dynamic filamentation instabilities in addition to the multi-longitudinal mode beatings.

Preliminary studies of current modulation of the MOPA device have already been carried out. Modulation of MOPAs is an important consideration in potential communications applications. Experimental investigations of integrated MOPAs under current modulation (CM) and electro-absorption modulation (EAM) of the MO have taken place, and have demonstrated some of the advantages and limitations that may exist in both schemes. For CM the main limitation to achieving high power is the tendency for the PA to lase independently of the MO, when the MO current remains at or below its threshold value for longer than the turn-on time delay in the PA. Another problem is that transverse mode instabilities may arise

at high PA currents. For example, Figure 1(a) shows the temporal evolution of the output power from the MOPA under sinusoidal current modulation of the MO at 4 GHz, close to the threshold for transverse mode instabilites in the device. Under DC bias conditions the output power is stable and constant, but it becomes irregular and unstable under modulation. Our model permits us to resolve the transverse mode behavior (Figure 1(c)) and determine how the profile changes in the course of the emission of a pulse.
We can also explore the spatio-temporal dynamics of the MOPA under EAM. An extra section is added to the MOPA between the MO and PA, which can be switched between a nearly transparent "on" state and a nearly opaque "off" state with a reverse bias. This arrangement suppresses the tendency for the PA to lase independently of the MO. However, during the "off" states, the carrier density in the PA rises to a high level, so that when the EAM is switched to the "on" state considerable feedback occurs and undamping of the relaxation oscillation in the MO occurs. This places a limitation on the PA operating current and hence on the output power.
Our simulation results suggest a modification in the design which should increase this window of stable operation, namely designing the PA current pump as a trumpet flare matching the actual beam divergence from the MO output facet. Color Plate III contrasts the new design with the existing linear flared device. Discussions are currently underway with Opto Power Corporation to build a prototype high-brightness source based on this design. We emphasize that the model used here and developed in detail in reference [1], is not confined to the MOPA structure but can be used to study single and multi-section lasers of arbitrary geometry. We are in the process of including thermal processes at the level of ultrafast plasma and lattice heating through to quasistatic bulk heating effects.

References

[1] C.Z. Ning, R.A. Indik, and J.V. Moloney, Generalized Bloch equations for semiconductor lasers and amplifiers, (in press IEEE J. Quant. Electron.); J.V. Moloney, R.A. Indik, and C.Z. Ning, Full space-time simulation of high brightness semiconductor lasers, (in press IEEE Photonics Tech. Letts, **9**, (June 1997).

[2] A. Egan, C.Z. Ning, J.V. Moloney, R.A. Indik, M.W. Wright, D.J. Bossert and J.G. McInerney, Dynamic instabilities in MFA-MOPA semiconductor, Submitted to Applied Physics Letters.

Conferences:

AFOSR/ACMS Nonlinear Optics Workshop, Tucson, Arizona, October 10-12, 1996.

SPIE Photonics West, "Space-time simulation of high brightness semiconductor lasers" San Jose, California, February 10-14, 1997.

Figure Captions

Figure 1 : For $I_{PA} = 2.75$A, (a) the total power output from the device and the power contained to the Full Width at Half Maximum (FWHM), (b) the modulated current applied to the MO and (c) the evolution of the FWHM of the central lobe of the farfield intensity profile.

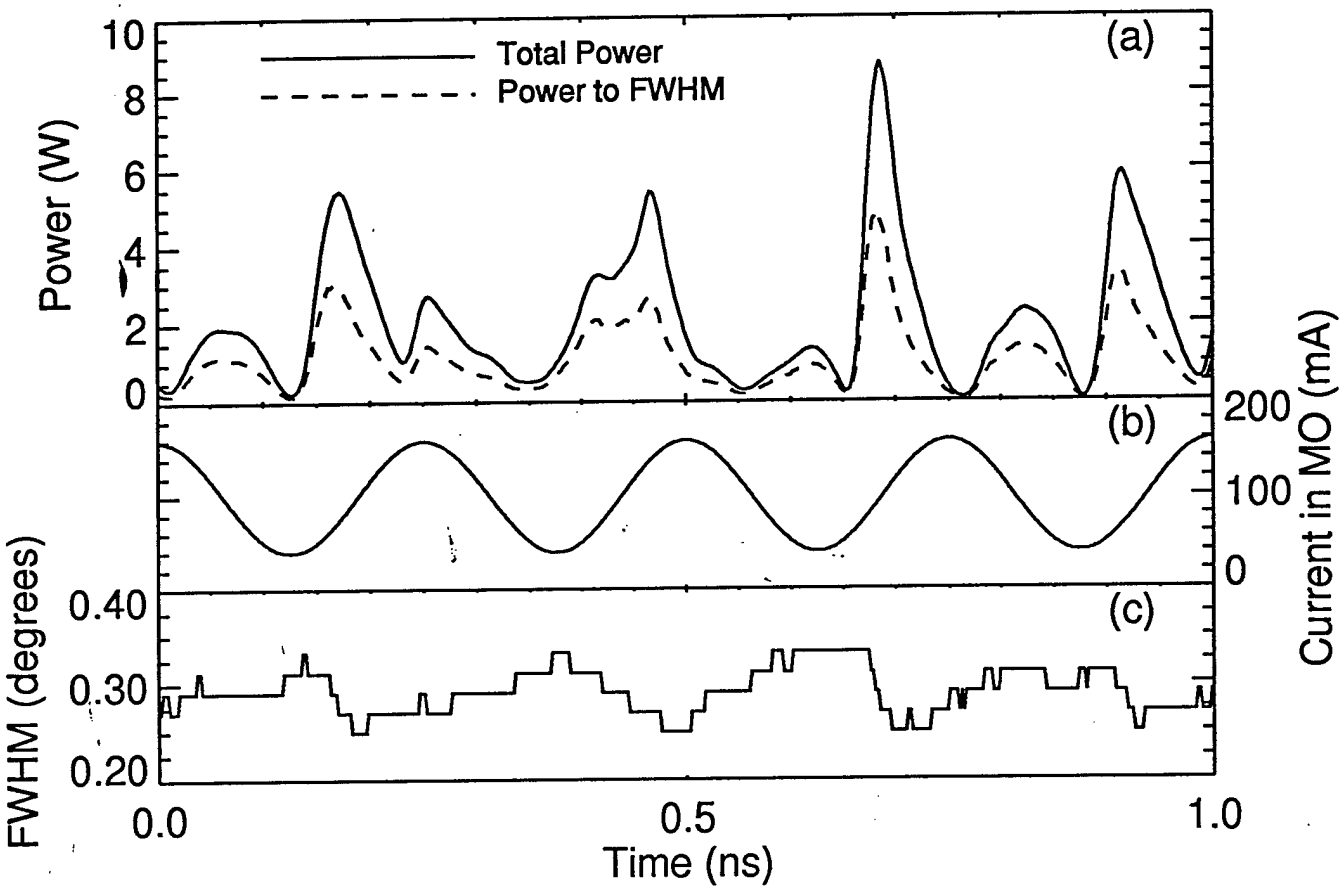

Figure 1 : For $I_{PA} = 2.75$A, (a) the total power output from the device and the power contained to the Full Width at Half Maximum (FWHM), (b) the modulated current applied to the MO and (c) the evolution of the FWHM of the central lobe of the farfield intensity profile.

Figure 1.

Color Plate I

• Microscopic Many–Body Theory of Semiconductor Optical Response

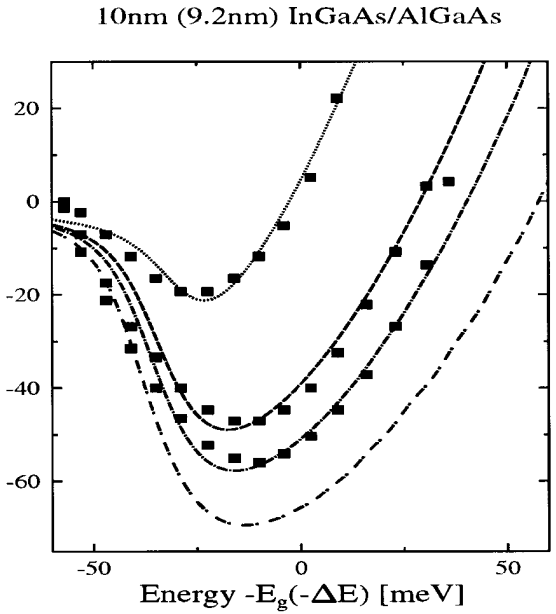

- *first quantitative agreement with experimentally measured quantum well gain spectra.*
- *femtosecond scale carrier–carrier scattering strongly modifies gain spectra.*
- *theory in collaboration with S.W. Koch and A. Girndt (Optical Sciences and Marburg)*
- *Experimental measurements (blue squares) by D. Bossert , USAF Phillips Laboratory.*

• Full Scale Nonlinear PDE Propagation Model.

$$\pm\frac{\partial E^{\pm}}{\partial z} - \frac{i}{2K}\frac{\partial^2 E^{\pm}}{\partial x^2} + \frac{n_g}{c}\frac{\partial E^{\pm}}{\partial t} = -\epsilon(E^{+}+E^{-}) + i\kappa E^{\mp} + \frac{iK}{2\epsilon_0\epsilon_b}(P_0^{\pm}+P_1^{\pm}+\ldots)$$

$$\frac{dP_j^{\pm}(t)}{dt} = \{-\Gamma_j(N) + i[\delta_0 - \delta_j(N)]\}P_j^{\pm}(t) - i\epsilon_0\epsilon_b A_j(N)E^{\pm}(t)$$

$$\frac{dN}{dt} - D_N\frac{\partial^2 N}{\partial x^2} = -\gamma_1 N + \frac{\eta J}{ew} + \frac{i}{4\hbar}\left(\left[(P_0^{+}+P_1^{+})^{*}E^{+} + (P_0^{-}+P_1^{-})^{*}E^{-}\right] + c.c.\right)$$

Arizona Center for Mathematical Sciences

Color Plate II

Stable Operation of MOPA after Transient Switch–on:

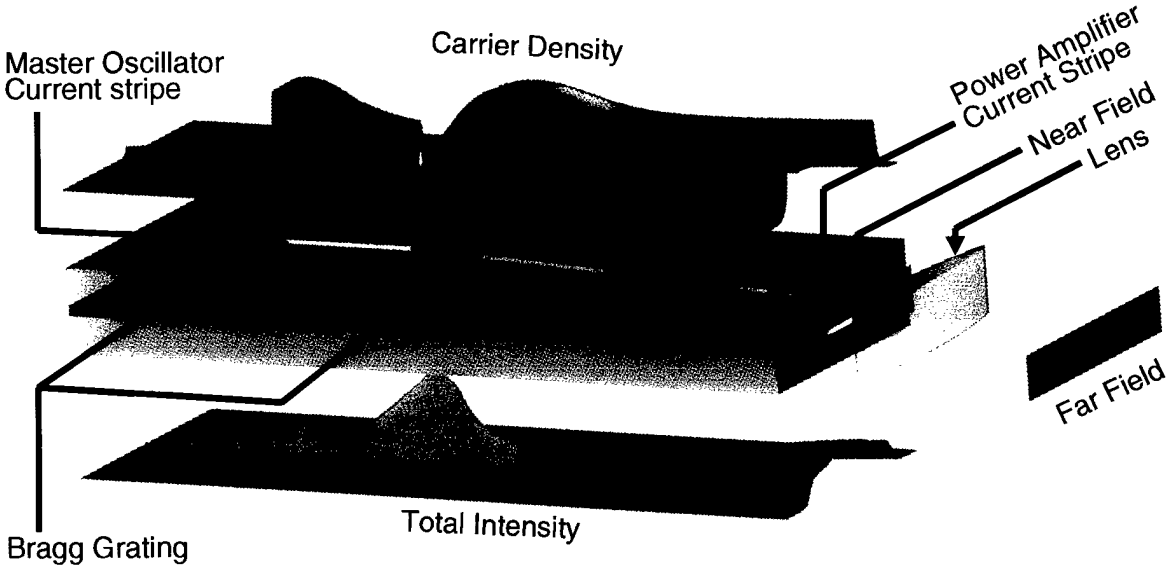

Simulations agree with experimental observations on linearly flared MOPAs – M.M. Wright, USAF Phillips Laboratory

- ***Highly nonuniform optical field intensity and carrier density – precludes use of standard linear gain model***
- ***Unsaturated carrier density at flare edges near MO output – recipe for destabilization of MO***

Arizona Center for Mathematical Sciences

Color Plate III

Alternative Design Strategy to Minimize Optical Feedback:

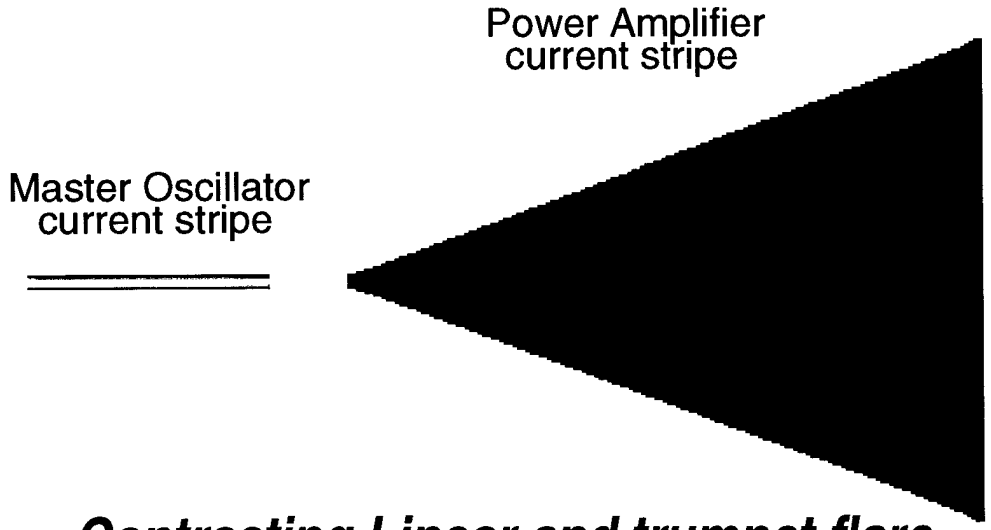

Simulations on nonlinearly flared MOPA predict increase in stable output power beyond linear flare by a factor of 2.

Contrasting Linear and trumpet flare

- ***Trumpet-shaped flare matches nonlinear modification of self-channeled optical intensity – provisional patent submitted.***
- ***Optical Feedback of back-reflected intensity minimized.***

Arizona Center for Mathematical Sciences

Plasma and Lattice Heating Effects in Quantum Well Lasers and VCSELs

C.Z. Ning, R. Indik, J.V. Moloney

Summary

Heating or thermal effects are a serious problem for semiconductor lasers in general and for some state-of-the-art devices, such as the Vertical-Cavity Surface-Emitting Lasers (VCSELs) in particular. There is much experimental evidence showing that heating can influence the device operation significantly. Furthermore, both theoretical and experimental investigations indicate that the lattice and plasma can each attain individual temperatures that are generally different from the ambient temperature during laser operation. It is thus of crucial importance to develop a self-consistent theory of heating in semiconductor lasers including lattice and plasma temperatures as independent dynamical variables, in order to understand the underlying physics and to help design semiconductor laser devices. We have developed such a self-consistent theory and applied it to CW operation of VCSELs. Many phenomena observed experimentally can be explained using our approach. These include the increase of CW-density and change of frequency shift with pumping, and thermal switch off. Furthermore our approach predicts a novel threshold bistability of VCSELs. The well-known gain nonlinearity can also be justified or improved using our present theory.

The model

Our starting point is the free-carrier model for the semiconductor laser with k-resolved polarizations adiabatically eliminated. This set of equations is generally equivalent to an infinite hierarchy of moment equations. We cut off the infinite hierarchy at the second order moment and close the hierarchy by assuming that the k-resolved densities obey the Fermi distribution. This leads to two equations for the total carrier density (N) and energy (W). The energy equation is transformed to an equation for plasma temperature (T_p). The lattice temperature equation is established phenomenologically by considering different cooling and heating mechanisms of the lattice. The coupling among different parts of the total system is schematically shown in Fig.1. The whole set of equations are given as follows (with A being the complex amplitude of the field):

$$\dot{A} = \frac{i\omega_0 L_m}{2n^2 L}\beta\chi A - \kappa A \tag{1}$$

$$\dot{N} = \gamma_{\parallel}(N_0 - N) - \frac{1}{2}\beta G_N |A|^2 \tag{2}$$

$$\dot{T}_p = \gamma_{\parallel}\left[J_W(W_0 - W) - J_N(N_0 - N)\right] - \frac{1}{2}\beta G_{T_p}|A|^2 - \gamma_T(T_p - T_l) \tag{3}$$

$$\dot{T}_l = -\gamma_a(T_l - T_a) + \gamma_T(T_p - T_l) + \gamma_{nr}\frac{\hbar\omega_0}{c_q}N + \frac{S^2 R}{c_q V_t}j^2 \tag{4}$$

Plasma heating

Plasma heating in CW operation is studied by fixing the lattice temperature at 300 K and solving the set of nonlinear equations (1-3) self-consistently. We observe significant plasma heating effects including the dependence of the cw-carrier density and frequency shift on pumping. An example of the CW solutions is shown in Fig.2.

Gain nonlinearity

Gain nonlinearity (or gain compression) means a nonlinear dependence of the gain on the laser intensity in the semiconductor rate equations. This nonlinear gain is very important in reconciling the disagreement

between experiments on directly modulated lasers and the simple rate equation (without nonlinear gain) predictions. Here we show that plasma heating leads to a nonlinear gain: Starting from equations (1-3), we eliminate the plasma temperature adiabatically. This leads to an elevated plasma temperature relative to the lattice temperature. Formally we have:

$$\dot{T}_p = 0 \quad \longrightarrow \quad T_p = T_p(N, |A|^2) \tag{5}$$

Substitute this stationary plasma temperature in to equations (1) and (2) we have:

$$\chi(T_p, N) \longrightarrow \chi\left(T_p(N, |A|^2), N\right) = \bar{\chi}(N, |A|^2) \tag{6}$$

By solving the plasma temperature equation we show that the resulting nonlinear gain can be fitted by the following non-perturbative form

$$-Im\bar{\chi}(N, |A|^2) = \frac{a}{\left(1 + \frac{|A|^2}{I_s}\right)^b} = \frac{G_I}{\omega_0} \tag{7}$$

The fitting to (7) (diamonds) and the solution to (5) (solid line) for different heat transfer constants are shown in Fig.3

Thermal switch-off

In experiments one often observes a strong saturation or even switch-off of the laser output at quite moderate pumping strength. To understand this phenomenon theoretically, we solve numerically the whole set of equations (1-4). Examples from our CW-solutions are shown in Fig.4

Thershold bistability

Under appropriate conditions the threshold of VCSELs can become bistable as shown in Fig.5. This rather unexpected phenomenon results from the complicated interplay between lasing on the one hand and plasma and lattice heating on the other. The occurrence of this phenomenon depends on the ambient temperature and the rate of heat transfer to the device substrate. Currently we are collaborating with a group of experimentalists at University of New Mexico to compare quantitatively this predication with experiments.

Future directions

The research reported above needs to be extended in several directions and some related work still needs to be done. The following directions are of special interest:

- Inclusion of many-body interactions in our present formalism. This would be very important if a quantitative comparison with experiments is intended, because of the band gap renormalization due to these interactions. This research is currently being carried out in a collaboration with Stephan Koch of the University of Marburg in Germany.
- Investigations of the transverse structure in VCSELs, especially under the transverse heat conduction and carrier diffusion.
- Dynamics and patterns in coupled VCSEL-arrays using a parameterized coupled rate-equation approach.

- The influence of plasma and lattice heating on modulation bandwidth.
- A noise theory including thermal effects that could provide us with a correct linewidth enhancement factor.

References

[1] C.Z. Ning, R. Indik, and J.V. Moloney, "A self-consistent approach to thermal effects in vertical-cavity surface-emitting lasers", JOSAB, **12**, (10), 1993, (1995).

[2] C.Z. Ning and J.V. Moloney, "Plasma heating induced intensity-dependent gain in semiconductor lasers", Appl. Phys. Lett., **66**, 559(1995)

[3] C.Z. Ning and J.V. Moloney, "Thermal effects on threshold of vertical-cavity surface-emitting lasers: first and second order phase transitions", Opt. Lett., **20**, (10), 1151-1153, (1995).

[4] C.Z. Ning, R. Indik, J.V. Moloney, and S.W. Koch, "Effects of plasma and lattice heating in VCSELs", SPIE-Physics and simulation of optoelectronic devices III, 6-9 Feb, 1995, San Jose, SPIE-Proceedings 2399, Eds. W. Chow and M. Osinski,

Conferences:

SPIE-Physics and simulation of optoelectronic devices III, 6-9 Feb, 1995, San Jose.

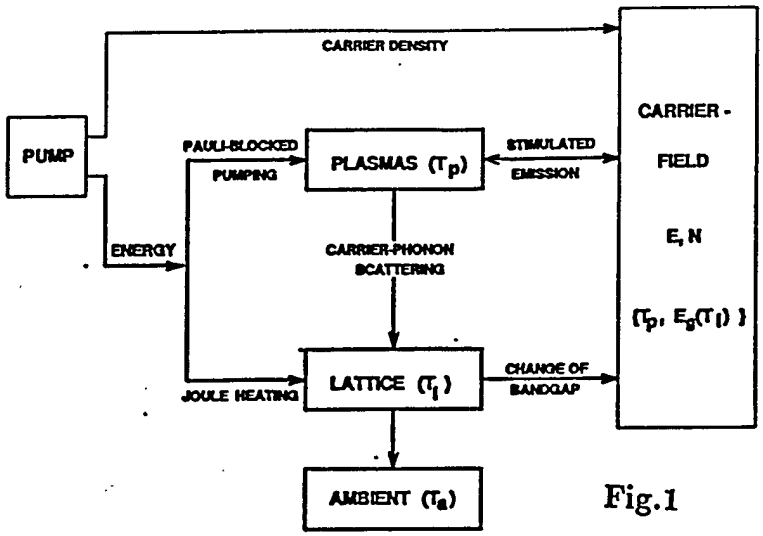

Fig.1

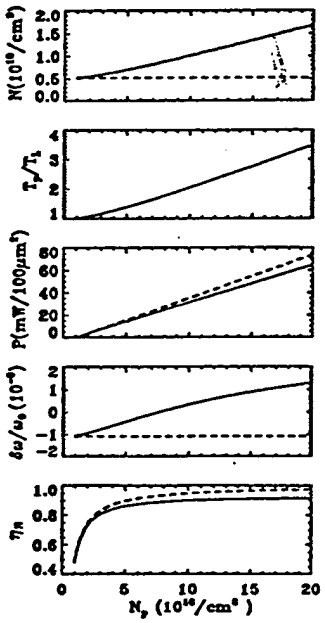

Fig.2

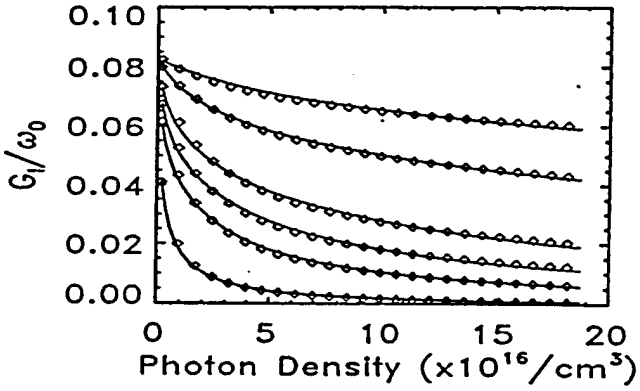

Fig.3

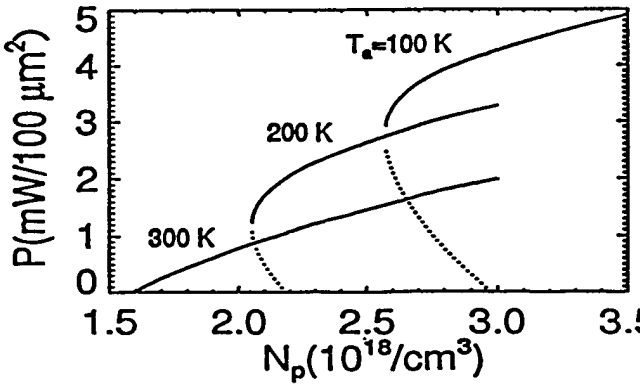

Fig.5

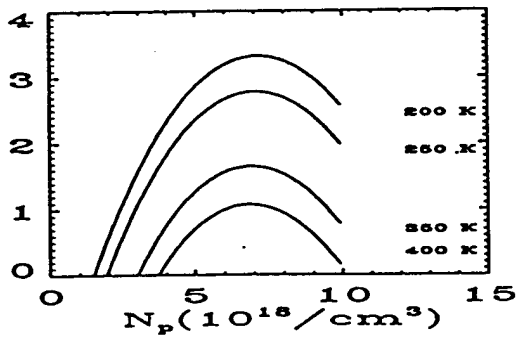

Fig.4

Polarization Patterns in Wide Aperture 3-level and Semiconductor Lasers

Polarization pattern forming instabilities in lasers

Q. Feng, M. San Miguel, J.V. Moloney and A.C. Newell

Transverse pattern formation in lasers has attracted much attention in recent years and a rich variety of pattern forming instabilities has been found. Most of studies have concentrated on systems in which the direction of the electric field in the laser cavity is fixed (by, e.g. Brewster windows). In this study we consider the case where the degree of freedom of the electric field polarization is unconstrained. We analyze the stability of solutions corresponding to transverse patterns: linearly polarized traveling waves and polarized standing waves. The interplay between the polarization and transverse effects leads to new instabilities whose natures are identified with amplitide equations. Here we report results for the positive detuning case (results for negative detuning have been reported elsewhere[1]).

The system we considered is a wide aperture, single longitudinal mode, ring cavity laser with transverse flat end reflectors. The basic equations are the vectorial Mawell-Bloch equationsgoverning space-time evolution of the slowly varying complex envelopes of the electric field in the laser cavity, $E_\pm = \frac{1}{\sqrt{2}}(E_x \pm iE_y)$, which are the left- and right-circularly polarized components. For positive detuning, lasing modes with finite transverse wavenumbers lose stability as the pump (r) is increased above threshold (r_c). From the vectorial Maxwell-Bloch equations we derived the amplitude equations which are valid near threshold:

$$\begin{aligned}
\tau(\partial_t + v_g\partial_x)z_1 &= \epsilon z_1 + \xi^2(1+ic_1)\partial_x^2 z_1 \\
&\quad - \left[\alpha|z_1|^2 + 2\alpha|z_2|^2 + \beta|z_3|^2 + \beta|z_4|^2\right] z_1 - \beta z_2 z_3^* z_4, \\
\tau(\partial_t - v_g\partial_x)z_2 &= \epsilon z_2 + \xi^2(1+ic_1)\partial_x^2 z_2 \\
&\quad - \left[\alpha|z_2|^2 + 2\alpha|z_1|^2 + \beta|z_3|^2 + \beta|z_4|^2\right] z_2 - \beta z_3 z_4^* z_1, \\
\tau(\partial_t - v_g\partial_x)z_3 &= \epsilon z_3 + \xi^2(1+ic_1)\partial_x^2 z_3 \\
&\quad - \left[\alpha|z_3|^2 + 2\alpha|z_4|^2 + \beta|z_1|^2 + \beta|z_2|^2\right] z_3 - \beta z_4 z_1^* z_2, \\
\tau(\partial_t + v_g\partial_x)z_4 &= \epsilon z_4 + \xi^2(1+ic_1)\partial_x^2 z_4 \\
&\quad - \left[\alpha|z_4|^2 + 2\alpha|z_3|^2 + \beta|z_1|^2 + \beta|z_2|^2\right] z_4 - \beta z_1 z_2^* z_3,
\end{aligned}$$

where z_1 (z_2, z_3 and z_4) is the amplitude of right- (right-, left- and left-) circularly polarized, traveling wave traveling in $+x$ ($-x$, $-x$ and $+x$) direction, respectively. The coefficients α and β are related to the material parameters: $\alpha = b^{-1}$, $\beta = (b^{-1} + c^{-1})/2$, where b is the decay rate of the population inversion between the atomic levels ($J = 1$, $J_z = \pm 1$) and ($J = 0$), c the decay rate of the coherence between the levels ($J = 1$, $J_z = \pm 1$) (they are measured in units of material polarization decay rate). Usually $c > b$ and we will restrict ourself to this case through this study.

The Amplitude equations admit linearly polarized traveling wave solutions,

$$(z_1, z_2, z_3, z_4) = (v, 0, 0, v)e^{i(Qx - \nu t)}.$$

A linear stability analysis determines the stability wavenumber $|Q|$ band (for given $\epsilon = r - r_c$). We found four types of instabilities, each of which sets in at wavenumber $|Q| > |Q_i|$, $i = 1, 2, 3, 4$, respectively, where

$$Q_1^2 = \frac{1}{3}\frac{\epsilon}{\xi^2},\quad Q_2^2 = \frac{c-b}{b+7c}\frac{\epsilon}{\xi^2},\quad Q_3^2 = \frac{1}{2}\frac{\epsilon}{\xi^2},\quad Q_4^2 = \frac{c-b}{4c}\frac{\epsilon}{\xi^2}.$$

The instability occuring at Q_1 is the well-known Eckhaus instability (the typical $\frac{1}{3}$-rule), which is caused here by the long-wavelength perturbation in the sum of the phases of z_1 and z_4, the right- and left-circularly

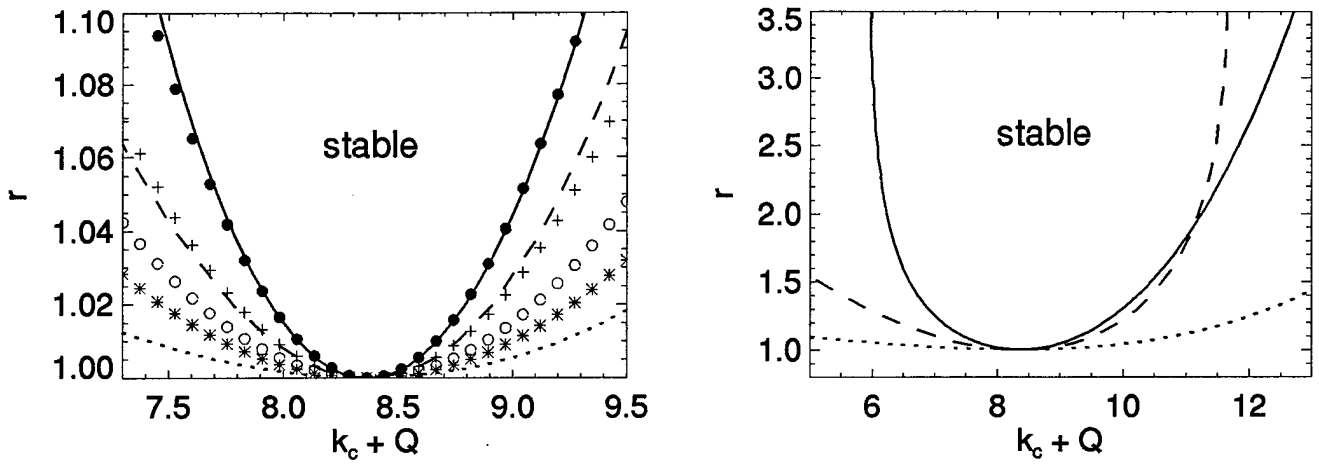

Figure 3: *Stability diagrams for positive detuning. The open circles, filled circles, crosses and asterisks correspond to Q_1, Q_2, Q_4 and Q_3, respectively (see text). The dotted line is the neutral curve. The solid and dashed lines are stability boundaries obtained from direct stability analysis based on the vectorial Maxwell-Bloch equations.*

polarized traveling waves (traveling in the same direction). The Q_2-instability is the one due to the long-wavelength perturbation in the phase difference of z_1 and z_4. The Q_3-instability is the amplitude instability due the interaction with a wave, with the same polarization, traveling in the opposite direction[2]. The Q_4-instability is another amplitude instability which is caused by an orthogonally polarized, oppositely traveling wave. Both Q_2 and Q_4 depend on relative magnitudes of the decay rates: $Q_2 \to 0^+$ and $Q_4 \to 0^+$ as $c \to b^+$. This means that the stable band disappears as $c \to b^+$. Near threshold the Q_1-instability limits the stability band, while far above threshold it is the amplitude instability originating from the Q_4-instability that limits the stability band (see Fig.1). The instabilities in the far above threshold region are obtained from the numerical stability analysis based on the vectorial Maxwell-Bloch equations.
The amplitude equations have another type of stable solutions, the polarized standing waves,

$$(z_1, z_2, z_3, z_4) = (ve^{i(Qx-\nu t)}, 0, ve^{i(-Qx-\nu t)}, 0),$$

which correspond to standing waves in both x and y components of the electric field. We have also studied the stability of these solutions and found four types of instabilities: two phase instabilities and two amplitude instabilities. Among the two phase instabilities, however, the Eckhaus $\frac{1}{3}$-rule-instability is now caused by the long-wavelength perturbation in the phase difference of z_1 and z_3, while the instability which sets in at Q_2 is caused by the long-wavelength perturbation in the sum of the phases. We have performed a series of numerical simulation on the vectorial Maxwell-Bloch equations with different transverse boundary conditions. The linearly polarized traveling waves tend to be destabilized, while the polarized standing waves may be more robust to survive under realistic boundaries.

References

[1] M. San Miguel, Q. Feng, J.V. Moloney, and A.C. Newell, in *Fluctuation Phenomena: Disorder and Nonlinearity*, edited by L. Vazquez (World Scientific, Singapore, 1995).

[2] Q. Feng, J.V. Moloney and A.C. Newell, Phys. Rev. Lett., **71**, 1705(1993).

Light polarization dynamics in surface emitting semiconductor lasers
M. San Miguel, Q. Feng and J.V. Moloney

The basic modeling of semiconductor laser dynamics is provided by rate equations and their generalization to include the dynamics of the phase of the electric field. The rate equations take for granted a fixed direction of polarization. Although they have been very useful both in basic and applied research in semiconductor laser devices, no such laser modeling seems to be available to describe the polarization of the electric field. On the other hand, a number of polarization-sensitive applications of semiconductor laser devices require detailed polarization control, and polarization coexistence between orthogonal modes (polarization partition) and polarization switching have been observed. The purpose of this work[1] is to introduce and analyze a basic model of semiconductor dynamics in which the key aspects of polarization dynamics of a semiconductor laser can be studied. The semiconductor engineering involving polarization control would benefit from a basic modeling of the key physical issues.

We introduce a four-level model which takes into account the spin sublevels of the conduction and valence band and therefore allows us to consider different polarizations of light associated with transitions between different spin sublevels (see the included figure for a schematic illustration). Generalized rate equations which include polarization degrees of freedom are obtained from the four-level model. Analysis of these equations privodes physical important insight into the nature of polarization instabilities in surface emitting semiconductor lasers. In particular, we show that the type dynamical response of the polarization degrees of freedom is linked to the relative time scale of spontaneous-emission and spin-relaxation processes.

The polarization dynamics is closely interrelated with transverse effects in lasers with large Fresnel number. In order to study general issues of the coupling of the polarization and the transverse degrees of freedom, we have included in our vectorial rate equations a general modeling of transverse effects for broad area lasers. Near threshold we derive an amplitude equation description which avoids the unphysical high-wavenumber instability resulted from the adiabatic elimination of the dipole polarization variables in the usually approach[2, 3]. We predict the existence of stable transverse spatially homogeneous intensity outputs, corresponding to off-axis emissions, with arbitrary direction of linear polarization in the transverse plane. The stability of the off-axis emission solutions to long-wavelength perturbations is investigated and, in addition to the Eckhaus instability associated with a global phase, we predict a new type of polarization instability associated with a relative phase of the complex field vector. We also explore the role of laser cavity anisotropies and their interplay with transverse effects. Linear phase anisotropies associated with birefrigence stabilize two prefered orthogonal directions for off-axis linearly polarized light. An important conclusion is that transverse effects discriminate between these two prefered directions so that, for given sign of the anisotropy, they extend the range of stability of the x-polarized emission while the stability range of the y-polarized solution shrinks.

References

[1] M. San Miguel, Q. Feng and J.V. Moloney, Phys. Rev. A., **52**, 1728, (1995).

[2] P. Ru, J.V. Moloney and R. Indik, Phys. Rev. A, **50**, 831(1994).

[3] P.K. Jakobsen, J.V. Moloney, A.C. Newell and R. Indik, Phys. Rev. A, **45**, 8129(1992).

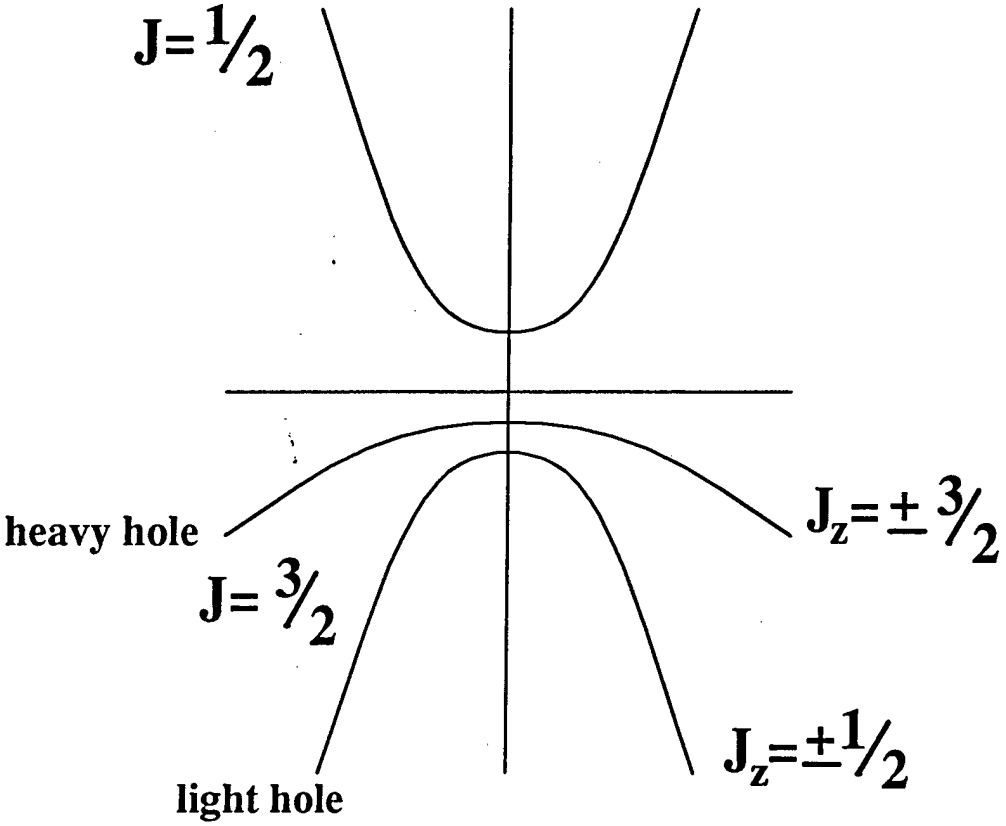
J= 1/2
heavy hole
J= 3/2
light hole
Jz= ± 3/2
Jz= ± 1/2

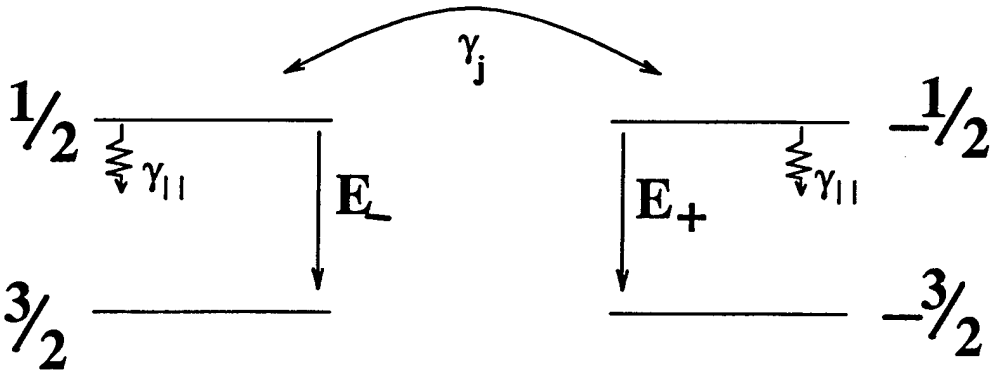
γj
1/2
γ||
E_
3/2
E+
γ||
_1/2
_3/2

1D-3D Vector Maxwell Solvers

R.G. Flesch and J.V. Moloney

We have developed a suite of modular one, two and three-dimensional vector Maxwell solvers to be used in the study of the propagation of ultrashort (< 100 fs) pulses in a variety of nonlinear materials. These codes serve two purposes:
(1) To solve problems where a vector Maxwell description is essential.
(2) To validate envelope theories (and their corrections) is regimes where the envelope assumption becomes suspect.
The former category includes ultrashort intense pulses propagating through structures with wavelength and sub-wavelength dimensional inhomogeneities. Examples are: periodic linear/nonlinear index gratings, Quantum-Well stacks, quantum wires, semiconductor micro-cavities, linear/nonlinear surfaces and the vicinity of the critical focus of a collapsing beam. In 1D many of the simulations can be carried out in real time on our new Power Challenge L machine. This offers the opportunity to develop a CAD-like interactive computing and graphical visualization environment which will significantly enhance our efficiency in modeling a wide variety of nonlinear optical structures.
Maxwell's equations have the following form:

$$\frac{\partial B}{\partial t} = -\nabla \times E \qquad \frac{\partial D}{\partial t} = \frac{1}{\mu_0}\nabla \times B \tag{1}$$

The equations for D, E and B are closed by adding the constitutive relation

$$D = \epsilon_0 \varepsilon_\infty E + P_L + P_{NL} \tag{2}$$

which allows for both a linear and nonlinear polarizations which we may write in general as

$$P_L = \mathcal{O}_L(D, E) \tag{3}$$
$$P_{NL} = \mathcal{O}_{NL}(D, E)\,. \tag{4}$$

The complete solution of the coupled system consists of the following three steps:

1. Given values for E and B, obtain updates for B and D. The Maxwell equations are solved by the FT-TD method.
2. Using the values from step 1, calculate the linear and nonlinear polarizations.
3. Obtain a new value for E from the constitutive relationship given D, P_L and P_{NL} from steps 1 and 2.

To date we have used a linear Lorentz medium for the linear polarization vector and a mixed Kerr and Raman response for the nonlinear polarizations. To verify and debug the code we have investigated the following situations:

- Reflection of a pulse from a layered set of dielectrics.
- Soliton formation for very short (< 100 fs FWHM) pulses.
- Propagation of "superluminal" pulses.
- Precursor phenomena.
- Carrier wave shocks.

- Paraxial corrections to the linear focusing (in vacuum) of a very narrow (two wavelengths FWHM) Gaussian pulse.
- Nonlinear self focusing of a Gaussian pulse.

The shocking of the carrier wave is of particular interest and to our knowledge has not yet been addressed in the literature. Carrier shocking, as depicted in Fig 1, is due to the nonlinear dependence of the wave velocity on the amplitude. Using a simple analysis for a medium without dispersion one can predict a shock time for the carrier which is independent of the pulse width for pulses which contain at least two wavelengths. Assuming a Kerr nonlinearity $P_{NL} = \chi^{(3)}(E \cdot E)E$ the estimated time to breaking of the carrier wave is given by

$$T_B = \frac{2}{3}\frac{T_{opt}}{\chi^{(3)}E_0^2}\frac{(1+4.5\chi^{(3)}E_0^2)^{3/2}}{\sqrt{(1+3\chi^{(3)}E_0^2)(1+6\chi^{(3)}E_0^2)}}\,. \tag{5}$$

In Fig. 2 we present results of the numerically-determined breaking times which agree rather well with the results in Eq. 5. Included in this figure is the curve (dots) of envelope breaking times for an optical pulse of 300 fs duration.

To model a more realistic situation we add a small amount of dispersion. This introduces a mismatch between the phase and group velocities of both the fundamental and harmonic freqencies which in most cases prevents carrier wave shock formation. As a pulse enters the nonlinear medium we see the carrier steepen, followed by the harmonic components separating according to their phase velocities. The presence of dispersion and hence nonzero GVD allows for envelope shock formation which has also been observed.

Carrier shock formation is of fundamental importance in the study of the critical collapse of a Gaussian packet in three spatial dimensions because the high field amplitudes which occur during the collapse can give rise to carrier shock. The dynamics is extremely rich due to the complex interplay of the carrier shocks, envelope shocks and self-focusing. For a full 3D simulation of the coupled system we require several Gigabytes of memory and the equivalent of hours of Cray CPU time. The large memory requirements are due to fact that the carrier frequency (and possibly third harmonics) of the pulse must be well enough resolved to avoid numerical dispersion from overwhelming any actual dispersion in the problem. The code has been implemented and optimized for the Vicksburg C90 and the AHPCRC CM5. We anticipate developing a PVM version which will run on the Mauii SP2

As an example of our three-dimensional results, we present preliminary results of the linear and nonlinear focusing of a Gaussian beam in a medium *without* dispersion. In the linear focusing case we see in Fig. 3 that in addition to the original x polarization (a), a longitudinal (b) and additional transverse component (c) develop as the pulse approaches the linear focal point. The transverse structure of each of these polarizations is shown in Fig. 4. These polarizations represent corrections to the paraxial approximation in which only the initial transverse polarization is of order one. To study critical collapse we wish to concentrate on the nonlinear effects and hence we choose a beam which is much wider thus initially avoid strong paraxial corrections. As the pulse propagates further the width becomes too narrow and our transverse resolution is too small. As in the one dimensional dispersionless case we also observe carrier shock here. Although the addition of some dispersion prevents the carrier shock from forming and allows us to follow the focusing further, we have not yet been able to observe the inhibition of self-focusing due to the GVD.

References

[1] R.G. Flesch, A. Pushkarev, J.V. Moloney, " Carrier Wave Shocking of Femtosecond Optical Pulses", Phys. Rev. Let., **76**, (14), 2488, (1995).

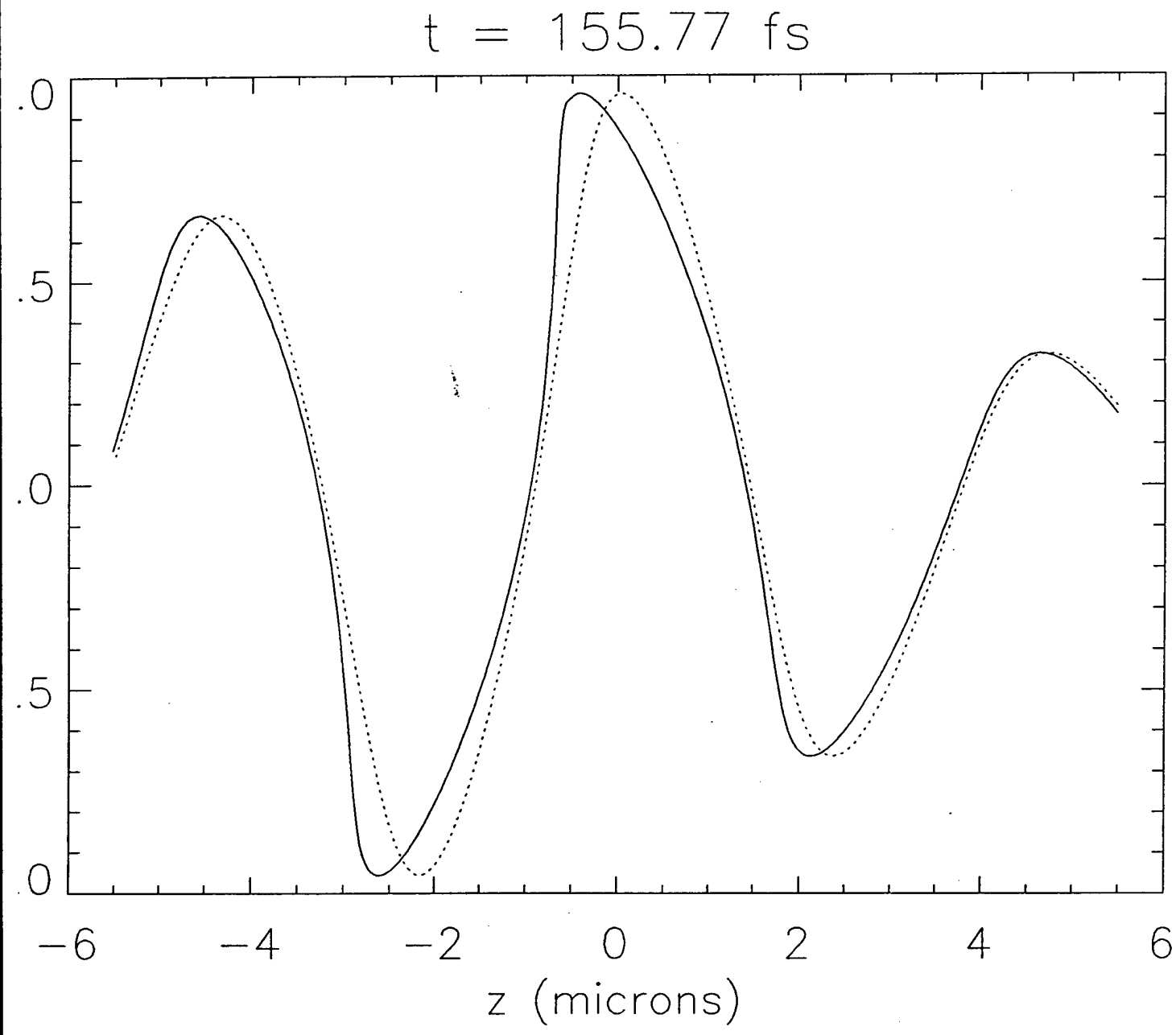

Figure 1.

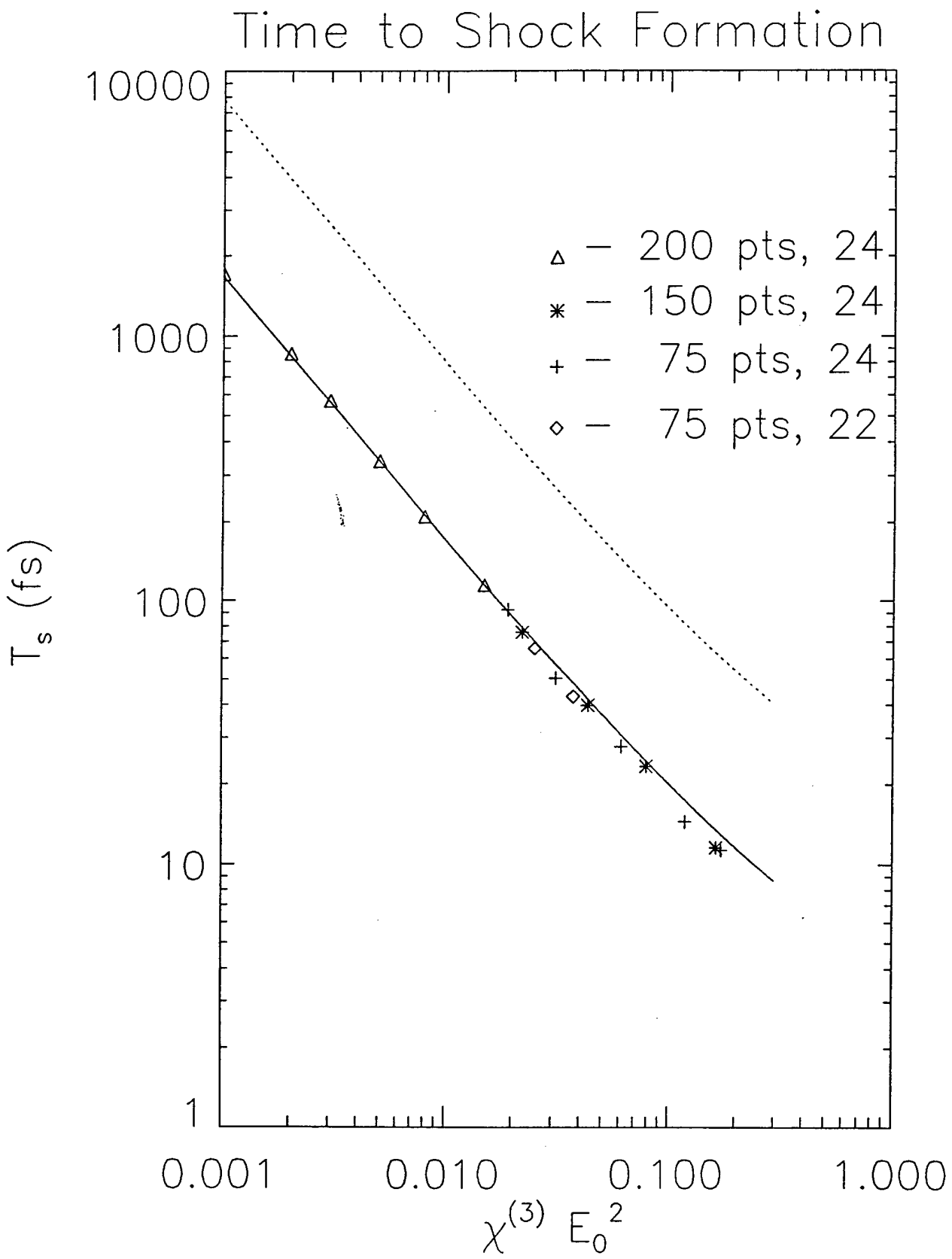
Time to Shock Formation
10000
1000
100
10
1
T_s (fs)
0.001
0.010
0.100
1.000
$\chi^{(3)} E_0^2$
Δ — 200 pts, 24
✳ — 150 pts, 24
+ — 75 pts, 24
◇ — 75 pts, 22

Figure 2.

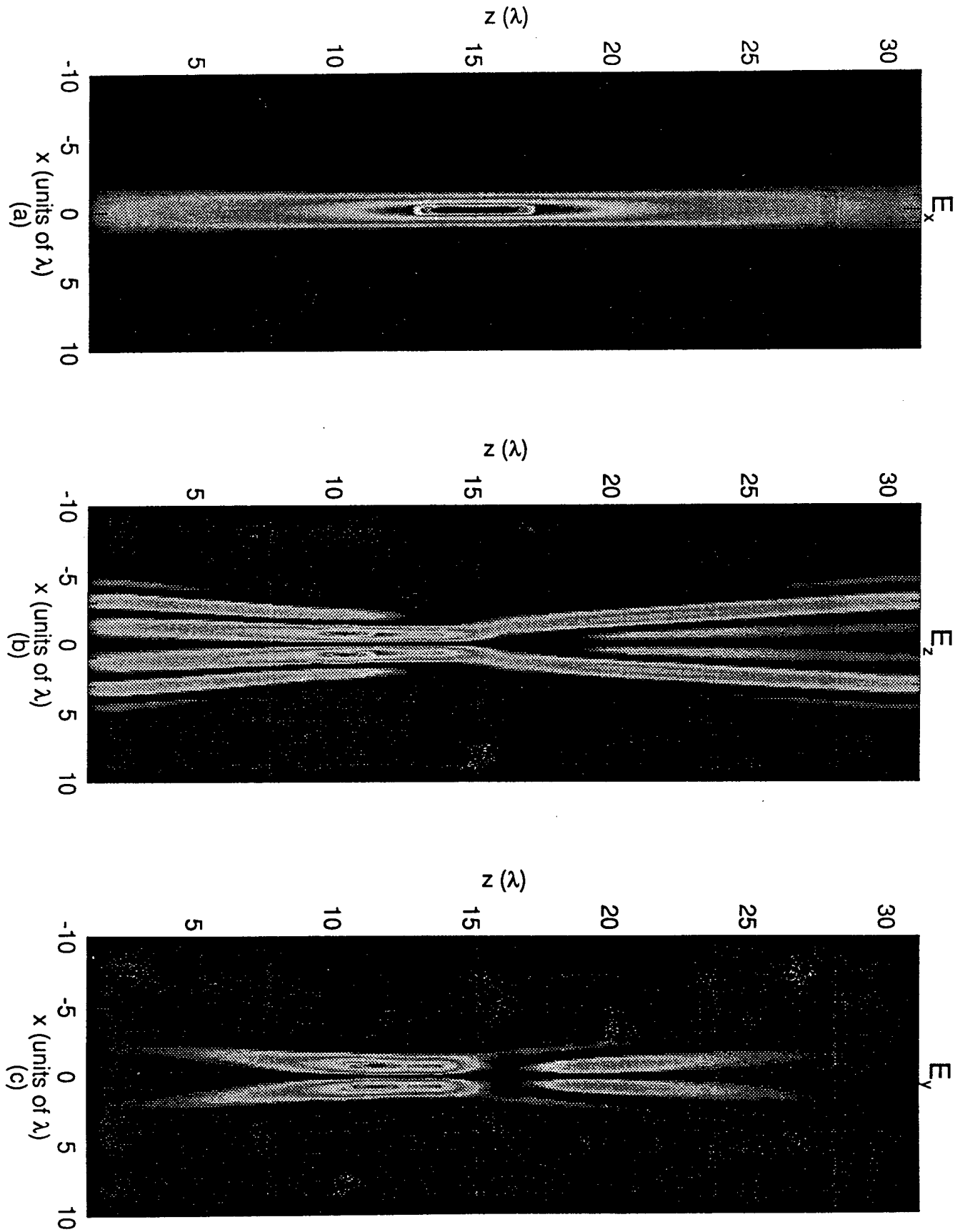

Figure 3.

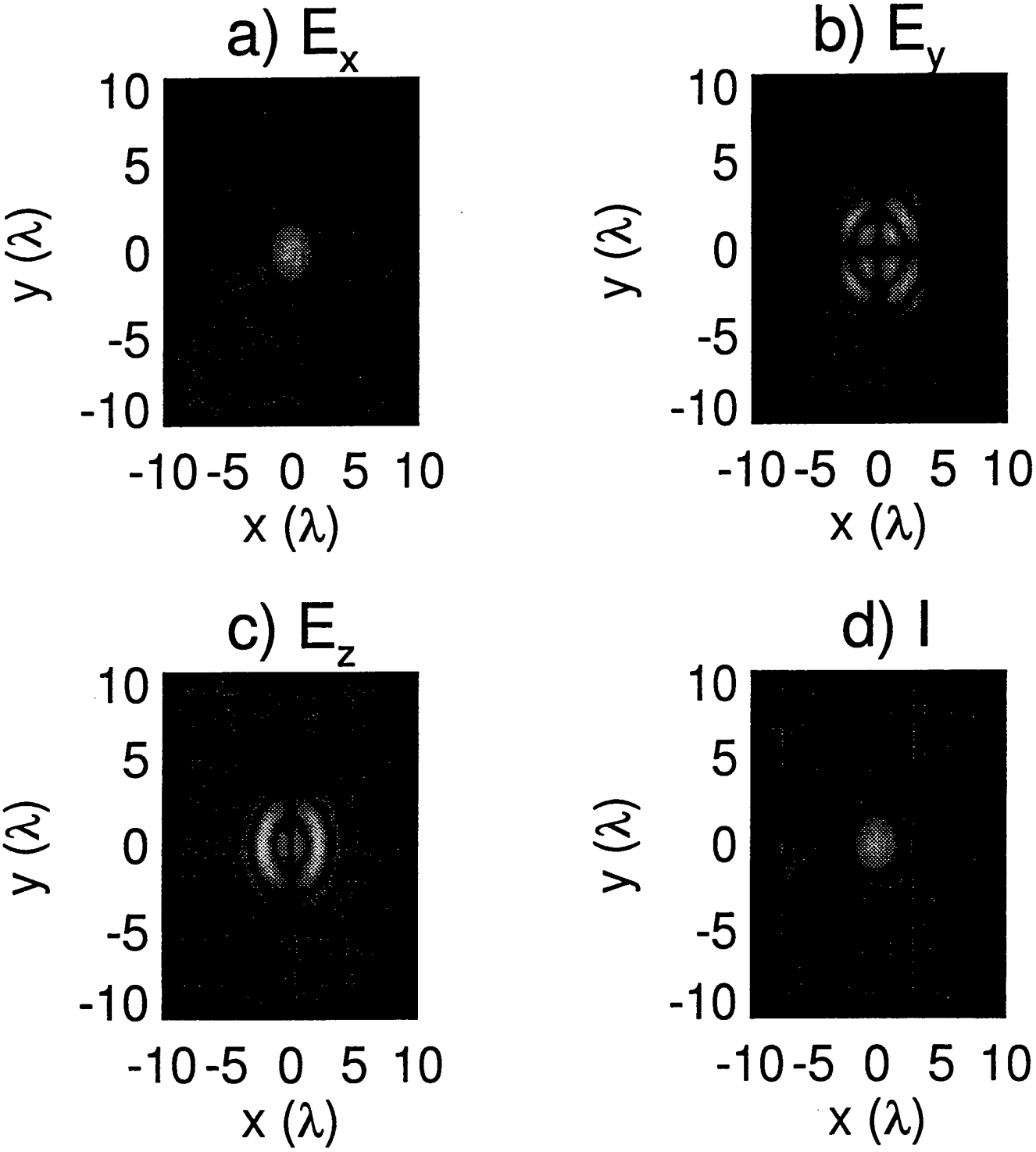

Figure 4.

Dynamic Nonlinear Optical Skin Effect

W. Forysiak, E.M. Wright and J. V. Moloney

The propagation of an intense optical field incident from air on a saturable absorber can give rise to a self-reflected wave, if the absorption is sufficiently large. The reflected wave arises at a wavelength-scale, spatial transition between the saturated and unsaturated regions of the absorber, akin to the skin effect at a linear boundary, and is self-reflected in the sense that the transition region is induced by the incident field itself.

The FD-TD method discretises the differential form of Maxwell's equations directly and allows one to determine the evolution of an optical field in a nonlinear medium, subject to the given constitutive relations between the electric field and polarisation, and without recourse to the SVEA. We examine pulse shaping in the near-field, close to the absorber boundary, and predict a new nonlinear focusing effect, which we attribute to the formation of a transient, focusing mirror in the absorber. As the incident pulse impinges on and strongly saturates the absorber, it excites a moving reflection front [1] which is shaped according to the transverse profile of the incident pulse. If the incident pulse transverse profile is bell-shaped, so too is the resulting mirror, and the reflected pulse is focused according to the waist and intensity of the incident pulse. In addition to being re-shaped, the reflected pulse is spectrally broadened and red-shifted due to the Doppler effect at the moving mirror [1].

We consider the time-dependent propagation of a 2-D transverse electric (TE) polarised pulse, in which the electric field is polarized along the y-axis and also assumed uniform along that axis, $E(r,t) = yE_y(x,z,t)$. Then the Maxwell's equations for the electric and magnetic field quantities, E_y, B_x and B_z, are,

$$\frac{\partial B_x}{\partial t} = \frac{\partial E_y}{\partial z}, \qquad \frac{\partial B_z}{\partial t} = \frac{\partial E_y}{\partial x}, \qquad \frac{\partial D_x}{\partial t} = \frac{1}{\mu_0}\left(\frac{\partial B_x}{\partial z} - \frac{\partial B_z}{\partial x}\right), \tag{1}$$

where the z-axis is the propagation direction, and the x-axis is the transverse direction. The nonlinear optical response of the saturable absorber is included using a two-level model via the constitutive relation, $D_y = \epsilon_0 E_y + P_y$, where the macroscopic polarisation, $P_y = Np(\rho_{21} + c.c.)$, is determined by the Bloch equations,

$$\frac{\partial \rho_{21}}{\partial t} + (\gamma_2 + i\omega_{21})\rho_{21} = i\frac{pE_y}{\hbar}n, \qquad \frac{\partial n}{\partial t} + \gamma_1(n-1) = 2i\frac{pE_y}{\hbar}(\rho_{21} - \rho_{21}^*). \tag{2}$$

Here, N is the density, ρ_{21} is the off-diagonal density matrix element, $n = (\rho_{11} - \rho_{22})$ is the population difference, ω_{21} is the transition frequency, p is the dipole moment, and $\gamma_1 = 1/t_1$ and $\gamma_2 = 1/t_2$ are the population and polarization damping constants.

The conditions for self-reflection of a continuous plane-wave incident field require that the normalised parameters, $\psi = \frac{p^2 N}{\epsilon_0 \hbar \gamma_2}$, and, $F = \frac{pE_0}{\hbar(\gamma_1\gamma_2)^{1/2}}$, are greater than unity, with E_0 the peak input field. Physically, this requires the linear absorption to be large on a wavelength scale, and the incident field to be strong enough to saturate the absorption. In the case of ultrashort pulses, we also require that the incident pulse duration t_p is greater than the polarization decay time but less than the population decay time, $t_1 > t_p > t_2$ [1]. To meet these conditions for the sub-100 fs pulses to which we were restricted by computational resources, we adopted the following medium parameters for illustrative purposes: $t_1 = 0.5$ ns, $t_2 = 10$ fs, $\omega = \omega_{21} = 2 \times 10^{15}$ rads^{-1} ($\lambda = 942$nm), $p = 4 \times 10^{-29}$ Cm and $N_0 = 2 \times 10^{20}$ cm^{-3}. For these values a normalised field strength of $F = 1$ corresponds to an electric field strength of $E_0 = 1.15 \times 10^6$ V/m. The linear complex refractive index of the absorbing medium is given by, $n_L^2 = 1 + \psi\frac{\delta+i}{1+\delta^2}$, where $\delta = (\omega_{21} - \omega)/\gamma_2$ is the normalised detuning. For the assumed parameter values $\psi = 3.8$, and n_L has a substantial imaginary contribution so that the linear skin effect is to be expected at the absorber boundary. The nonlinear Maxwell's equations were numerically integrated using Yee's second-order FD-TD scheme for the field updates and a fourth-order Runge-Kutta method for the medium updates. On the driving face ($z = 0$) of the computational domain, the incident pulse was defined to be Gaussian-shaped in space

and time. Periodic boundary conditions were imposed at the transverse boundaries ($x = \pm L_x/2$) which were placed far enough away for the optical intensity to be reduced by more than 50dB compared with pulse center. The medium was initialised uniformly with $\rho_{21} = 0$ and $n = 1$ for $z > z_a$.

Figures 1 and 2 show results from a pair of sample calculations for incident pulses with peak fields of (a) $E_0 = 7 \times 10^6$ V/m, and (b) $E_0 = 7 \times 10^8$ V/m. The computational domain was 132×113 μm ($L_z \times L_x$), discretised onto a 3000×250 numerical grid, with the saturable absorber interface situated at $z_a = 125$ μm. The incident pulse was 80fs long (FWHM of the electric field), with a beam waist of $w_0 = 20$ μm ($1/e$ half-width of the field), and was initialised such that its peak entered the computational domain at $z = 0$ when $t = 120fs$. The temporal snapshots are taken after reflection from the interface (at $t = 770$ ps) when the pulses are travelling back towards $z = 0$. In Fig. 1 only the extracted field envelopes are shown, since the carrier is not easily discernible. The corresponding spectra in Fig. 2 were obtained from the full electric field data.

Figures 1(a) and 2(a) show that for low incident pulse intensities the self-reflected pulse, though diminished in amplitude, is unchanged spatially or spectrally. The pulse energy is reduced during the absorptive reflection, and the calculated reflectivity of 24% compares favourably with the predicted steady-state linear value of 22% from Fresnel's law and the expression for the complex refractive index above. The pulse waist remains unchanged, evolving almost imperceptibly on the time scale of the computation, because of its long diffraction length ($L_D = \pi w_0^2/\lambda_0 > 1000$ μm). In this case, therefore, since the pulse is too weak to significantly saturate the absorber, the physical properties of the interface remain unmodified and the pulse is partially reflected, according to the linear skin effect, as if from a flat mirror.

In contrast, Figs. 1(b) and 2(b) show that the high intensity pulse undergoes significant nonlinear spatial and spectral reshaping at the interface. Figure 1(b) shows the pulse profile after it has propagated away from the interface, close to its focal point, where the pulse waist (at maximum E_y) is reduced to 2.2 μm, a considerable reduction in spot size in comparison to the linear case in Fig. 1(a). At this point, the peak electric field is actually fractionally greater than the peak incident field, despite the decreased reflectivity of 18%. The reflectivity is reduced compared to the linear case because the high power pulse reduces the medium absorption and as a result the pulse penetrates further into the interface.

The spectral broadening that results from the nonlinear saturation of the absorber is clearly evident in Fig. 2(b) in comparison to Fig. 2(a). The longitudinal spectral broadening (in K_z) and red-shifting of the reflected field are due to the self-reflection of the incident pulse from an absorption front which initially accelarates and then deccelarates into the saturable medium, which in turn causes the reflected light to be red-shifted and chirped.

The formation of a curved focusing reflection front is shown in Fig. 3, where the spatial distribution of the population difference, n, is plotted after its creation by the leading edge of the pulse. Once this curved mirror is formed, the rest of the pulse is reflected towards the $x = 0$ axis, leading to the tight focus seen in Fig. 1(a). The spectral width of the broadest feature in Fig. 2(b) accurately reflects the inverse incident pulsewidth. Furthermore, we note the signature of the ordinary (unfocused) plane-wave reflection at the leading edge of the pulse in Fig. 1(a), on a timescale of approximately t_2, during which the mirror formation takes place.

References

[1] W. Forysiak, R.G. Flesch, J.V. Moloney, and E.M. Wright, "Doppler shift of self-reflected optical pulses at an interface: the nonlinear optical skin effect", Phys. Rev. Lett., **76**, 3695–3698, (1996).

[2] W. Forysiak, J.V. Moloney, and E.M. Wright, "Nonlinear Focusing of Femtosecond Pulses Due to Self-Reflection from a Saturable Absorber", Optic Letters, **22**, (4), 239-241, (1997).

[3] A. Schulzgen, S. Hughes, J.V. Moloney, and N. Peyghambarian, "Observation of Self-Reflection Due to Dynamic Nonlinear Skin Effect in a Semiconductor", submitted to Phys. Rev. Letts., 1997.

Figure Captions

Fig. 1 Surface plots of the calculated field envelope profiles at t=770fs for peak input fields of (a) $E_0 = 7 \times 10^6$ V/m and (b) $E_0 = 7 \times 10^8$ V/m, after reflection from the interface.

Fig. 2 Contour plots of the spatial Fourier transforms of the field distributions in Fig. 1.

Fig. 3 The population difference of the saturable absorber following self-reflection of the $E_0 = 7 \times 10^8$ V/m (high power) pulse in Fig. 1(b) at t = 770 fs. The contour at $n = 0.5$ is superimposed.

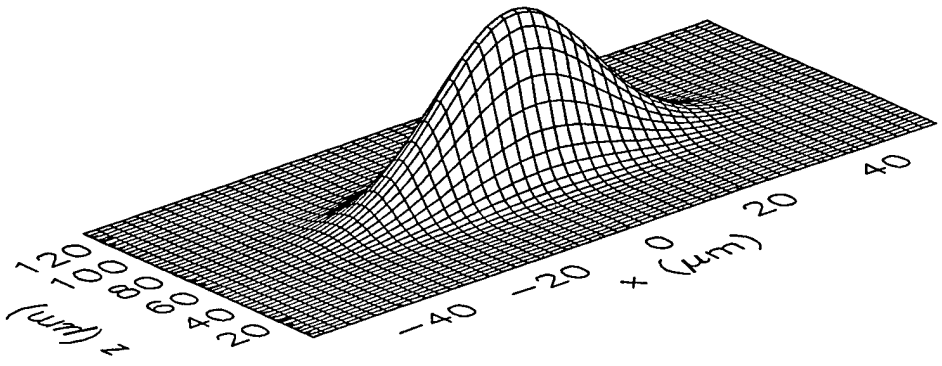
120
100
80
60
40
20
z (μm)
−40
−20
0
20
40
x (μm)

(a)

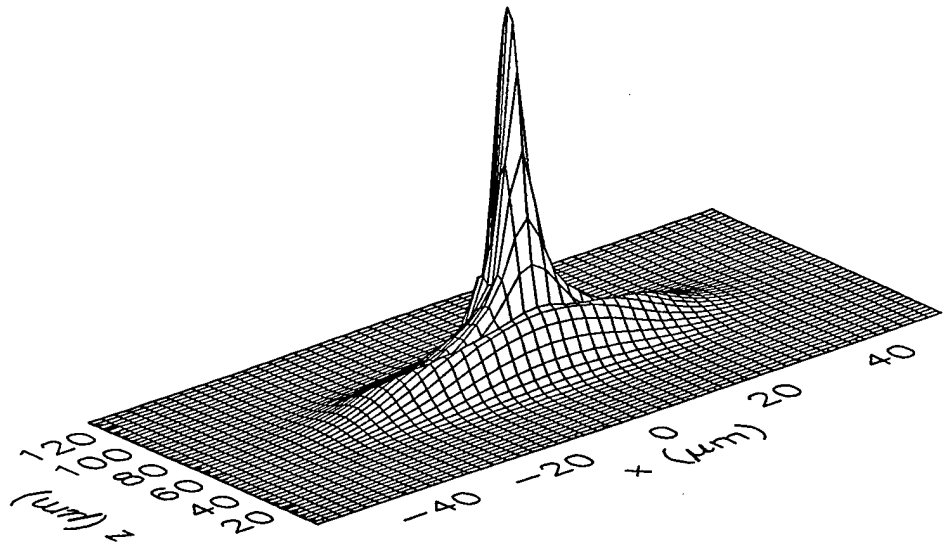
120
100
80
60
40
20
z (μm)
−40
−20
0
20
40
x (μm)

(b)

Figure 1.

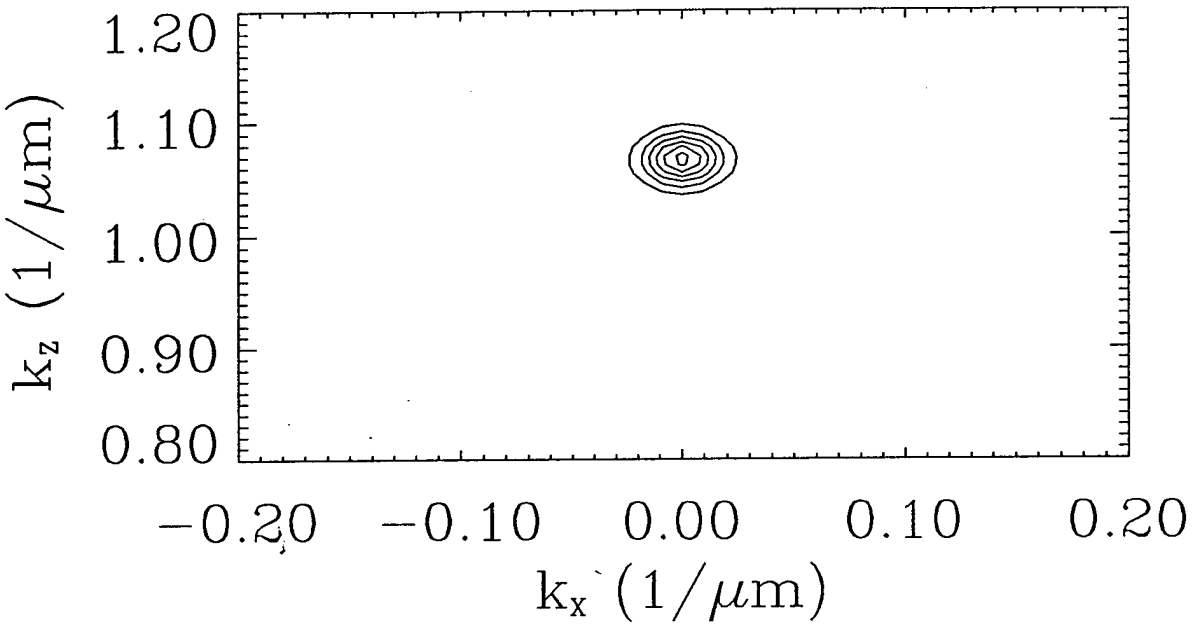
1.20
1.10
1.00
0.90
0.80
k_z $(1/\mu m)$
−0.20
−0.10
0.00
0.10
0.20
k_x $(1/\mu m)$

(a)

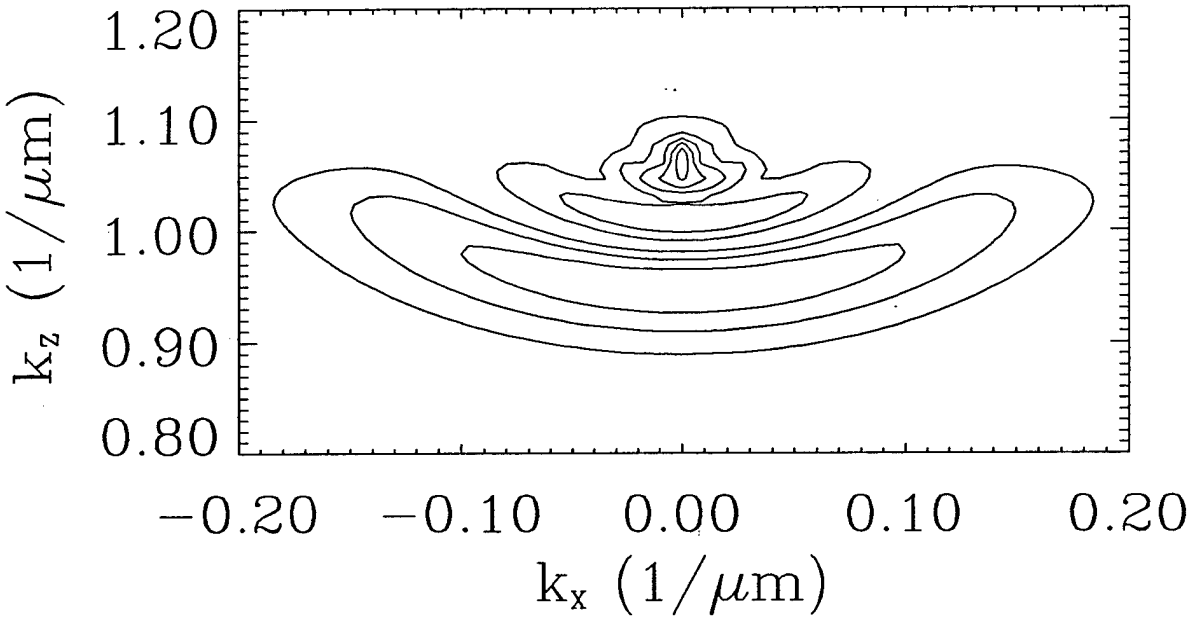
1.20
1.10
1.00
0.90
0.80
k_z $(1/\mu m)$
−0.20
−0.10
0.00
0.10
0.20
k_x $(1/\mu m)$

(b)

Figure 2.

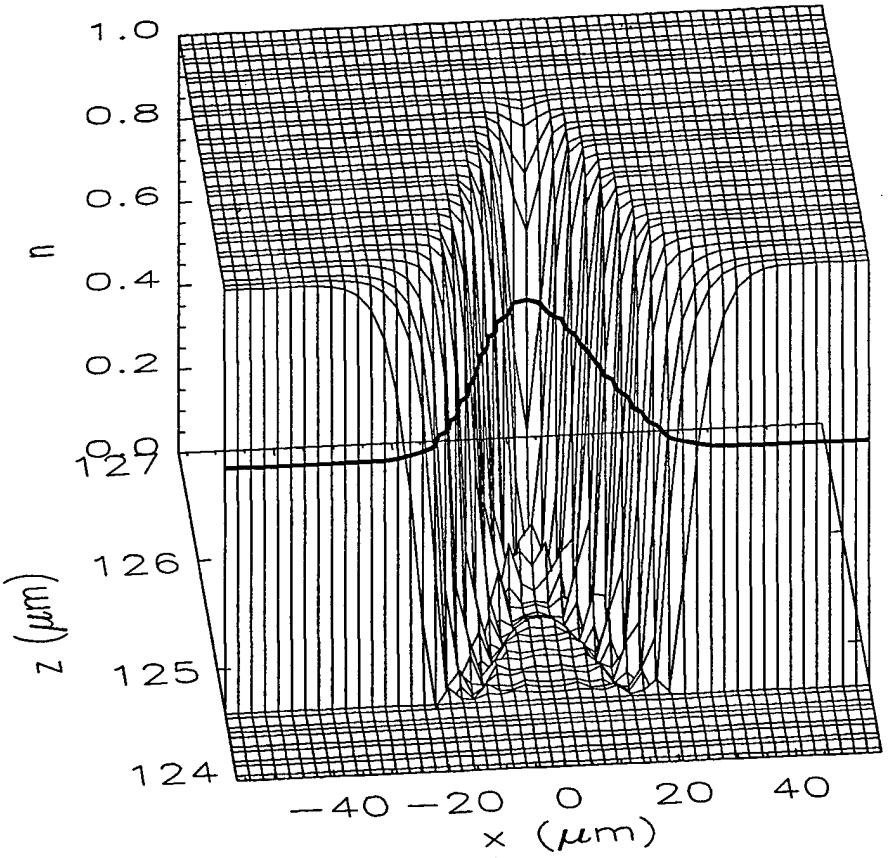

Figure 3.

1D and 2D Femtosecond Light Bullets and Bubbles

S. Glasgow, J. Xin, N. Ercolani and J.V. Moloney

The existence of localized (non-collapsing) femtosecond duration optical pulses with very high local intensities but very low energies, presents a fascinating opportunity to revisit the optical breakdown problem which has plagued high power laser design for decades. In many instances, the envelope approximations to the vector Maxwell equation predict collapse to a singularity in finite time. An open issue is whether higher-order corrections to envelope approximations can introduce regularization of blow-up or whether one has to resort to a full-fledged Maxwell description. We have been studying these phenomena in 1D and 2D with the view to establishing a connection between these distinct levels of treatment. In 1D we have explored localization with an instantaneous cubic nonlinear term and the analog of critical collapse with an instantaneous quintic nonlinear term.

Maxwell's equations have the following form:

$$\epsilon_\infty \mathcal{E}_{tt} + c^2 \nabla \times \nabla \times \mathcal{E} = -\mathcal{P}_{tt} \tag{1}$$

$$\mathcal{P}_{tt} + \omega_0^2 \mathcal{P} = (\epsilon_s - \epsilon_\infty)\frac{N}{N_0}\mathcal{E} \tag{2}$$

$$N_t = -4\mathcal{E} \cdot \mathcal{P}_t. \tag{3}$$

which allows for both a linear and nonlinear polarizations within a simple quantum oscillator model. This model was initially used to revisit many well-established nonlinear optical interactions but now occurring on femtosecond timescales. The validity of traditional envelope approximations becomes an issue as the pulse gets progressively shorter. Moreover, as the pulse shortens, its energy decreases and mucher higher peak intensities can be achieved before material breakdown becomes an issue. The need for a full reappraisal of light-material coupling on such ultra-short timescales becomes essential.

Our recent work showed that the assumption of an instantaneous nonlinear optical response would lead to shocking of femtosecond pulses. We have now adopted the more realistic quantum oscillator model above, which includes linear and nonlinear dispersion, and from which all of the known classical envelope descriptions can be obtained via singular perturbation expansions. We have confirmed the existence of a 2D TE light bullet and have evidence to show that a recently re-discovered 1D unipolar (half-cycle) light bubble is unstable in higher space dimensions. The 1D version of this latter object has been shown to be integrable by us. Figure 1 shows numerically computed 2D TE light bullet (a) and bubble (b). The latter is decaying slowly.

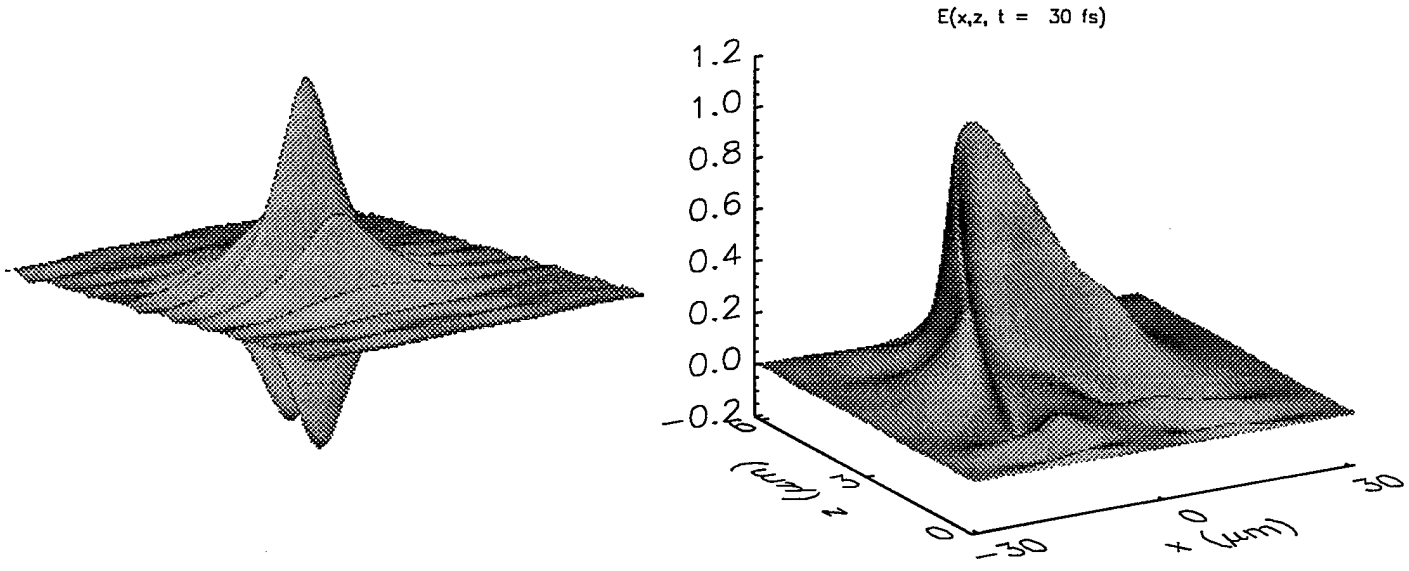

Large Scale Computational Nonlinear Optics

Maxwell semiconductor Bloch equations

R. Indik and J.V. Moloney

To model the behavior of ultrashort pulses in semiconductor media, we use the Maxwell-Semiconductor Bloch equations. As mentioned earlier in this report, these equations describe how the electric field E evolves in the traveling frame of reference $\xi = z - tc/n$. In practice, we assume isotropy in q, and motivated by device geometries assume strong guiding in one of the transverse spatial dimentions. This reduces the problem to calculation of the dynamics of integro-differential equation in 3 dimensions.

$$\frac{\partial E}{\partial \xi} - \frac{1}{2ik_0}\frac{\partial^2 E}{\partial x^2} = \frac{i\mu_0\omega_0^2}{k_0 V}\int_q P_q\, q^2 dq\ . \tag{1}$$

This evolution is given in terms of the momentum resolved polarization P_q. The evolution of this polarization and the electron/hole distribution functions $n_q^{e/h}$ in time t is given by

$$\begin{aligned}
\frac{\partial P_q}{\partial t} &= -i\left(\Delta_q - \omega_0\right)P_q - i\Omega_q(n_q^e + n_q^h - 1) + \left.\frac{\partial P_q}{\partial t}\right|_{\text{coll}} \\
\frac{\partial n_q^{e/h}}{\partial t} &= iP_q^\star\Omega_q - iP_q\Omega_q^\star + + \left.\frac{\partial n_q^{e/h}}{\partial t}\right|_{\text{coll}}\ ,
\end{aligned}$$

with the renormalized Rabi frequency

$$\Omega_q = \frac{d_{cv}E}{2\hbar} + \frac{1}{\hbar V}\int q' V_{q,q'} P_{q'}\, q^2 dq$$

and renormalized energy dispersion

$$\Delta_q = \varepsilon_q - \frac{1}{\hbar V}\int_{q'} V_{q,q'}(n_{q'}^e + n_{q'}^h\, q^2 dq).$$

$V_{q,q'}$ is the angle averaged coulumb interaction. The details of the collision terms are described in an earlier section of this report. They have little impact on the methodology of the numerical implementation.
These are differential equations in t, ξ and x, and integral in q, the magnitude of the momentum. The integrals in this calculation lead to a tight coupling of the equation across the momentum variable q. This is precisely as a result of the inclusion of the Coulumb interaction, which enters in these equations through the band-gap renormalization Δ_q and the generalized Rabi frequency $Omega_q$.
Numerical integration of the Maxwell-Semiconductor-Bloch (MSB) equations quickly becomes a large problem. Even in the plane-wave case, where a strong transverse guiding assumption in x reduces the system from dynamics in three dimensions to two dimensions, the parabolic band structure leads to the necessity of integrating the behavior of tightly coupled oscillators whose frequencies vary over a large fraction of the underlying optical frequency, each of which has a decay rate of the order of 50 fs. In practice, this forces explicit step sizes to be of order 0.5 fs. If we are primarily interested in the behavior of very thin slabs of semiconductor, the computations are not too onerous. However propagation through thick samples is another matter, and when the transverse guiding assumption is relaxed, and the 3 dimensional problem with propagation is considered, the calculation becomes quite challenging.
We have implemented a code that can follow the three dimensional dynamics of a pulse in a slab amplifier without transverse confinement. This code has been developed using PVM and run on the IBM SP2 at the Mauii High Performance Computing Center (MHPCC), on the Thinking Machines CM5 at the Army High Performance Computing Center at the Minnesota Supercomputing Center, as well as on a network of Sun

Sparc-stations, Silicon Graphics Indy work stations and a four processor Silicon Graphics Power Challenge at the University of Arizona. The code takes advantage of the natural parallelism of the problem in the transverse dimension to achieve very efficient parallel execution. The same code has been used to make exploration in parameter space for the plane wave problem. The problem is discretized in momentum, time and space, and is solved using the method of lines. The time equations are integrated using fourth order Runge-Kutta, while the spatial propagation is done using second order central differences and second order Runge-Kutta. A typical long propagation computation including transverse structure uses 2.5-5 cpu hours on 64 nodes of the IBM SP2 at MHPCC.

The structure of the code is illustrated in figure 1. We use a domain decomposition, to parcel the work of calculation over many processors. Each processor is responsible for calculating the propagation of the $E(x,t,\xi)$ at a point $x = x_i$. The only place in the calculation which requires that processors exchange information (other than the initialization and for output) is in the calculation of the diffraction term $\partial^2 E/\partial x^2$. Since we are using second order central differences, this requires nearest neighbor exchange of the values of E. This is a very small amount of information that must be communicated compared to the amount of data in the q resolved polarization P_q and densities $n_q^{e/h}$. Not only is little data shared between processors, that data is only shared relatively infrequently. The vast bulk of the time that is required for the computation is spent in integrating the local material equation in time t. The values of the field E can be sent to nearest neighbors before the calculation of the material response $P_q, N_q^{e/h}$ is started, so that the propagation of E in ξ (requiring the values of the neighboring E values) is done after the material response has been computed. Thus even though communication between processors can be quite slow, the computation need not wait. In practice, more than one tarnsverse value may be executing on one processor, as we take advantage of the virtual machines that PVM provides. This allows us to run the same code on our local network as we run on the remote sites.

Our experience using the The CM-5 at the AHPCC of the MSC (Minnesota Supercomputing Center) and the SP2 at the MHPCC (Mauii High performace Computing Center) has led us to conclude that for the very coarse grained parallelism in our code, the SP2 in dedicated mode is nearly ideal. The individual machines (processors) execute the code independently and quite efficiently, and the communication overhead is minimal. As the usage at MHPCC has increased, the performance of our code has degraded dramatically. This is due to the uneven load across the many machines. At any given time, our code executes at the speed of the slowest of the machines. In addition, although dedicated machine time has been available, the waiting time to get that time has been quite long. We are hopeful that the implementation LoadLeveler at MHPCC will improve this situation dramatically. This should be installed in mid March 1995. We have found that the user support services at both MSC and particularly at MHPCC have been excellent.

References

[1] R.A. Indik, A.C. Newell, "Computing for pattern forming systems in nonlinear optics", Mathematics and Computers in Simulation **37** (1994) 385-403

[2] R. Indik, R. Binder, W.W. Chow, A. Knorr,J.V. Moloney, and S.W. Koch "Many-body effects in the propagation of short pulses in a semiconductor amplifier", SPIE-Physics and simulation of optoelectronic devices III, 6-9 Feb, 1995, San Jose, SPIE-Proceedings 2399, Eds. W. Chow and M. Osinski

[3] J.V. Moloney and R.A. Indik, "Femtosecond Nonlinear Optical Proves of Microscopic Many-Body Interactions", DoD Mission Success from High Performance Computing, 1996.

Conferences:

AFOSR Meeting for Contractors and Grantees in Computaional and Physical Mathematics, June 1-3 Kirtland AFB.

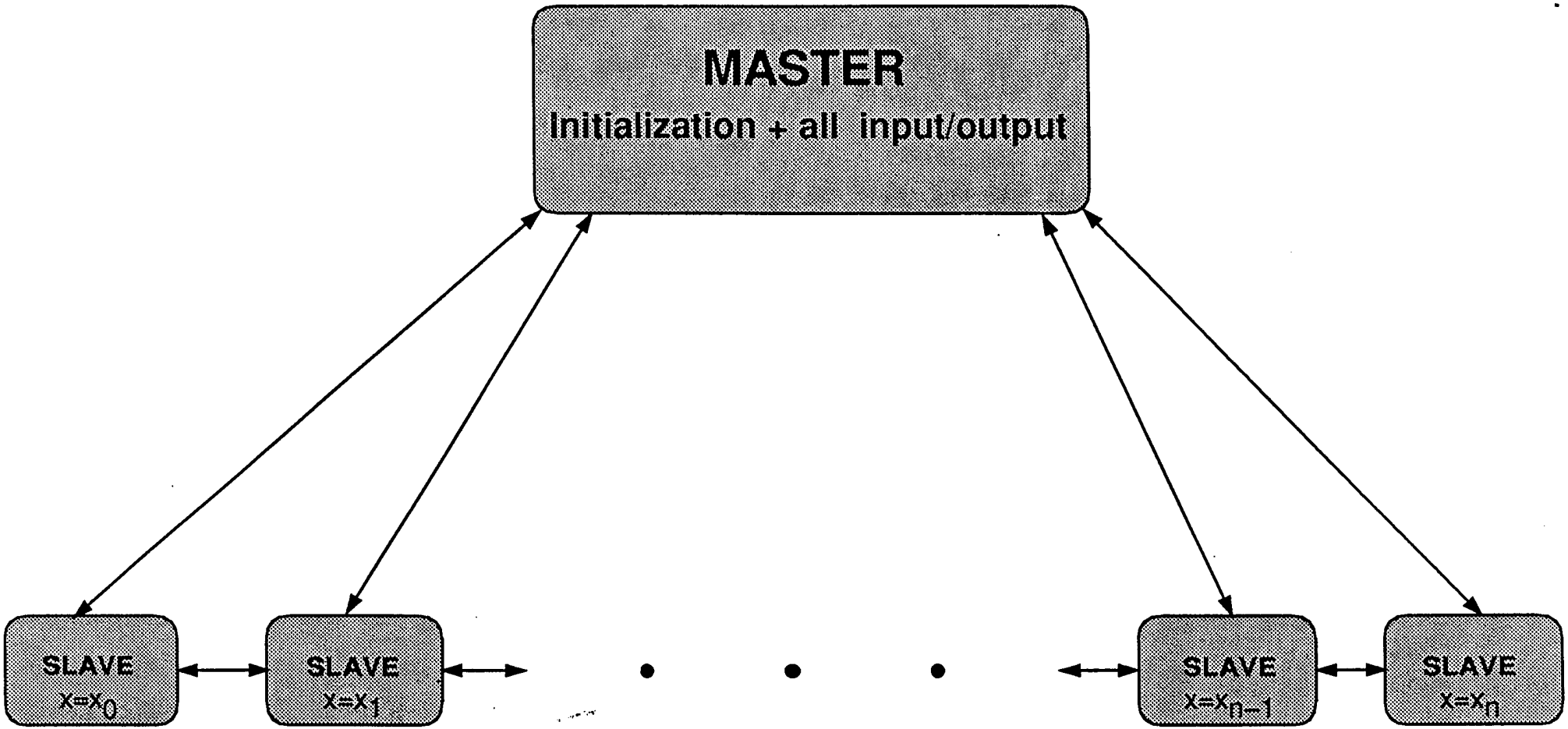

Slaves do all of the work, and communicate among themselves to calculate diffraction

- The master does very little computation
- Slaves compute the material response P(t) (99% of CPU) and propagate the light field E(t) in space (z direction)
- P(t)=P(E(t'), 0<t'<t), is computed locally
- In the propagation of the light field E(t), diffraction couples nearest neighbors.

Nonlinear Optics and Guided waves Study Centre of the European Science Foundation, Aug 1-20 1994, University of Edinburgh.

SPIE-Physics and simulation of optoelectronic devices III, 6-9 Feb, 1995, San Jose, California.

Large Scale Computational Nonlinear Optics - Maxwell's Equations
R.G. Flesch, and J.V. Moloney

Solution of Maxwell's equations in three spatial dimensions plus time places such memory, speed and disk storage demands on the systems as to put it is the class of Grand Challenge projects like lattice gauge theory. Resolutions of only 20 points per wavelength in the longitudinal direction can lead to executables as large as 10 Gbytes. Clearly the only machines which have such resources are the largest supercomputers such as the CM5 at the AHPRC and the SP2 in Maui. That is not to say that one cannot make good progress with more modest resources. Our strategy has been to develop the codes on our Power Challenge and do preliminary parameter searches with smaller grid resolution. Once an interesting regime has been uncovered we can test and further probe the phenomena on the larger machines at increased resolution to ensure accuracy. A sketch of the computational domain illustrating one means of visualization in movie format is shown in the figure.

Algorithmically, the solution process cleanly breaks into two steps, first the Maxwell field updates followed by computation of the material response. The first of these two steps requires a great deal of communication while the second in completely local. Both steps require roughly the same amount of time, the communication in the Maxwell steps is balanced by the more intense number of actual flops in the material. As is the case in any multi-processor machine, each processor is allocated an equal fraction of grid points. To minimize interprocessor communication, it is essential to minimize the surface area to volume ratio, something which is the default data layout on the CM5. The high interprocessor bandwidth and relatively low latency make the CM5 the optimal choice we have examined to date. We have yet to port the code to the SP2 as the PVM paradigm will require complete recoding. The success of the port will depend on how well the high speed switch on the SP2 handles the large amount of communication. As the second step requires no communication, the CM5, C90 and Power Challenge all parallelize that section of the code very well.

One very important numerical aspect of the problem which we had to address is the presence of numerical dispersion in the finite differencing schemes used in the Maxwell step. There have recently been a significant number of publications on this issue. We have run our own tests using a model system in which there is no physical dispersion. We have observed the phase shifts reported in the literature using both the (2,2) and (2,4) numerical schemes and have been able to control it by using a larger number of grid points. However we have found that the actual shifts in the position of the packets we propagate to be very small. For example have found no real difference in the carrier shock times if we use 200 or 1000 points per wavelength. This is in great part due to the fact that we use ultrashort pulses and propagate them hundreds or a thousand wavelengths. The process is cumulative and would introduce more errors for longer propagations. Equally important is that for realistic material models the physical dispersion far exceeds the numerical.

Another aspect which is essential to a successful implementation of this research program is the visualization of the large date sets generated. Visualization of a three dimensional three component vector field has always been a difficult task and one must normally resort viewing cross sections. One software tool which greatly eases this task is AVS, enabling one to load in an entire 3D data set and view any desired slice. But often this also does not suffice because due to the rapid longitudinal variation due to the carrier can

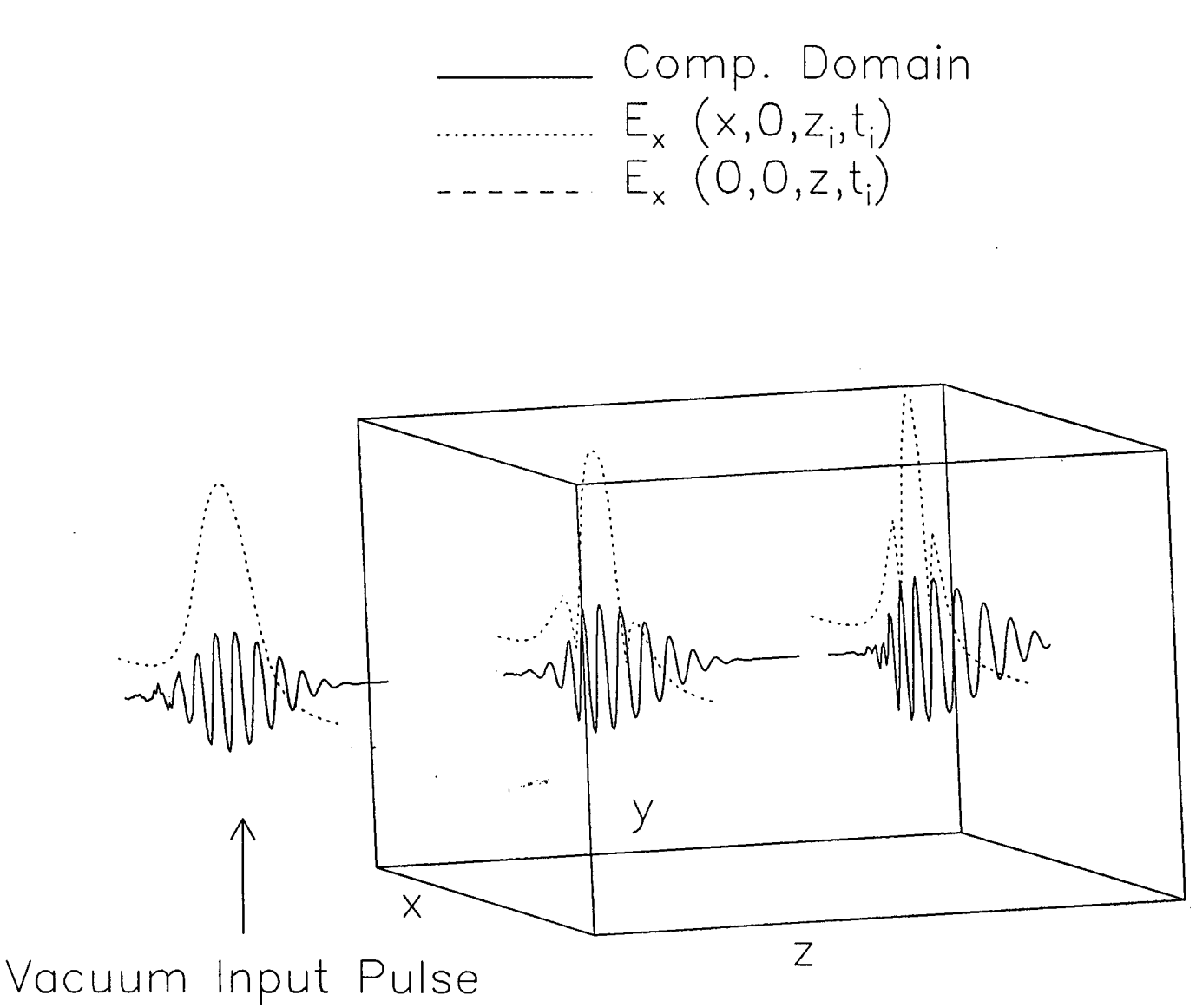
Comp. Domain
E_x $(x,0,z_i,t_i)$
E_x $(0,0,z,t_i)$
y
x
z
Vacuum Input Pulse

obstruct field values. To avoid this we have written some GL code for our Silicon Graphics machines. With this code we are able to rotate and animate two dimensional surfaces of the field avoiding the obstruction problems. The hardware graphics present in the Indigo 2 allow us to do these rotations in real time.

Relaxation processes in semiconductor light amplifiers: the role of charge carrier correlations

Y. Lvov, R. Binder and J.V. Moloney

One of the most important aspects of a microscopic approach to semiconductor lasers and semiconductor light amplifiers is the problem of charge carrier relaxation and thermalization processes. Being far away from thermal equilibrium, the coupled semiconductor-light system is generally not well described in terms of equilibrium concepts. Many theories use the concepts of quasi-thermal equilibrium amended by phenomenological thermalization terms. In the quasi-thermal equilibrium approach, the conduction band electrons and valence band holes are assumed to be independently in equilibrium, and the thermalization terms account for carrier-carrier and carrier-phonon scattering which tends to establish the quasi-equlibrium if, for example due to the presence to the light field, the system is not in the quasi-equilibrium state. Since the incoherent scattering processes crucially affect the optical gain dynamics of the systems (in other words, determine the filling of energy states which contributes to stimulated emission), a microscopic treatment of these terms is clearly desirable.

In recent years, several research groups have already implemented basic versions of microscopic scattering models in their analysis of optical properties of semconductors. Most of these models are based on the combination of three approximations: the screened-Hatree-Fock approximation (i.e., the scattering probability being proportional to the square of the screened Coulomb interaction matrix element, and being solely determined by carrier distribution functions, not carrier correlation functions), the Markov approximation, and the completed scattering approximation (i.e., the scattering contains an energy-conserving delta-function). These are typical features of the so-called Kadanoff-Baym theory, which was developed to describe systems very close to equilibrium.

In systems which deviate considerably from equilibrium, such as lasers operating far above threshold, lasers with fast external modulations and light-amplifiers amplifying sub-ps pulses, these approximations become questionable. Also, novel laser systems like ZnSe-based lasers cannot simply be described on the basis of commonly used weakly-correlated plasma theories. Although the lasing processes in these structures are still being investigated (with special emphasis on excitonic, biexcitonic, and carrier-phonon processes), it seems appropriate at the present time to amend existing theories and include charge-carrier correlations beyond the screened-Hartree-Fock approximation.

In the present project we are deriving equations of motion for carrier-correlation functions, which ultimately should allow us to study relaxation mechanisms in systems with strong Coulomb correlations.

Due to the nature of the quantum mechanical Coulomb interaction Hamiltonian, the time evolution of the distribution functions (two operator expectation values) $n_k =< a_k^+ a_k >$ are determined by four operator expectation values $N_4(k_1, k_2, k_3, k_4) =< a_{k_1}^+ a_{k_2}^+ a_{k_3} a_{k_4} >$. The time evolution of the four operator expectation values is defined by six operator expectation values, and so on. This infinite hierarchy of operator equations is known as BBGKY hierarchy. In order to obtain finite sets of equations one has to decouple the hierarchy with, for example, the help of Green's function formalisms. This is done in the Kadanoff-Baym approach. Using this formalism one can obtain Boltzmann kinetic equations, which within the certain limits describe the time evolution of two operator expectation values. The Green's function approach, although being a very practical approach, has two disadvantages: the two-time structure of the one-particle Green's functions and the lack of precise and systematic error studies of given approximations (i.e., without going beyond the screened-Hartree Fock approximation no definite statements about its accuracy can be made).

We propose an alternative approach for studying carrier-carrier collisions and correlations which combines the method of nonlinear optical suseptibilities for Coulomb systems, recently developed by Axt and Stahl) with the method of multiple scales. The combination of these approaches should enable us to obtain generalized Boltzmann equations including charge-carrier correlation functions. As this project is based

on a highly demanding and complex theory, we are planning the following a two step approach.
In the first step, we neglect all contributions of the optical field and study correlations functions in a certain order of the interaction potential (which, at this point, we assume to be small). We can then apply the multiple scales method to obtain an equation of motion for the four operator expectation value $\delta N_4 = N_4 - n \times n$, where $n \times n$ denotes the corresponding Hartree-fock factorized form of N_4. Initial calculations indicate a strong formal similarity of the generalized Boltzmann equation with the conventional Boltzmann equation.
We are also interested in studying stationary solutions of the systems described by the above mentioned relaxation equations and additional (more or less phenomenological) carrier source and sink terms. These questions are related to the well-known Kolmogorov solutions in conventional, classical scattering investigations.
After acquiring a certain familiarity with the temporal evolution of correlation functions in weakly interacting systems (i.e. sytems which allow for a classification of solutions corresponding to the order of the interaction potential), we plan to generalize the approach and include the optical polarization, similar the the Axt-Stahl approach. Of course, in contrast to their investigation, we have to go to higher than third order in the optical field to properly describe relaxation effects.

Feedback and Multimode Behavior of a Fabry-Pérot Laser: A Travelling Wave Model

M. Homar, J.V. Moloney and M. San Miguel

Summary

We report the results of a numerical study of multimode behavior of a Fabry-Pérot laser[1]. The model is based on travelling-wave equations for the slowly varying amplitudes of the counterpropagating waves in the cavity, coupled to equations for spatially dependent population inversion and polarization of a two-level active medium. Variations in polarization and population inversion over wavelength scales are taken into account by means of an expansion in a Fourier series. Results are given for typical semiconductor laser parameters. Spatially distributed spontaneous emission noise and carrier diffusion are taken into account. The competing role of Spectral Hole Burning (SHB), spontaneous emission noise and carrier diffusion in determining multimode behavior is elucidated: With no carrier diffusion, spontaneous emission noise excites a large number of modes close to threshold, while SHB leads to a fixed number of significant lasing modes well above threshold. Carrier diffusion restores dominant single-mode emission well above threshold. We have also studied the effects of optical feedback and opportunities for mode selection with short external cavities: For a cavity of $L_{ext} = 75\mu$m a chosen single mode can be selected for an external field mirror reflectivity of 1%. For a reflectivity of 40% two groups of intracavity modes separated by the external cavity mode interspacing are selected. For a cavity of $L_{ext} = 450\mu$m the laser can be forced to lase in two intracavity modes for a reflectivity of 2%. Mode selection is not found, even for weak feedback, for external cavities longer than 0.1cm.

Traveling wave model

The interaction of the electromagnetic wave with the medium is governed by the Bloch equations for two-level atoms.

$$\frac{\partial E^+}{\partial t} + \frac{\partial E^+}{\partial z} = -P^+_{(0)} \tag{1}$$

$$\frac{\partial E^-}{\partial t} - \frac{\partial E^-}{\partial z} = -P^-_{(0)} \tag{2}$$

$$\frac{\partial P^+_{(p)}}{\partial t} = -\gamma_\perp \left[\left(1 + \imath\frac{\delta}{\gamma_\perp}\right) P^+_{(p)} + \left(N_{(p)}E^+ + N_{(p+1)}E^-\right)\right] + \xi^+_{(p)}(z,t) \tag{3}$$

$$\frac{\partial P^-_{(p)}}{\partial t} = -\gamma_\perp \left[\left(1 + \imath\frac{\delta}{\gamma_\perp}\right) P^-_{(p)} + \left(N^+_{(p)}E^* + N^*_{(p+1)}E^-\right)\right] + \xi^-_{(p)}(z,t) \tag{4}$$

$$\frac{\partial N_{(p)}}{\partial t} = -\gamma_\parallel \left[N_{(p)} + \left(E^{-*}P^+_{(p-1)} + E^+P^{-*}_{(p-1)} + E^{+*}P^+_{(p+1)} + E^{-*}P^{-*}_{(p+1)}\right)\right] \tag{5}$$

$$\frac{\partial N_{(0)}}{\partial t} = -\gamma_\parallel \left[(N_{(0)} - N_0) + \left(E^+P^{+*}_{(0)} + E^-P^{-*}_{(0)} + (*)\right)\right] \tag{6}$$

In the equations above we have also included Langevin noise terms $\xi_{(p)}(z,t)$ as polarization sources. Such spatially distributed noise terms model independent spontaneous emission process in different points of the cavity. They are taken to be Gaussian white noise in space and time with zero mean and correlations $\langle \xi_0(z,t)\xi_0^*(z',t')\rangle = \delta_0\delta(t-t')\delta(z-z')$. Longitudinal carrier diffusion is also taken into account.
We denote by r_1 and r_2 the reflectivities of the cavity mirrors placed at $z = 0$ and $z = L$, respectively. In addition we consider an external mirror of reflectivity r_3 placed on the right of the laser cavity. Thus, our boundary conditions are,

$$\begin{aligned} E^+(z=0,t) &= r_1E^-(z=0,t) \\ E^-(z=L,t) &= r_2E^+(z=L,t) - r_3\sqrt{1-r_2^2}E^+(z=L,t-\tau) \end{aligned}$$

where τ is the round trip time of the field in the external cavity of length L_ext. Note that these boundary conditions take into account multiple reflections on the external mirror.

References

[1] M. Homar, J. V. Molor.ey and M. San Miguel, "Feedback and multimode behavior of a Fabry-Perot laser: A traveling wave model", manuscript in preparation.

Circularly symmetric distributed feedback semiconductor lasers

Ewan M. Wright and K. Kasunic

We are currently investigating the modal properties of circularly symmetric distributed feedback (CSDFB) lasers using both coupled-mode and beam propagation techniques. CSDFB lasers offer a number of advantages over conventional surface emitting lasers including circularly symmetric output, low-divergence output beam, and the ability to phase-lock a two-dimensional array.

Previous work on CSDFB lasers concentrated on the mode properties and the calculation of the laser threshold using coupled-mode theory. We have extended this work to deal explicitly with issues related to CSDFB semiconductor lasers including index anti-guiding associated with the gain profile, azimuthal mode selection, and the laser linewidth. The key issue we have addressed is that of the azimuthal mode selection since this determines whether or not the output is circularly symmetric. However, as one increases the azimuthal mode selection we find that the laser linewidth also increases, meaning that as a result more azimuthal modes may actually oscillate close to threshold! Our initial result indicate that CSDFB lasers may typically oscillate on several azimuthal modes, and hence have non-circular output beams, close to threshold. Far above threshold the laser linewidth narrows and the output beam may then become circularly symmetric.

To extend our understanding of CSDFB semiconductor lasers we are currently developing beam propagation codes which also incorporate the nonlinear optical response of the semiconductor medium. This will allow us to address the problem of nonlinear transverse mode selection and also the laser stability which is beyond the previous coupled mode theories.

Our most recent work has concentrated on the above-threshold, nonlinear properties of CSDFB lasers. Specific issues addressed in our research are gain saturation [1], index saturation [2], and solutions to the time-dependent coupled-mode equations on a finite interval.

By including radially-varying gain saturation and uniformly-distributed surface emission in the above-threshold solution of the coupled-mode equations, we have obtained 2 significant results. First, there exists an optimum coupling strength κ for efficient conversion of pump power into useful output power. From the perspective of device design, these results allow appropriate selection of κ for high-power operation, alleviating potential problems with overheating. Second, for relatively large κ, high-power operation of the CSDFB laser will result in multi-mode operation, a consequence of an above-threshold mode competition. Fortunately, this multi-mode behavior can be avoided by designing these lasers with the optimum κ for power conversion.

We have also modeled the effects of gain/index coupling, by including index saturation *via* the linewidth enhancement factor α. The results here show that even for large κ, single-mode behavior is possible over a limited (above-threshold) power range. We also believe our results help explain the difficulties found in experimentally obtaining above- threshold, single-mode output.

Finally, we have started the numerical modeling of the time-dependent coupled-mode equations describing self-pulsing and soliton formation in nonlinear periodic structures. To date, we have successfully modeled self- pulsing in conventional DFB structures. Our future work will extend these results to the CSDFB laser.

References

[1] K. J. Kasunic and M. Fallahi, "Gain Saturation in Circular-Grating Distributed-Feedback Semiconductor Lasers", accepted by JOSA-B, 20 Dec. 1996.

[2] K. J. Kasunic and M. Fallahi, "Gain and Index Saturation in Circular-Grating Distributed- Feedback Semiconductor Lasers", *Proc SPIE* **2994** (1997).

PUBLICATIONS (AFOSR F49620-94-0144DEF)

1. P.M.W. Skovgaard, J.G. McInerney, J.V. Moloney, R.A. Indik, and C.Z. Ning, "Enhanced stability of MFA-MOPA semiconductor lasers using a nonlinear, trumpet shaped flare", *IEEE-Photonics Tech. letts.*, in press, (1997).

2. D. Hochheiser, J.V. Moloney, and J. Lega, "Controlling Optical Turbulence", *Phys. Rev. A.*,**55**, (6) in press (1997 June).

3. J.V. Moloney, R.A. Indik, and C.Z. Ning, "Full Space-time simulation for high brightness semiconductor lasers", *IEEE-Photonics Tech. Letts.* **9**, (6), in press (1997 June).

4. C.Z. Ning, J.V. Moloney, A. Egan, R.A. Indik, "A First-Principles Fully Space-Time Resolved Model of a Semiconductor Laser", *JEOS/Quantum and Semiclassical Optics* in press (1997).

5. I. Aranson, D. Hochheiser, J.V. Moloney, "Boundary Driven Selection of Patterns in Large Aspect Ratio Lasers." *Phys. Rev. A.*, in press (1997, April).

6. C.Z. Ning, R.A. Indik, J.V. Moloney, W.W. Chow, A. Girndt, S.W. Koch, and R. Binder, "Incorporating many-body effects into modeling of semiconductor lasers and amplifiers", *SPIE Proceedings*, **2994**, (1997).

7. J.V. Moloney, C.Z. Ning, R.A. Indik, and A. Egan, "Full Space-time simulationof high brightness semiconductor lasers,"*SPIE Proceedings*, **2994**, (1997).

8. C.Z. Ning, W.W. Chow, D.J. Bossert, R.A. Indik, and J.V. Moloney, "Influences of Unconfined States on the Optical Properties of Quantum Well Structures. *(IEEE - J. Selected Topics in Quantum Electronics)*(Accepted Feb. 1997).

9. A. Egan, C.Z. Ning, J.V. Moloney, R.A. Indik,M.M Wright, and D.J. Bossert, "Dynamic Instabilities in MFA-MOPA Semiconductor Lasers" *Submitted to Appl. Phys. Letts.*, (1997).

10. W. Forysiak, J.V. Moloney, E.M. Wright, "Nonlinear focusing of femtosecond pulses due to self-reflection from a saturable absorber", *Optic Letters*, **22** (4), 239-241, (1997 Feb 15).

11. C.Z. Ning, R.A. Indik and J.V. Moloney, Arizona Center for Mathematical Sciences, "Effective Bloch Equations for Semiconductor Lasers and Amplifiers", *JQE, IEEE/LEOS*, (February 1997).

12. J. Xin and J.V. Moloney, "Global Weak Solutions and Attractors of the Three Dimensional Maxwell-Bloch Two Level Laser Systems", *Communications in Math. Physics*, **179**, 511-528, (1996).

13. J.V. Moloney, and R.A. Indik, "Femtosecond Nonlinear Optical Probes of Microscopic Many-Body Interactions", *DoD Mission Success from High Performance Computing - a report by the DoD high Performance Computing Modernization Office, Ofc. Sec. of Defense*, 100, (1996).

14. R.G. Flesch, A. Pushkarev and J.V. Moloney, "Carrier Wave Shocking of Femtosecond Optical Pulses", *Phys. Rev. Let.*, **76**, (14), 2488, (1996).

15. S. Hughes, A. Knorr, S.W. Koch, R. Binder, R.Indik and J.V.Moloney, "The Influence of Electron-Hole-Scattering on the Gain Spectra and the Saturation Behavior of Highly Excited Semiconductors", *Solid State Comm.*, **100**, 555 (1996).

16. M. Homar, J.V. Moloney and M. San Miguel, "Travelling Wave Model of a Multimode Fabry-Perot Laser in Free Running and External Cavity Configurations", *IEEE JQE*, **32**, (3), 553-566, (1996).

17. W. Forysiak, R.G. Flesch, J.V. Moloney and E.M. Wright, "Doppler Shift of Self-Reflected Optical Pulses at an Interface: The Dynamic Nonlinear Optical Skin Effect", *Phys. Rev. Lett.*, **76**, (20), 3695-3698, (1996).

18. R.A. Indik, M. Mlejnek, J.V. Moloney, R. Binder, S. Hughes, A. Knorr and S.W. Koch, "The role of plasma cooling, heating and memory effects in sub-picosecond pulse propagation in semiconductor amplifiers", *Phys. Rev. A*, **53**, (5), 3614-3620, (1996 May).

19. M.E. Bleich, D. Hochheiser, J.V. Moloney, and J.E.S. Socolar, "Controlling Extended Systems with Spatially Filtered, Time-Delayed Feedback." *Phys. Rev. E.*, **55**, 2119, (March 1996).

20. C.Z. Ning, R.A. Indik, and J.V. Moloney, "A Self-consistent approach to thermal effects in vertical-cavity surface-emitting lasers," *J. Opt. Soc. Am. B.*, **12** (10), 1993-2004, (1995 Oct).

21. Hu Gang, C.Z. Ning, H. Haken, "Inverse Problem and Singularity of the Integration Kernal", *Phys. Letts. A.*, **205**, 130-136, (1995).

22. R.F. Pawula, "Relations Between Rice *Ie*-function and Marcum *Q*-function with Applications to Error Rate Calculations", *Elec. Lett.*, **31**, (20), 1717-1719 (1995).

23. C.Z. Ning and J.V. Moloney, "Plasma-heating induced intensity-dependent gain in semiconductor lasers", *Appl. Phys. Lett.* **66** (5), 559-561 (1995 Jan 30).

24. W.W. Chow, R. Indik, A. Knorr, S.W. Koch, and J.V. Moloney, "Time-resolved nondegenerate four-wave mixing in a semiconductor amplifier", *Phys. Rev. A*, **52** (3), 2479-2482, (1995 Sept).

25. C.Z. Ning, R.A. Indik, and J.V. Moloney, "Effects of plasma and lattice heating in VCSELs", *SPIE Proceedings - Physics and Simulation of Optoelectronic Devices III*, **2399**,(617), (1995, Feb 6-9, San Jose, CA).

26. J.K. White, J.G. McInerney, and J.V. Moloney, "Effects of the injection current profile shape on sidelobes in large-aperture semiconductor laser amplifiers", *Opt. Letts.*, **20**, (6), 593-595 (1995 Mar 15).

27. C.Z. Ning and J. V. Moloney, "Thermal effects on the threshold of vertical-cavity surface-emitting lasers: first and second order phase transitions", *Opt. Letts.*, **20**, (10), 1151-1153, (1995 May).

28. J. Lega, J.V. Moloney, and A.C. Newell, "Universal Description of Laser Dynamics Near Threshold", *Physica D*, **83**, 478, (1995).

29. M. San Miguel, Q. Feng, J.V. Moloney, and A.C. Newell, "Polarization Instabilities in Transverse Laser Patterns", *Fluctuation Phenomena: Disorder and nonlinearity*, (1995).

30. J.K. White, J.G. McInerney and J.V. Moloney, "Formation of sharply peaked sidelobes in large aperture single pass semiconductor laser amplifiers", *Electron. Lett.*, **31**(1), 38-39, (1995).

31. C.Z. Ning and J. V. Moloney, "Thermal effects on threshold of vertical-cavity surface-emitting lasers: first and second order phase transitions", *Opt. Lett.*,**20**(10), 1151-1153, (1995).

32. M. San Miguel, Q. Feng, and J.V. Moloney, "Light polarization dynamics in surface-emitting semiconductor lasers," *Phys. Rev. A.*, **52** (2) 1728-1738 (1995 August).

33. W.W. Chow, R. Indik, A. Knorr, S.W. Koch, and J.V. Moloney, "Time-resolved nondegenerate four-wave mixing in a semiconductor amplifier", *Phys. Rev. A.*,**52** (3), 2479-2482 (1995).

34. O. Hess, S.W. Koch, and J.V. Moloney, "Filamentation and Beam Propagation in Broad-Area Semiconductor Lasers," *IEEE JQE* **31** (1) (1995).

35. R.A. Indik, J.V. Moloney, R.H. Binder, W.W. Chow, A. Knorr and S.W. Koch, "Many–body effects in the propagation of short pulses in a semiconductor amplifier", *SPIE Proceedings* **2399**, 650-659, (1995).

36. R.A. Indik, J.V. Moloney, R. Binder, A. Knorr and S.W.Koch, "Self-induced channeling of subpicosecond optical pulses in broad area bulk semiconductor amplifiers",*Opt. Lett.*, **20** (22) 2315-2317 (1995 Nov 15).

37. P. Ru, W.W. Chow, J.V. Moloney, and S.W. Koch, "Quantum Confinement and Strain Effects on the Lateral Mode Stability of an Unstable Resonator Semiconductor Laser", *Appl. Phys. Lett.*, **64**, (12), 1469-1471, (1994).

38. P.K. Jakobsen, J. Lega, Q. Feng, M. Staley, J.V. Moloney, and A.C. Newell, "Nonlinear transverse modes of large-aspect-ratio homogeneously broadened lasers: I. Analysis and numerical simulation", *Phys. Rev. A.*, **49**, (5), 4189-4200, (1994 May).

39. J. Lega, P.K. Jakobsen, J.V. Moloney, and A.C.Newell,"Nonlinear transverse modes of large-aspect-ratio homogeneously broadened lasers: II. Pattern analysis near and beyond threshold", *Phys. Rev. A.*, **49**, (5), 4201-4212, (1994 May).

40. P. Ru, J.V. Moloney, and R. Indik, "Mean-field approximation in semiconductor-laser modeling", *Physical Review A*, **50**, (1), 831-838, (1994).

41. R. Indik, A. Knorr, R. Binder, J.V. Moloney, and S.W. Koch, "Propagation-Induced Adiabatic Following in a Semiconductor Amplifier", *Optics Letters*, **19**, (13), 966-968, (1994).

42. J. Lega, J.V. Moloney, and A.C. Newell, "Swift-Hohenberg Equation for Lasers", *Phys. Rev. Letts.*, **73**(22), 2978-2981, (1994 Nov 28).

43. Q. Feng, J.V. Moloney, and A.C. Newell, "Transverse patterns in lasers", *Phys. Rev. A.*, **50** (5), R3601-R3604 (1994).

44. J.B. Geddes, R.A. Indik, and J.V. Moloney, and W.J. Firth "Hexagons and squares in a passive nonlinear optical system", *Phys. Rev. A*, **50** 3471 (1994).

45. J.B. Geddes, J.V. Moloney, E.M. Wright, and W.J. Firth, "Polarisation patterns in a nonlinear cavity", *Optics Communications*, **111**, 623, (1994).

46. J.B. Geddes, J. Lega, J.V. Moloney, R.A. Indik, E.M. Wright, and W.J. Firth, "Pattern Selection in Passive and Active Nonlinear Optical Systems",*Chaos, Solitons and Fractals*, **4**, 1261-1274, (1994).

47. G.K. Harkness, W.J. Firth, J.B. Geddes, J.V. Moloney, and E.M. Wright, "Boundary Effects in Large Aspect Ratio Lasers", *Phys. Rev. A.*, **50**, 4310-4317, (1994).

48. R.A. Indik and A.C. Newell, "Computing for Pattern Forming Systems in Nonlinear Optics", *Mathematics and Computers in Simulation*, **37**, 385-403 (1994).

CONFERENCES, SEMINARS, INVITED PAPERS (AFOSR F49620-94-0144DEF)

1. D. Hochheiser, Controlling Optical Turbulence in High Brightness Semiconductor Lasers, SIAM Conference of the Applications of Dynamical Systems, Snowbird, Utah, May 18-22, 1997.

2. J.V. Moloney, AFOSR Annual Contractors Meeting on Dynamics and Control, Wright-Patterson AFB,Dayton, Ohio, May 21-23, 1997.

3. C.Z. Ning, Comprehensive simulation and modeling of optoelectronic devices, April 4, 1997, New Technology Seminar, NASA Ames Research Center, Mountain View, California.

4. C.Z. Ning, R.A. Indik, and J.V. Moloney, W.W. Chow, A. Girndt, S.W. Koch, R. Binder, Incorporating many-body effects into modeling of semiconductor lasers and amplifiers, Invited talk, Feb., 1997, SPIE Photonics West, San Jose, CA.

5. J.V. Moloney, C.Z. Ning, R.A. Indik, and A. Egan, Space-time simulation of high brightness semiconductor lasers, invited talk, Feb., 1997, SPIE Photonics West, San Jose, CA.

6. D. Hochheiser, Controlling Optical Turbulence, presented at Dynamcis Days Arizona, Arizona State University, Tempe, Arizona, January 8-11, 1997.

7. J.V. Moloney, invited speaker, Materials for Nonlinear Optics Applications, Application of Mathematics to Materials Sciences", (IMA), University of Minnesota, Minneapolis, U.S.A., February - March 1996.

8. C.Z. Ning, W.W. Chow, D.J. Bossert, R.A. Indik, and J.V. Moloney, Unconfined-state contribution to the linewidth enhancement factor in quantum well lasers, presented at OSA Annual Meeting, Rochester, N.Y., October 20-24, 1996

9. J.V. Moloney, C.Z. Ning, R.A. Indik, and A. Egan, Space-time simulation of Instabilities in high brightness semiconductor lasers, Post-deadline paper presented at OSA Annual Meeting, Rochester, N.Y., October 20-24, 1996

10. J.V. Moloney, invited speaker, National Academy Review Meeting, Washington, D.C., Febuary 1996.

11. C.Z Ning, R. A. Indik, J.V. Moloney, S.W. Koch, Effects of plasma and lattice heatings in VCSELs, SPIE-meetings, San Jose, California, Feb. 6-9, 1995.

12. SPIE-Physics and simulation of optoelectronic devices III, 6-9 Feb, 1995, San Jose.

13. Dynamics Days 14-th Annual International Workshop, Houston, Jan. 4-7, (19-5).

14. Third SIAM Conference on the Applications of Dynamical Systems, Snowbird,-Utah, May 21-24, (1995).

15. C. Z. Ning, J.V.Moloney, and S.W. Koch, A self-consistent many-body theory for plasma heating in vertical-cavity surface-emitting lasers, OSA Annual Meeting, Portland, Oregon, Sept. 10-15, 1995.

16. J.V. Moloney, invited speaker, Issues Relating to the Arrest of Critical Collapse of Femtosecond Pulses in Normally Dispersive Self-Focusing Media, Nonlinear Coherent Structures in Physics and Biology, Heriot-Watt University, Edinburgh, 10-14 July 1995.

17. J.V. Moloney, invited colloquium speaker, Issues in the Arrest of Critical Collapse of Femtosecond Optical Pulses in Optically Transparent Media, Physics Colloquium, Free University, Amsterdam, 28 June 1995.

18. J.V. Moloney, invited plenary paper, Pattern Evolution in Large Aspect Ratio Nonlinear Optical Systems, Third SIAM Conference on Applications of Dynamical Systems, Snowbird, Utah, U.S.A., May 21-24, 1995.

19. J.V. Moloney, invited speaker, Space-Time Behavior of Wide Aperture Semi Conductor Lasers and Amplifiers, 8th Annual Diode Laser Technology Conference, USAF Phillips Lab, Fort Walton Beach, Florida, 25-28 April 1995.

20. J.V. Moloney, invited colloquium speaker, Arrest of Critical Collapse of Ultra-Short Pulses in Optically Transparent Media, Physics Colloquium, Georgia Tech., 24 April 1995.

21. J.V. Moloney, invited plenary speaker, Pattern Evolution in Large Aspect Ratio Nonlinear Optical Systems, Dynamics Days Texas, an international workshop, Houston, Texas January 4-7, 1995.

22. J.V. Moloney, invited speaker, Computational insights into nonlinear optics, European Science Foundation's Summer School on Nonlinear Optics and Guided Waves, and a member of the organizing committee. Edinburgh, Scotland, United Kingdom, August 1-20, 1994.

23. AFOSR Meeting for Contractors land Grantees in Computational and Physical Mathematics, June 1-3 Kirtland AFB.

24. R. Indik, J.V. Moloney, S.W. Koch, R. Binder, A. Knorr OSA Annual Meeting, Dallas, Oct. 2-7 (1994)

25. J.K. White, J.G. McInerney, J.V.Moloney, "Modeling spatio-temporal dynamics of broad area/flared semiconductor laser amplifiers", AFOSR/ACMS Nonlinear Optics Workshop, University of Arizona, (1994).

26. J.K. White, J.V. Moloney, W.W. Chow, J.G. McInerney, "Issues of spatial and dynamical stabilities in the scaling of flared semiconductor laser amplifiers", OSA Annual Meeting, Dallas, (1994).

27. J.K. White, J.G. McInerney, J.V. Moloney, Workshop on Singularities and Patterns in Collapse, University College, Cork, Ireland, (1994).

28. J.K. White, J.G. McInerney, J.V. Moloney, International Summer School in Nonlinear Optics, University of Edinburgh, Scotland (1994).

29. J.V. Moloney, invited colloquium speaker, Modelling spatiotemporal evolution in high power wide aperture semiconductor amplifiers and lasers, presented at a colloquium at the Phillips Universitat, Marburg, Germany, June 21, 1994.

30. J.V. Moloney, invited speaker, Patterns in Large Aspect Ratio Lasers, at the Scientific Workshop on Pattern Singularities and Collapse: Applications to Semiconductor Lasers and Critical Focusing of Ultrashort Optical Pulses, University College Cork, Cork, Ireland, August 21-26, 1994.

31. J.V. Moloney, Chair and Organizer, Materials Issues in Nonlinear Optics section of SIAM Conference on Emerging Issues in Mathematics and Computation from the Materials Sciences, Pittsburgh, Pennsylvania, U.S.A., April 19-20, 1994.

32. J.V. Moloney, invited paper, Modeling the nonlinear dynamics of wide aperture semiconductor lasers and amplifiers, presented at Physics and Simulation of Optoelectronic Devices II, part of SPIE's OE/LASE 94, Los Angeles, California, U.S.A., January 22-29, 1994.

33. FSU-USA Conference on Chaos, Woods Hole, Massachussetts, July 19-23, (199-).

34. Nonlinear Optics and Guided Waves, A Study Center of the European Science-Foundation, Aug. 1-20, 1994.

35. Workshop on "Singularities in Patterns and Collapse: Applications to Semiconductor Lasers and Critical Focusing of Ultrashort Optical Pulses", University College Cork, Ireland, Aug. 21-27, 1994.

36. AFOSR/ACMS Nonlinear Optics Workshop, University of Arizona, Oct. 9-11, 1994.

37. Gordon Research Conference on Nonlinear Optics and Lasers, Aug. 1-6, (1993), Wolfeboro, NH.

Multi-band Bloch Equations and Gain Spectra of Highly Excited II-VI Semiconductor Quantum Wells

A. Girndt, F. Jahnke, A. Knorr, and S.W. Koch

Fachbereich Physik und Zentrum für Materialwissenschaften,

Phillips-Universität, Renthof 5, D-35032 Marburg, Germany

W.W. Chow

Sandia National Laboratories, Albuquerque, NM 87185-0601, U.S.A.

(April 16, 1997)

Abstract

Quasi-equilibrium excitation dependent optical probe spectra of II-VI semiconductor quantum wells at room temperature are investigated within the framework of multi-band semiconductor Bloch equations. The calculations include correlation effects beyond the Hartree-Fock level which describe dephasing, interband Coulomb correlations and band-gap renormalization in second Born approximation. In addition to the carrier-Coulomb interaction, the influence of carrier-phonon scattering and inhomogeneous broadening is considered. The explicit calculation of single particle properties like band structure and dipole matrix elements using $\mathbf{k} \cdot \mathbf{p}$ theory makes it possible to investigate various II-VI material combinations. Numerical results are presented for CdZnSe/ZnSe and CdZnSe/MgZnSSe semiconductor quantum-well systems.

Keywords: A. semiconductors B. optical properties C. carrier-carrier interaction

I. INTRODUCTION

Wide band gap semiconductor materials, in particular II-VI compounds, are promising candidates for optical device application in the blue-green wavelength region. Especially for device optimization, a detailed understanding of the electronic interaction processes and their influence on optical gain spectra is desirable. Several recently investigated II-VI heterostructures are composed of quantum layers with $Zn_xCd_{1-x}Se$ active material within ZnSe barriers [1–4]. Hence, the theoretical description of the optical properties of II-VI heterostructures requires not only the inclusion of the relevant many-body processes in a highly excited semiconductor but also the particular composition and geometry dependence of the band structure properties.

In this paper we theoretically investigate the optical probe spectra of II-VI heterostructures. Concentrating on room temperature properties of structures with weak interface roughness, the optical gain can be assumed to result from electrons which, after their incoherent injection, have relaxed into the available electronic states at the bottom of the band whereas higher bound states, such as biexcitons [5], are of minor importance. In our model, the interaction of the light field with the inverted material is treated semiclassically by calculating the absorption in the framework of the multi-band semiconductor Bloch equations. The observable in a typical experiment, where the probe light propagates in the plane of the quantum-well heterostructure, is the absorption coefficient,

$$\alpha(\omega) = \mu\Gamma\frac{\omega}{n_b}\,\mathrm{Im}\left[\frac{\tilde{P}(\omega)}{\tilde{E}(\omega)}\right], \tag{1}$$

where n_b the refractive index, $\tilde{E}(\omega) = \int dt\, e^{i\omega t}\, E(t)$ is the Fourier transform of the applied probe pulse $E(t)$ and $\tilde{P}(\omega)$ is the corresponding Fourier transform of the induced polarization density $P(t)$. Note that for a weak probe field the induced polarization $\tilde{P}(\omega)$ is directly proportional to $\tilde{E}(\omega)$ so that $\alpha(\omega)$ is independent of the probe-pulse parameters.

When light propagation in the quantum-well plane is experimentally investigated, the field overlaps with the quantum well(s) and the barrier layers. To account for the resulting

reduced effective absorption or gain, we have introduced in Eq. (1) the confinement factor $\Gamma = 0.003/nm$.

II. EQUATIONS OF MOTION

In this section, we calculate the polarization density $P(t)$ from a microsocopic theory including band-structure effects as well as many body interactions. We expand the polarization density in a quantum-well Bloch basis,

$$P(t) = \frac{1}{A}\sum_{\nu,\nu'}\sum_{\mathbf{k}} \mu_{\mathbf{k}}^{\nu,\nu'} P_{\mathbf{k}}^{\nu,\nu'}(t) + \text{c.c.}, \tag{2}$$

where $\mathbf{k}$ is the in-plane carrier momentum, $\nu = \lambda, n$ contains the band index $\lambda = e, h$ and the sub-band index n and A is the active area of the quantum well. In Eq. (2), we consider all optically allowed single valence band to conduction band ($|\nu'\rangle \rightarrow |\nu\rangle$) transitions with the interband dipole matrix elements $\mu_{\mathbf{k}}^{\nu,\nu'}$. The polarizations for the different bands obey the multi-band semiconductor Bloch equations [6],

$$\frac{d}{dt}P_{\mathbf{k}}^{\nu,\nu'}(t) = -\frac{i}{\hbar}\Delta_{\mathbf{k}}^{\nu,\nu'} P_{\mathbf{k}}^{\nu,\nu'}(t) - \frac{i}{\hbar}\left[1 - f_{\mathbf{k}}^{\nu} - f_{\mathbf{k}}^{\nu'}\right]\Omega_{\mathbf{k}}^{\nu,\nu'}(t) + \left.\frac{dP_{\mathbf{k}}^{\nu,\nu'}(t)}{dt}\right|_{\text{corr}}, \tag{3}$$

where $P_{\mathbf{k}}^{\nu,\nu'}(t)$ is the interband polarization between the bands $\nu = e, n$ and $\nu' = h, n$ and $f_{\mathbf{k}}^{e,n}$, $f_{\mathbf{k}}^{h,n}$ are the carrier distribution functions for electrons and holes in the sub-band n, respectively. For a weak probe beam, the polarization $P_{\mathbf{k}}^{\nu,\nu'}(t)$ remains linear with respect to the probe field $E(t)$ and the probe field induced changes of the carrier occupation $f_{\mathbf{k}}^{a,n}$ can be neglected. Hence the probe spectrum reflects the excitation of the system which is described by quasi-equilibrium Fermi-Dirac distribution functions $f_{\mathbf{k}}^{a,n}$ with fixed carrier temperature (T=300K) and a chemical potential determined by the total density in the sample.

In Eq. (2), the many-body effects can be devided into Hartee-Fock (mean field) and correlation contributions. The mean field corrections lead to renormalized single-particle energies,

$$\Delta_{\mathbf{k}}^{\nu,\nu'} = \epsilon_{\nu}(\mathbf{k}) - \epsilon_{\nu'}(\mathbf{k}) - \sum_{\mathbf{q}\neq\mathbf{k}} V_{|\mathbf{k}-\mathbf{q}|}\left(f_{\mathbf{q}}^{\nu} + f_{\mathbf{q}}^{\nu'}\right), \tag{4}$$

and to a renormalized Rabi energy,

$$\Omega_{\mathbf{k}}^{\nu,\nu'}(t) = \mu_{\mathbf{k}}^{\nu,\nu'} E(t) + \sum_{\mathbf{q}\neq\mathbf{k}} V_{|\mathbf{k}-\mathbf{q}|}\, P_{\mathbf{q}}^{\nu,\nu'}(t), \tag{5}$$

with the free-carrier energies $\epsilon_\nu(\mathbf{k})$ and the Rabi energy of the probe field $\mu_{\mathbf{k}}^{\nu,\nu'} E$. The particular properties of the heterostructure, such as quantum-well thickness and material composition, determine the dipole matrix transition elements $\mu_{\mathbf{k}}^{\nu,\nu'}$ as well as the bandstructure $\epsilon_\nu(\mathbf{k})$. In our approach, these quantities are calculated from a diagonalization of the Luttinger Hamiltonian using a 4×4 $\mathbf{k}\cdot\mathbf{p}$-theory within the envelope approximation [6].

The quantum-well matrix elements of the bare Coulomb potential, which couple various carrier states, have the general form

$$V^{\nu_1,\nu_2,\nu_3,\nu_4}(\mathbf{k}_1,\mathbf{k}_2,\mathbf{q}) = \frac{2\pi e^2}{\varepsilon_b\, q} \int dz\, dz' \tag{6}$$

$$\times\, \xi_{\nu_1}^*(\mathbf{k}_1,z)\, \xi_{\nu_2}^*(\mathbf{k}_2,z')\, e^{-q|z-z'|}\, \xi_{\nu_3}(\mathbf{k}_1+\mathbf{q},z')\, \xi_{\nu_4}(\mathbf{k}_2-\mathbf{q},z).$$

Because of the band mixing, the confinement functions $\xi_{\nu_i}(\mathbf{k}_i,z)$ of the band ν_i depend on the in-plane carrier momentum k_i. This band mixing is additionally complicated by the fact that the influence of barrier states on the top valence band states cannot be neglected. The dependence of the quantum-well Coulomb matrix elements on the band indices ν_i and the corresponding in-plane carrier momenta k_i considerably complicates the coupling of various bands in Eqs. (3)–(5) as well as the evaluation of screening. It would be desirable to use Eq. (6) without further approximations within the many-body problem. Then one would take into account that the Coulomb interaction explicitly depends on the momenta of the contributing carriers k_i and not only on the transition momentum q. In this paper, we study the influence of band mixing under the assumption that the various envelope functions $\xi_{\nu_i}(\mathbf{k}_i,z)$ in Eq. (6) are approximated by an effective (momentum independent) function $\xi_0(z)$. The resulting confinement Coulomb potential

$$V_q = \frac{2\pi e^2}{\varepsilon_b\, q} \int dz\, dz'\, |\xi_0(z)|^2\, e^{-q|z-z'|}\, |\xi_0(z')|^2 \tag{7}$$

will be used in Eqs. (4), (5) and below.

The mean-field contributions contain the lowest-order Coulomb effects which lead to excitonic resonances and a low-density band-gap renormalization. However, under high excitation conditions, correlation contributions [7–11] result in strong modifications of the Hartree-Fock terms. The correlation terms can be divided into diagonal (d) and non-diagonal (nd) contributions:

$$\left.\frac{dP^{\nu,\nu'}(\mathbf{k})}{dt}\right|_{\text{corr}} = -\left[\Gamma_{\text{d}}^{\nu}(\mathbf{k}) + \Gamma_{\text{d}}^{\nu'}(\mathbf{k})\right] P^{\nu,\nu'}(\mathbf{k}) + \sum_{\mathbf{q}} \left[\Gamma_{\text{nd}}^{\nu}(\mathbf{k},\mathbf{q}) + \Gamma_{\text{nd}}^{\nu'}(\mathbf{k},\mathbf{q})\right] P^{\nu,\nu'}(\mathbf{k}+\mathbf{q}). \quad (8)$$

The real part of Γ^{ν} describes the dephasing of the polarization due to scattering of carriers in the bands ν. The diagonal contribution, Re Γ_{d}^{ν}, leads to a momentum-dependent polarization decay rate whereas the non-diagonal contribution, Re Γ_{nd}^{ν}, mixes the polarizations of various k-states. Without higher-order polarization terms [8,11], which can be neglected in the regime where a weak probe field is treated, we find Re $\Gamma_{\text{d}}^{\nu}(\mathbf{k}) = \Sigma_{in}^{\nu}(\mathbf{k}) + \Sigma_{out}^{\nu}(\mathbf{k})$ where

$$\left.\frac{df^{\nu}(\mathbf{k})}{dt}\right|_{\text{corr}} = \Sigma_{in}^{\nu}(\mathbf{k})\,[1 - f^{\nu}(\mathbf{k})] \; - \; \Sigma_{out}^{\nu}(\mathbf{k})\, f^{\nu}(\mathbf{k}) \quad (9)$$

determines the redistribution of the carrier occupation probability f^{ν}. Hence the diagonal damping rate contains the sum of in and out-scattering rates in the carrier dynamics. For the considered quasi-equilibrium situation of the carrier system, the detailed balance condition leads to $\frac{d}{dt} f^{\nu}(\mathbf{k})|_{\text{corr}}=0$ whereas in and out-scattering results in a large damping rate Re Γ_{d} which corresponds to a decay time on the order of 100 fs. In Eq. (8), this diagonal damping rate is compensated to a large extend by the non-diagonal damping rate Re Γ_{nd}. In Ref. [9] it has been shown, that this compensation has to be considered in order to obtain the correct carrier generation rate for intense optical interband excitation. Also the excitonic damping [13] and the lineshape of the gain [10] can be properly described only by including both diagonal and non-diagonal damping.

On the other hand, the imaginary part of Γ^{ν} combines with the mean-field contributions, described by Eqs. (4) and (5), by adding screening contributions to the renormalized carrier energy and and the renormalized Rabi energy. Note, however, that in general the correlation

contributions cannot be written as corrections to single particle properties.

In the following we consider the influence of carrier-carrier Coulomb scattering as well as carrier-phonon scattering. In second Born approximation, where terms up to the quadratic order in the screened Coulomb potential are included, the carrier-carrier scattering leads to the diagonal contribution

$$\Gamma_{\rm d}^{\nu(cc)}(\mathbf{k}) = \frac{1}{\hbar}\sum_{\mathbf{k}',\mathbf{q}}\sum_{\nu'}\left(2|\bar{W}_{\mathbf{q}}|^2 - \delta_{\nu,\nu'}W_{\mathbf{q}}\,W_{\mathbf{k}+\mathbf{q}-\mathbf{k}'}\right)\,g(\epsilon_{\mathbf{k}}^{\nu} - \epsilon_{\mathbf{k}+\mathbf{q}}^{\nu} + \epsilon_{\mathbf{k}'}^{\nu'} - \epsilon_{\mathbf{k}'-\mathbf{q}}^{\nu'}) \\ \times\left[f_{\mathbf{k}+\mathbf{q}}^{\nu}\left(1-f_{\mathbf{k}'}^{\nu'}\right)\,f_{\mathbf{k}'-\mathbf{q}}^{\nu'} + \left(1-f_{\mathbf{k}+\mathbf{q}}^{\nu}\right)\,f_{\mathbf{k}'}^{\nu'}\,\left(1-f_{\mathbf{k}'-\mathbf{q}}^{\nu'}\right)\right], \tag{10}$$

whereas the non-diagonal scattering rate follows from

$$\Gamma_{\rm nd}^{\nu(cc)}(\mathbf{k},\mathbf{q}) = \frac{1}{\hbar}\sum_{\mathbf{k}'}\sum_{\nu'}\left(2|W_{\mathbf{q}}|^2 - \delta_{\nu,\nu'}W_{\mathbf{q}}\,W_{\mathbf{k}+\mathbf{q}-\mathbf{k}'}\right)\,g(-\epsilon_{\mathbf{k}}^{\nu} + \epsilon_{\mathbf{k}+\mathbf{q}}^{\nu} - \epsilon_{\mathbf{k}'}^{\nu'} + \epsilon_{\mathbf{k}'-\mathbf{q}}^{\nu'}) \\ \times\left[f_{\mathbf{k}}^{\nu}\,f_{\mathbf{k}'}^{\nu'}\,(1-f_{\mathbf{k}'-\mathbf{q}}^{\nu'}) + (1-f_{\mathbf{k}}^{\nu})\,(1-f_{\mathbf{k}'}^{\nu'})\,f_{\mathbf{k}'-\mathbf{q}}^{\nu'}\right]. \tag{11}$$

In the subband matrix element of the screened 2d-Coulomb potential, $W_{\mathbf{q}} = V_{\mathbf{q}}/\epsilon_{\mathbf{q}}$, the influence of excitation-induced screening is described by the dielectric function $\epsilon_{\mathbf{q}}$ which will be calculated using the static Lindhard formula [12]. Screening contributions of the crystal lattice (including phonons) and nonresonant transitions are included through a background dielectric constant ϵ_b in Eq. (7). With $\epsilon_b = \epsilon_0$ background contributions of phonons are taken into account. However, as part of the phonons and their interaction with the carriers will be treated explicitly, this dielectric constant has to be reduced [12]. Hence, when we consider correlation contributions due to carrier-phonon interaction, we use a background dielectric constant $\epsilon_b = \epsilon_\infty$ which does not include the influence of phonons. In this limiting case, the background phonon screening is slightly underestimated.

For the electron-phonon scattering, the diagonal rates in Eq. (8) are given by

$$\Gamma_{\rm d}^{\nu(ph)}(\mathbf{k}) = \frac{1}{\hbar}\sum_{\mathbf{q}}\gamma_{\mathbf{q}}^2\left\{\left[(1-f_{\mathbf{k}-\mathbf{q}}^{\nu})\,n_{LO} + f_{\mathbf{k}-\mathbf{q}}^{\nu}\,(1+n_{LO})\right]\,g(\epsilon_{\mathbf{k}}^{\nu} - \epsilon_{\mathbf{k}-\mathbf{q}}^{\nu} + \hbar\omega_{LO}) \right. \\ \left. + \left[(1-f_{\mathbf{k}-\mathbf{q}}^{\nu})\,(1+n_{LO}) + f_{\mathbf{k}-\mathbf{q}}^{\nu}\,n_{LO}\right]\,g(\epsilon_{\mathbf{k}}^{\nu} - \epsilon_{\mathbf{k}-\mathbf{q}}^{\nu} - \hbar\omega_{LO})\right\}, \tag{12}$$

and the non-diagonal rates are

$$\Gamma_{\rm nd}^{\nu(ph)}(\mathbf{k},\mathbf{q}) = \frac{1}{\hbar}\sum_{a=\nu,\nu'} \gamma_{\mathbf{q}}^2 \Big\{ [(1-f_{\mathbf{k}}^a)\, n_{LO} + f_{\mathbf{k}}^a\,(1+n_{LO})]\; g(\epsilon_{\mathbf{k}-\mathbf{q}}^a - \epsilon_{\mathbf{k}}^a + \hbar\omega_{LO}) + [(1-f_{\mathbf{k}}^a)\,(1+n_{LO}) + f_{\mathbf{k}}^a\, n_{LO}]\; g(\epsilon_{\mathbf{k}-\mathbf{q}}^a - \epsilon_{\mathbf{k}}^a - \hbar\omega_{LO}) \Big\}, \qquad (13)$$

where $\hbar\omega_{LO}$ is the energy of the LO-phonons and $\gamma_{\mathbf{q}}^2$ is the Fröhlich interaction matrix element of 3d LO-phonons and confined electrons with in-plane momentum $\mathbf{q}$,

$$\gamma_{\mathbf{q}}^2 = \int dq_z \, \frac{e^2}{4\pi\varepsilon_0\,\epsilon_{(|\mathbf{q}|^2+q_z^2)}\,(|\mathbf{q}|^2+q_z^2)} \left(\frac{1}{\epsilon_\infty} - \frac{1}{\epsilon_0}\right) \frac{\hbar\omega_{LO}}{2}. \qquad (14)$$

For the distribution function of phonons, n_{LO}, we use a Bose-Einstein function containing the lattice temperature.

The derivation of the scattering rates requires many body techniques such as Green's functions or projection formalism in density matrix theory. Here, within the assumption that gain spectra at room temperature can be described by using one-particle correlations, higher order correlation functions have been factorized. In the Green's functions technique, the random-phase approximation (RPA) as well as the first Coulomb vertex contribution have to be considered to obtain all scattering contributions in Eqs. (10) and (11) which are quadratic in the screened Coulomb potential W. Correlation contributions have a complicated time dependence, which includes memory effects. In Eqs. (10) – (13), this time-dependence has been approximated within an adiabatic treatment that leads to a generalized Heitler-Zeta function,

$$g(\epsilon) = \frac{i}{\epsilon + i\gamma}. \qquad (15)$$

This Heitler-Zeta function includes the effective quasi-particle broadening γ which will be treated as a small constant. While γ is a property of correlated carriers, we do not include any phenomenolagical polarization decay time.

At the end of this section, we outline some properties of the discussed theory for a 4 nm CdZnSe quantum well (see next section). The dependence of our results on the effective quasi-particle broadening γ is shown in Fig. 1 where, for simplicity, only a single valence band has been considered. While the diagonal scattering rate is reduced with increasing

γ, the compensation of diagonal and non-diagonal rates results in a spectrum which is basically independent on γ. In Fig. 2 we study the influence of various approximations for the polarization dephasing on the absorption spectrum. In the simplest approximation, correlation contributions in Eq. (2) are included phenomenologically. Polarization dephasing, which is described by the real part of Eq. (8), has often been approximated by a constant T_2 time. Screening corrections to the Hartree-Fock terms, Eqs. (4) and (5), which follow from the imaginary part of Eq. (8), have been approximated by replacing V by W and adding the Coulomb-hole term in Eq. (4) [12]. The resulting absorption spectra are shown in Fig. 2a. With increasing carrier density, we obtain a strong artificial red shift of the exciton resonance (at moderate densities) and of the gain peak (at high densities). As a next step, we consider correlation contributions due to carrier-carrier scattering. In Fig. 2b, only the complex diagonal rate $\Gamma_{\mathrm{d}}^{\nu(cc)}(\mathbf{k})$ has been used together with Eqs. (4)–(8), whereas in Fig. 2c also the non-diagonal rate $\Gamma_{\mathrm{nd}}^{\nu(cc)}(\mathbf{k},\mathbf{q})$ has been included. When only the diagonal rate is considered, dephasing is clearly overestimated which can be seen from the strong broadening of the exciton resonances. Only if both diagonal and non-diagonal rates are included, the exciton broadening is reduced to reasonable values and, in agreement with experimental observations, almost no shift of the exciton resonance is obtained with increasing carrier density. In Figs. 2d and e, we directly compare the approximations of Figs. 2a-c for carrier densities leading to gain. In the phenomenological model (dotted line) as well as in the pure dephasing limit (dashed line), the bandgap renormalization is drastically overestimated, the lineshape of the gain is modified and unphysical absorption below the renormalized bandedge is obtained in comparison to the full model (solid line). Especially the absorption energetically below the gain region, which occurs in simplified gain calculations, is a signature of overestimated dephasing and incorrect lineshape. The resulting strong broadening of carrier lineshape functions leads to an unphysical admixture of non-inverted states high above the band edge.

In conclusion, the large red shift of the exciton at low carrier densities, the overestimated band-gap shift at higher densities as well as the large damping are artifacts of simpler

models which are in clear contradiction to experimental results. Hence, a pure dephasing approximation is not appropriate and only the full model can reproduce the experimental results.

For a realistic description of quantum wells on the basis of II-VI compounds, additional excitation independent inhomogeneous broadening has to be considered in addition to the excitation dependent carrier-carrier and carrier-phonon interaction. In particular, small spatial variations of the concentration of the quantum-well and barrier materials as well as roughness of the well/barrier interfaces give rise to inhomogenous broadening. Correspondingly the calculated results are more realistic when the homogeneously broadened spectrum $\alpha_{hom}(\omega)$ is convoluted with a Gaussian distribution $\mathcal{G}(\omega)$ of given spectral width according to

$$\alpha_{inh}(\omega) = \int d\omega' \, \alpha_{hom}(\omega - \omega') \, \mathcal{G}(\omega'). \tag{16}$$

Figure 3 shows the influence of increasing additional inhomogenous broadening on the TE-spectrum of a 4 nm CdZnSe quantum well (see next section). Note that the influence of inhomogeneous broadening is stronger for smaller carrier densities where the spectrum contains sharp features. With increasing broadening, the lineshape is modified and the gain maxima can shift several meV. In the following results, we have included an inhomogenous broadening of 10 meV.

III. SPECTRA OF II-VI QUANTUM WELLS

The microscopic model discussed in the previous section will be used to compute the density-dependent absorption and gain spectra for CdZnSe quantum wells between 15nm ZnSe barriers and ZnSSe cladding layers (25% Cd and 6% S). Two samples with a quantum-well width w=4 nm (QW1) and w=7 nm (QW2) are compared.

Using the envelope approximation method [6], the energy gaps and the strain induced shifts for the heavy and light hole states are calculated. The conduction bands are always

assumed to be parabolic. Neglecting the split off band, the hole states are coupled via a 4×4 Luttinger Hamiltonian. The diagonalization of this system leads to the valence bands $\epsilon_\nu(\mathbf{k})$ and the dipol matrix elements $\mu_{\mathbf{k}}^{\nu,\nu'}$. All those bands are considered where the carriers are confined in the quantum well for at least small wavevectors $\mathbf{k}$. For the 4 nm and 7 nm quantum wells, the calculated band structure is shown in Fig. 4. In the 4 nm (7 nm) quantum well, one (two) conductions band and three (five) valence bands are confined. The compressive strain of the CdZnSe wells between the ZnSe barriers produces a heavy-hole light-hole splitting. For the 7 nm quantum well, the top three valence bands are heavy-hole like close to the band edge so that their coupling to the TM-mode is weak. Hence the exciton and gain corresponding to these transitions is small. The main contribution to the TM-mode follows from tansitions between the fourth and fifth valence band and the first conduction band.

The TE- and TM-spectra of the 4 nm and 7 nm quantum wells are plotted in Figs. 5 and 6, respectively. The shown carrier densities cover the region from no inversion between any bands to inversion between most of the confined bands for small wavevectors $\mathbf{k}$ [15].

The low-density TE-spectra of the 4 nm quantum well (left part in Fig. 5) show two strong excitonic absorption lines corresponding to the 1-1 and 2-2 transition. Here transitions are labeled i-j with i (j) refering to the conduction (valence) band involved. For our system, the second TE-absorption (2-2) line appears at the same spectral position as the TM-absorption (1-4) line; the differences of the band gaps for these transitions is less than 2meV. These excitonic absorption lines stay at their spectral position when the carrier density increases; after exciton bleaching the transition develops gain. For the highest carrier density, the TE-spectra of the 4 nm quantum well exhibit a shoulder due to inversion of the 2-2 transition. In addition, the left part of Fig. 5 shows that the absorption above the renormalized band edge does not decrease when the carrier density increases; the high-energy part of the spectra for large carrier densities is only shifted as a consequence of bandgap renormalization due to Coulomb interaction.

If the quantum well is wider, more bands are confined. This is illustrated in the right

part of Figs. 5 and 6. Due to the second conduction band in QW2, we obtain an additional excitonic transition in the TE-spectra while the TM-absorption remains similar to that of QW1. As the carrier density is distributed over more bands in QW2, the inversion becomes smaller and the gain is reduced. In addition, the polarization decay is increased for QW2 at low plasma densities which leads to a broader excitonic absorption line.

The band offset, i.e., the splitting of the confinement energy between the conduction and the valence band, cannot be determined unambiguously from experiments. In the previous calculations, a band offset of 60% for the conduction band has been assumed. The influence of band offset changes on our results is studied in Figs. 7 and 8 for the TE- and TM-spectra, respectively. For a conduction band offset between 30% and 60%, a single sub-band appears in the finite-hight quantum well confinement potential of the electrons using the above discussed material composition and 4 nm well width (QW1). However, the confinement potential of holes leads to four sub-bands within the quantum well for 30% and 40% offset and three sub-bands when 50% and 60% offset are considered. The TE-spectra for various band-offset values are shown in Fig. 7. The lineshape of the spectra at high densities is almost independent of the band offset; only the magnitude of the gain is slightly changed. Also the low-density spectra are similar, only the weak excitonic resonance of the fourth hole subband is missing for a band offset $\geq$ 50%. With increasing band offset, the envelope function of the light hole becomes less confined in the quantum well which leads to an reduced effective TM-dipol coupling with the conduction band. For that reason both the TM-absorption for low plasma densities and TM-gain at higher densities are reduced with increasing band offset as shown in Fig. 8.

As another application of our theory, we study the influence of compressive versus tensile strain on the quantum-well spectra of II-VI compounds. We investigate a 4 nm $Zn_{0.8}Cd_{0.2}Se$ quantum well with a lattice constant of 5.75 Å between ZnMgSSe barriers having a lattice constant of either 5.65 Å (QW3) or 5.83 Å (QW4) [16]. The corresponding band structure is shown in Fig. 9. In QW3, the first three valence bands are heavy-hole like at the zone center while in QW4 the tensile strain causes a top valence band with light-hole character.

Therefore, the TE-gain strongly exceeds the TM-gain for compressive strain whereas for tensile strain the TM-gain is dominant (Fig. 10). The carrier density dependence of the TE-spectrum for QW3 is shown in Fig. 11. At intermediate densities, a situation can be realized where a small gain exists while the excitonic enhancement is still present. A similar situation has recently been observed in ZnCdSe/ZnSSe/ZnMgSSe quantum wells [17].

IV. CONCLUSION

In summary, the gain spectra of II-VI quantum-well materials have been investigated within a microscopic plasma theory which is based on kinetic equations for an interacting electron-hole system in a multi-band semiconductor. These equations include many-body effects such as intraband as well as interband Coulomb correlations leading to carrier scattering and excitonic transitions. In addition, the influence of LO-phonons has been considered. The single-particle energies and the dipole coupling have computed using Luttinger-Kohn theory in envelope function approximation.

The model has been used for calculating the excitation density dependent absorption and gain spectra of several different examples. The possibility to optimize the gain spectra in terms of well-width and composition has been studied for II-VI compounds.

This work was supported by the Deutsche Forschungsgemeinschaft through the "Schwerpunktprogramm II-VI-Halbleiterstrukturen", the Leibniz prize, the AFOSR grant 49620-97-1-0002 and valuable discussions with J. Moloney and coworkers. We acknowledge a grant for CPU time at the Forschungszentrum Jülich.

REFERENCES

[1] M.A. Haase, J. Qui, J.M. De Puydt, and H. Cheng, Appl. Phys. Lett. **59** , 1272 (1991).

[2] A.V. Nurmikko, R.L. Gunshor, and M. Kobazyashi, J. Vac. Sci. Technol B **10**, 2056 (1992).

[3] See e.g. contributions to *Proceedings of the International Workshop on ZnSe-Based Blue-Green Laser Structures, 1994*, [Phys. Status Solidi B **187** (1995)].

[4] W.W. Chow, and S.W. Koch, Appl. Phys. Lett. **66** (22), 3004 (1995).

[5] F. Kreller, M. Lowitsch, J. Puls, and F. Henneberger, Phys. Rev. Lett. **75**, 2420 (1995).

[6] For a textbook discussion see, W.W. Chow, S.W. Koch, and M. Sargent. III, *Semiconductor-Laser Physics* (Springer, Berlin, 1994).

[7] M. Lindberg and S.W. Koch, Phys. Rev. **B 38**, 3342 (1988).

[8] T. Rappen, U.G. Peter, M. Wegener, and W. Schäfer, Phys. Rev. **B 49**, 10 774 (1994).

[9] F. Rossi and S. Haas and T. Kuhn, Phys. Rev. Lett. **72**, 152 (1994).

[10] A. Knorr, S. Hughes, T. Stroucken, S.W. Koch, Chem. Phys. **210**, 27 (1996).

[11] F. Jahnke, M. Kira and S.W. Koch, "Linear and Nonlinear Optical Properties of Quantum Confined Excitons in Semiconductor Microcavities", Phys. Rev. B., submitted.

[12] For a textbook discussion see, H. Haug and S.W. Koch, *Quantum Theory of the Optical and Electronic Properties of Semiconductors*, World Scientific, Singapore, 3rd ed., (1994).

[13] F. Jahnke, M. Kira, S.W. Koch, G. Khitrova, E.K. Lindmark, T.R. Nelson Jr., D.V. Wick, J.D. Berger, O. Lyngnes, H.M. Gibbs and K. Tai, Phys. Rev. Lett. **77**, 5257 (1996).

[14] S.Hughes, A.Knorr, S.W.Koch, R.Binder, R.Indik, and J.Moloney, Solid State Comm.

100, 555 (1996).

[15] For the inversion at the band edge $I^{\nu,\nu'} = f^{\nu}(\mathbf{k}=0) + f^{\nu'}(\mathbf{k}=0) - 1$ we obtain with the lowest carrier density $n = 0.5 \times 10^{12}$ cm^{-2}: $I^{1,1} = -0.63$, $I^{2,5} = -0.98$ and with the highest density $n = 8.0 \times 10^{12}$ cm^{-2}: $I^{1,1} = +0.79$, $I^{1,5} = +0.69$, $I^{2,1} = +0.50$, $I^{2,3} = +0.12$, $I^{2,4} = -0.22$, $I^{2,5} = -0.22$.

[16] W. Huang and F.C Jain Appl. Phys. Lett. **66**, 1596 (1995).

[17] J. Ding, V. Kozlov, P. Kelkar, A. Salokatve, and A.V. Nurmikko, phys. stat. sol. (b) **188**, 153 (1995).

FIGURES

FIG. 1. Complex scattering rate $\Gamma_d^{\nu(cc)}(\mathbf{k})$ for electrons (e) and holes (h) and absorption spectrum for a two-band model with carrier density 2×10^{12} cm^{-2} and various quasi-particle broadening γ.

FIG. 2. Influence of the polarization-dephasing model on the linear absorption spectrum of a 4 nm CdZnSe quantum well. Within a phenomenological model (a), a constant polarization decay rate T_2=100 fs and screened Hartree-Fock contributions have been considered. Using a microscopic model for correlation contributions due to carrier-carrier scattering, we compare the diagonal dephasing (b) with diagonal *and* non-diagonal dephasing (c). The carrier densities are 0.1, 0.5, 1, 2, 4 $\times 10^{12}$ cm^{-2} (from top to bottom). In (d) and (e) we directly compare the phenomenological model (dotted line) with the diagonal dephasing (dashed line) and diagonal + non-diagonal dephasing (solid line) for a fixed carrier density.

FIG. 3. Absorption spectrum of a 4 nm quantum well for a carrier density 2×10^{12} cm^{-2} and various inhomogeneous broadening.

FIG. 4. Energy bands for a 4 nm and 7 nm CdZnSe/ZnSe quantum well. The offset energy E_1 is 2.52 eV.

FIG. 5. Comparison of the TE-spectra of a CdZnSe/ZnSe quantum well with 4 nm well width (QW1) and 7 nm well width (QW2). The carrier densities are 0.5, 1, 2, 3, 4, 5, 6, 7, 8×10^{12} cm^{-2} (from top to bottom). An additional inhomogenous broadening of 10 meV is taken into account. The bottom figures show the same on a larger scale.

FIG. 6. Same as Fig. 5 for the TM-spectra.

FIG. 7. TE-spectra for QW1 where different band offsets are assumed. The densities are similar as in Fig.(6). For 30% or 40% conduction-band offset, four valence bands are confined in the well and three valence bands for higher offsets.

FIG. 8. Same as Fig. 7 for the TM-spectra. By increasing the conduction-band offset, i.e., reducing the potential well for the holes, the light hole becomes less confined and therefore the TM-coupling of the conduction bands with the confined valence bands decreases.

FIG. 9. Energy bands for a 4 nm CdZnSe/ZnMgSSe quantum well with compressive (QW3) and tensile (QW4) strain. The offset energy E_2 is 2.68 eV.

FIG. 10. TE- and TM-spectra for a 4 nm CdZnSe/ZnMgSSe quantum well with compressive (QW3) and tensile (QW4) strain at carrier density 6 $\times 10^{12}$ cm^{-2}. The bottom figures show the same on a larger scale.

FIG. 11. TE-spectra for a 4 nm CdZnSe/ZnMgSSe quantum well with compressive strain (QW3) for carrier densities 1.5, 1.8, 2.0, 2.2, 2.5 and 4.0 $\times 10^{12}$ cm^{-2} (from top to bottom). The bottom figure shows the same on a larger scale.

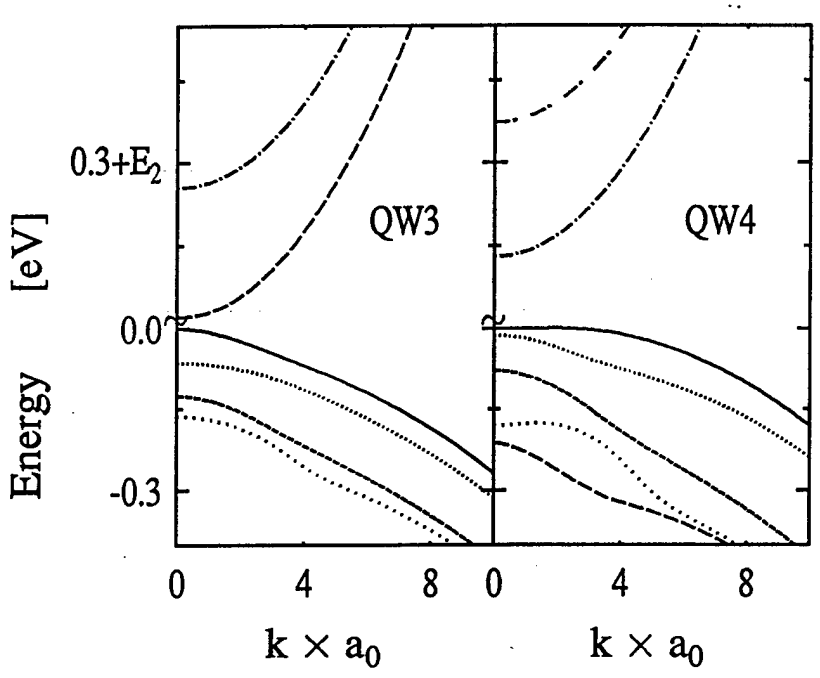
0.3+E2
0.0
-0.3
Energy [eV]
QW3
QW4
0
4
8
0
4
8
k × a0
k × a0

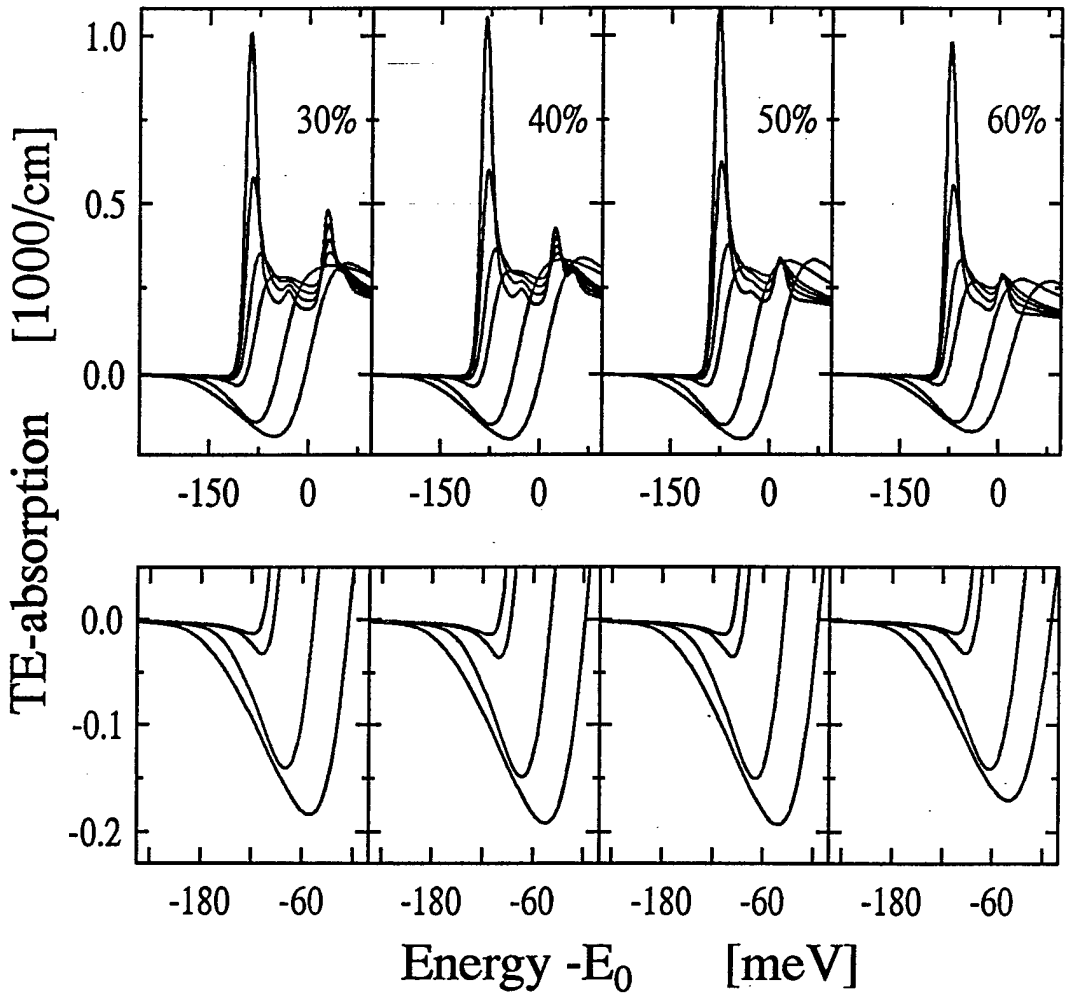
1.0
0.5
0.0
30%
40%
50%
60%
-150
0
-150
0
-150
0
-150
0
0.0
-0.1
-0.2
-180
-60
-180
-60
-180
-60
-180
-60
TE-absorption [1000/cm]
Energy -E0 [meV]

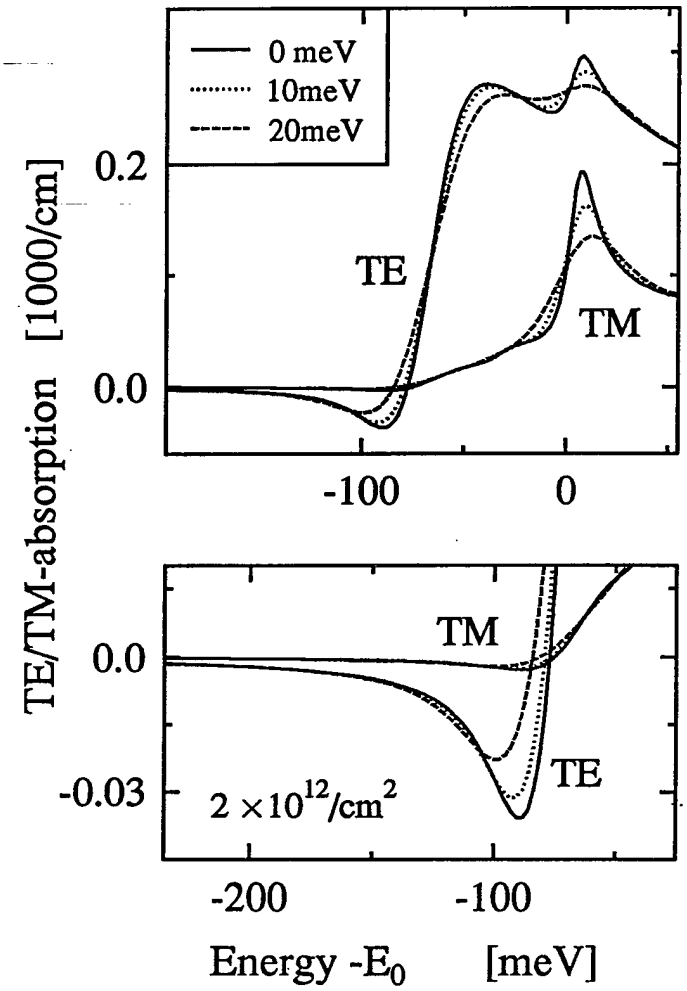
0 meV
10meV
20meV
0.2
0.0
TE
TM
-100
0
TE/TM-absorption [1000/cm]
TM
0.0
-0.03
TE
2 ×10^12/cm^2
-200
-100
Energy -E0 [meV]

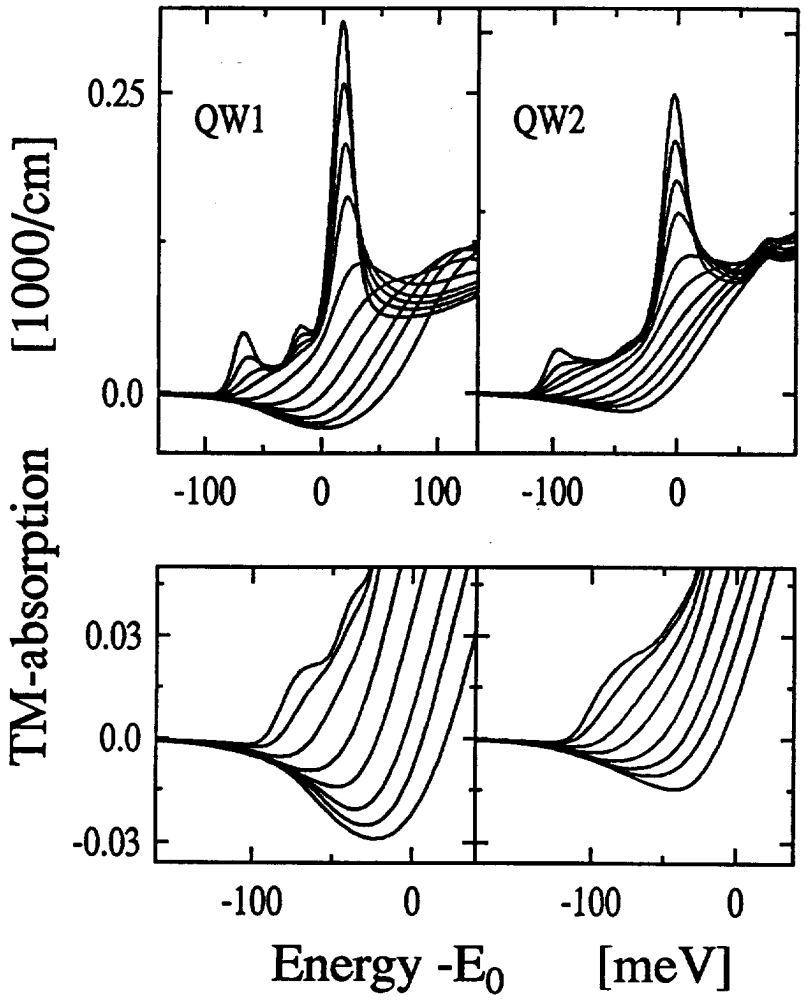
QW1
QW2
0.25
0.0
-100
0
100
-100
0
0.03
0.0
-0.03
-100
0
-100
0
TM-absorption [1000/cm]
Energy -E0 [meV]

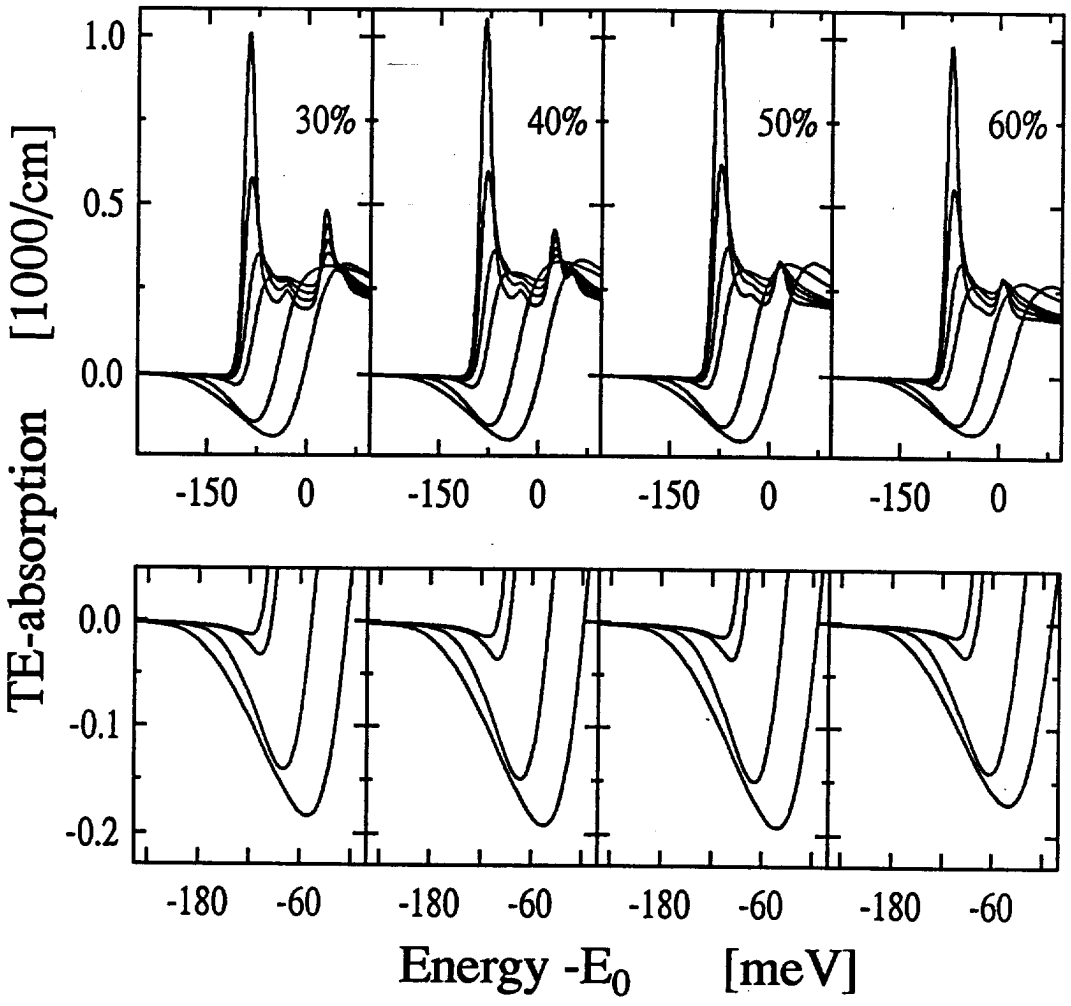
1.0
0.5
0.0
30%
40%
50%
60%
-150
0
TE-absorption [1000/cm]
0.0
-0.1
-0.2
-180
-60
Energy -E0 [meV]

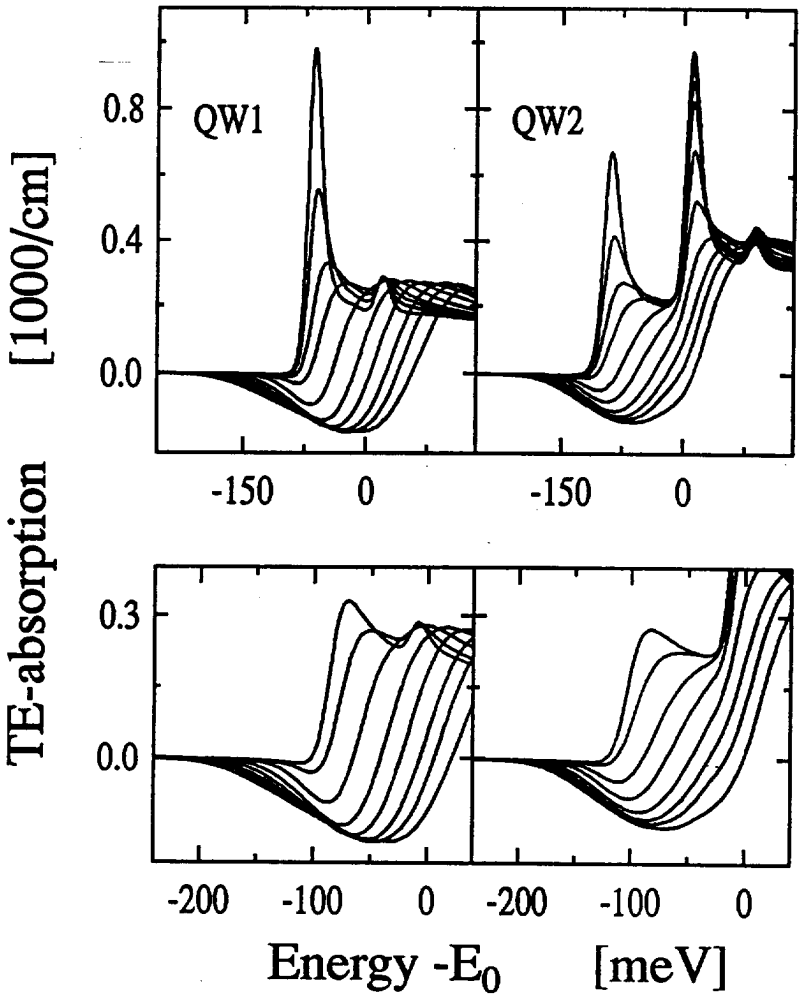
QW1
QW2
0.8
0.4
0.0
-150
0
-150
0
0.3
0.0
-200
-100
0
-200
-100
0
TE-absorption [1000/cm]
Energy -E0 [meV]

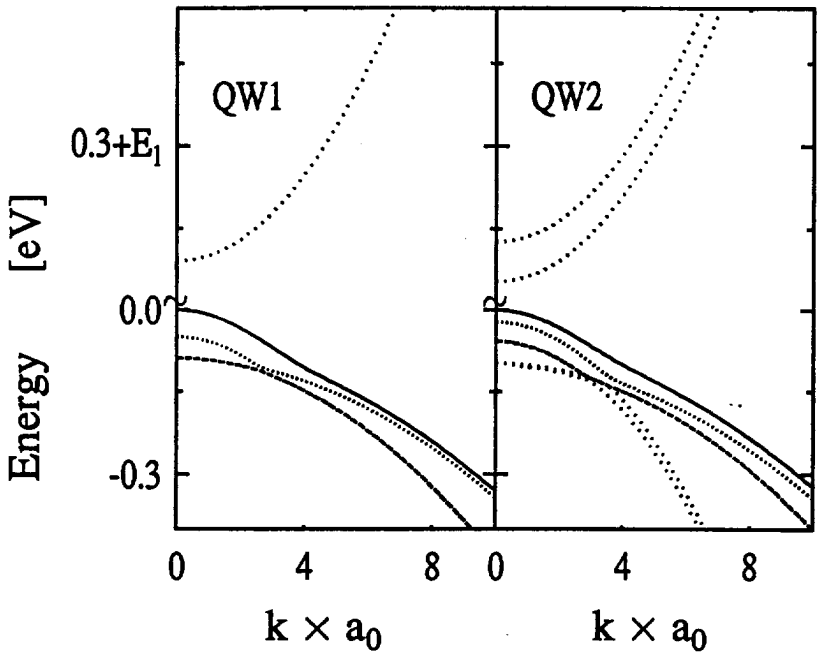
QW1
QW2
0.3+E1
0.0
-0.3
Energy [eV]
0
4
8
0
4
8
k × a0
k × a0

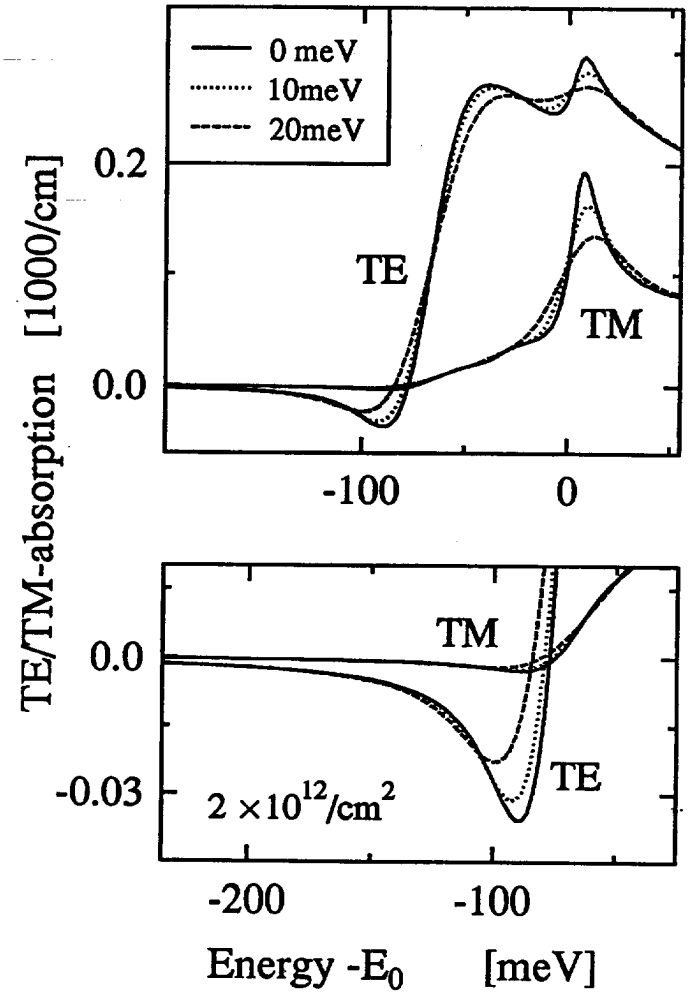
0 meV
10meV
20meV
0.2
0.0
TE
TM
-100
0
TE/TM-absorption [1000/cm]
TM
0.0
-0.03
TE
2 ×10^12/cm^2
-200
-100
Energy -E0 [meV]

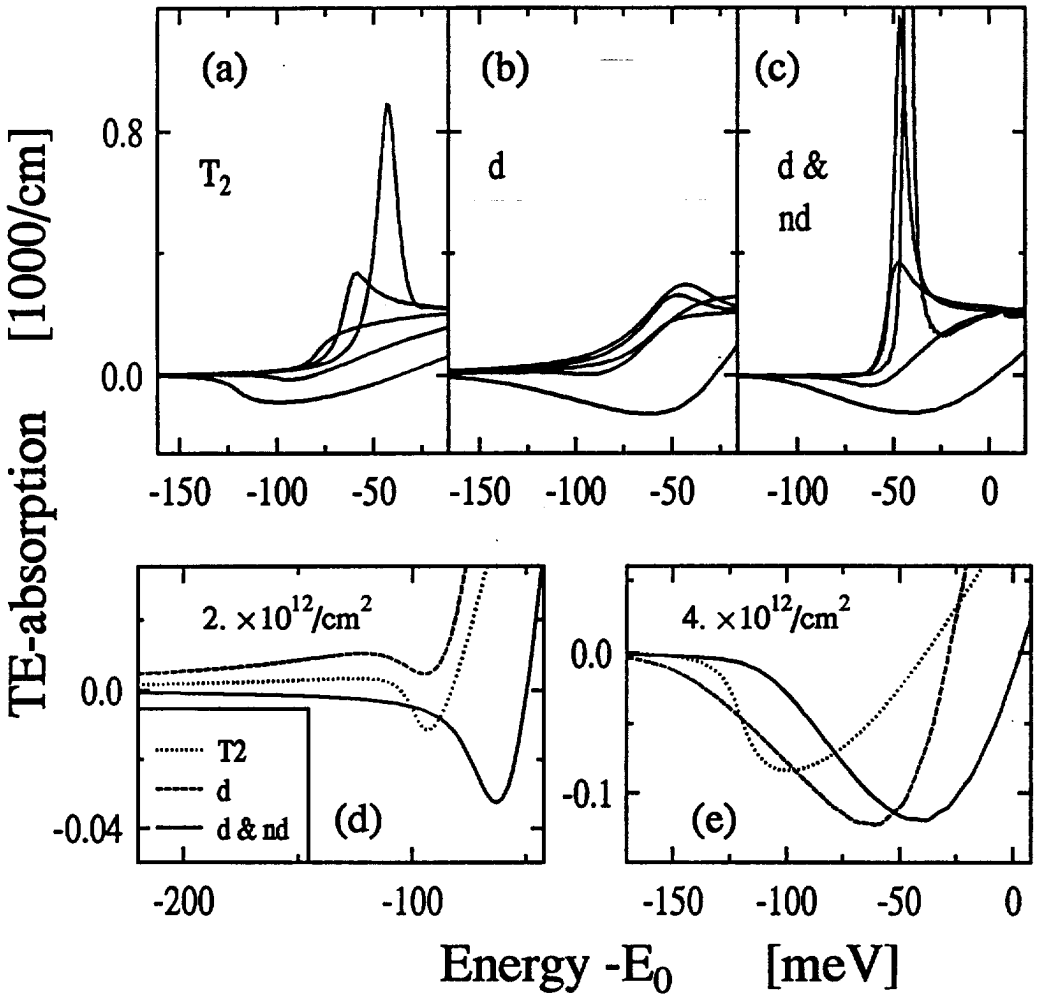
(a)
(b)
(c)
T_2
d
d &
nd
0.8
0.0
-150 -100 -50
-150 -100 -50
-100 -50 0
TE-absorption [1000/cm]
2. $\times 10^{12}$/cm^2
4. $\times 10^{12}$/cm^2
0.0
-0.04
0.0
-0.1
T2
d
d & nd
(d)
(e)
-200 -100
-150 -100 -50 0
Energy -E_0 [meV]

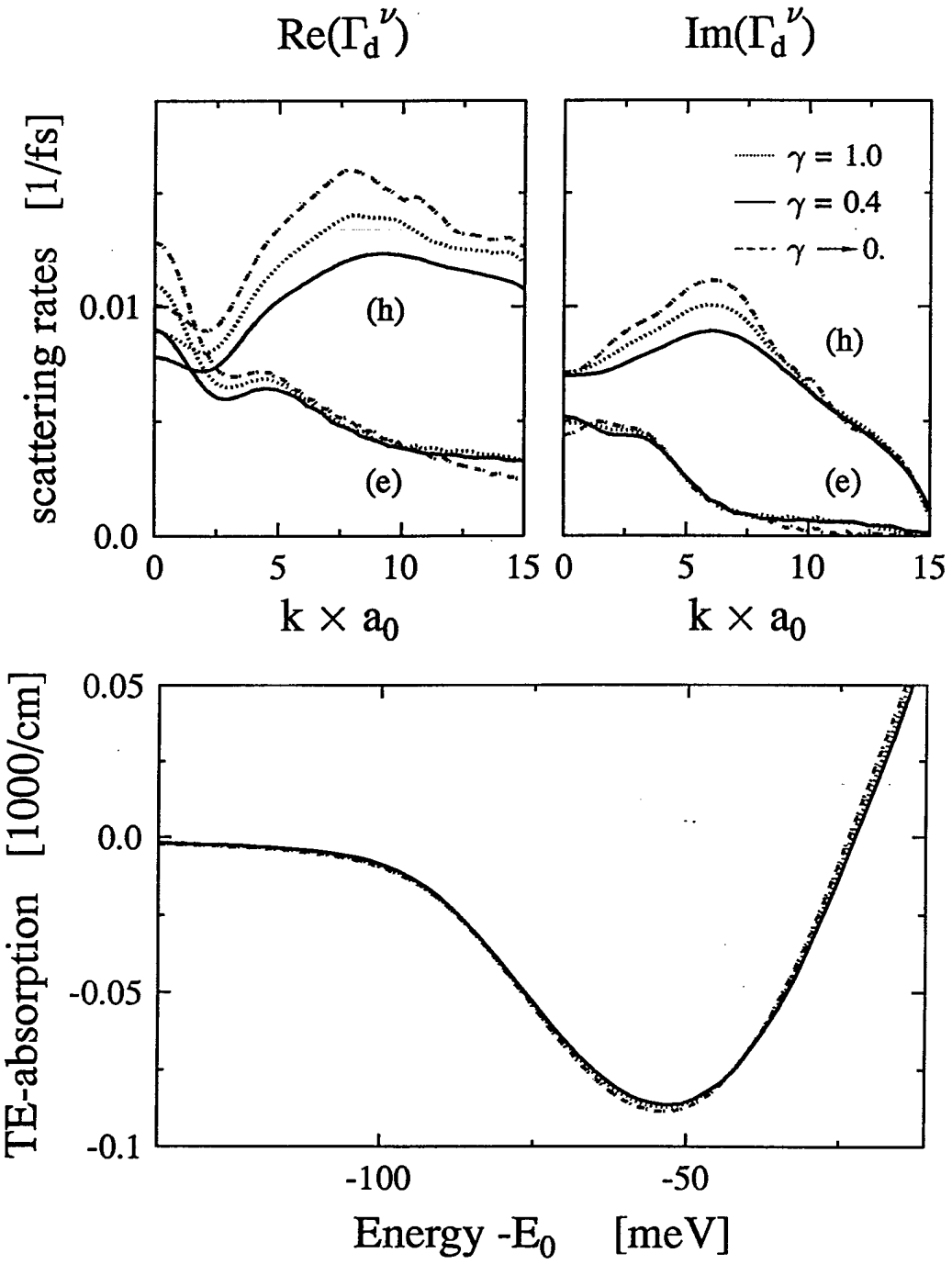
Re(Γ_d^{ν})
Im(Γ_d^{ν})
scattering rates [1/fs]
0.01
0.0
(h)
(e)
γ = 1.0
γ = 0.4
$\gamma \rightarrow$ 0.
0
5
10
15
k × a_0
TE-absorption [1000/cm]
0.05
0.0
-0.05
-0.1
-100
-50
Energy -E_0 [meV]

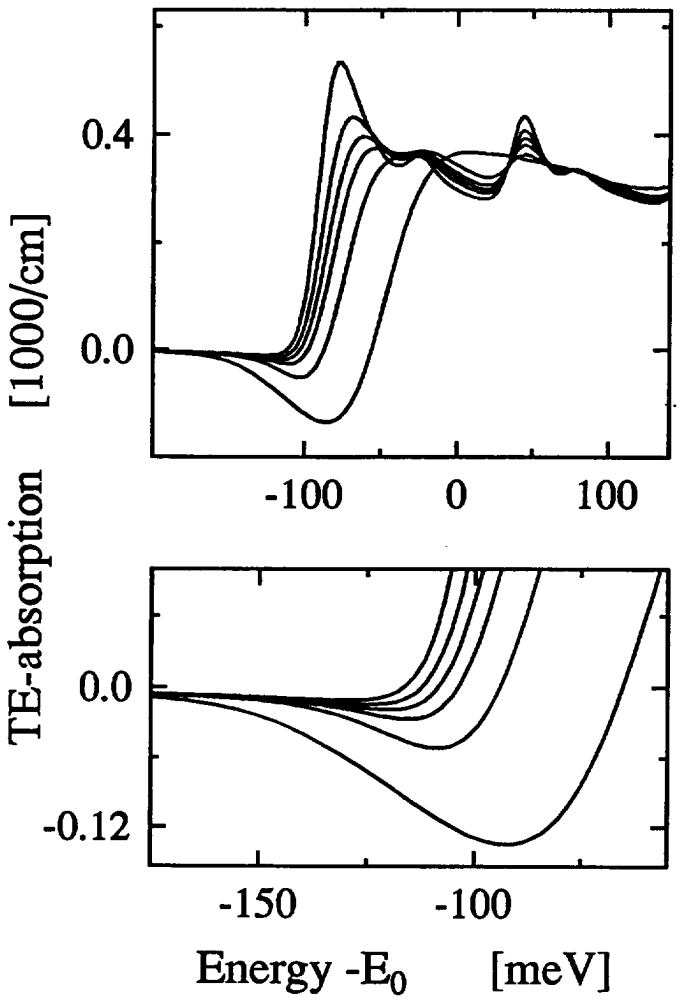
0.4
0.0
-100
0
100
TE-absorption [1000/cm]
0.0
-0.12
-150
-100
Energy -E0 [meV]

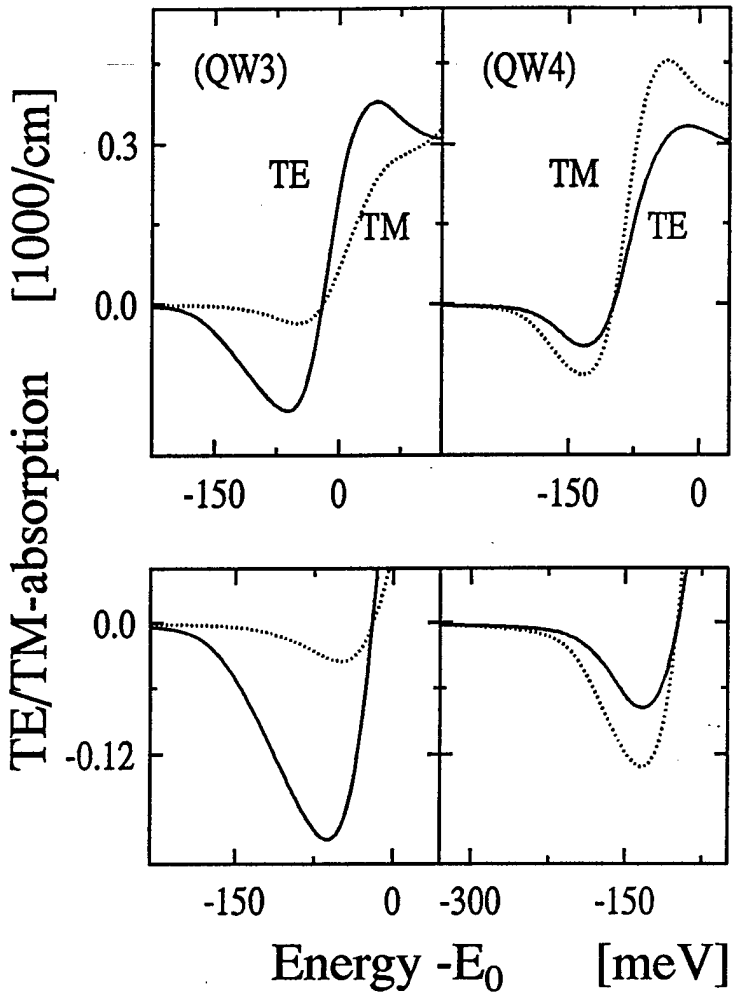
(QW3)
(QW4)
TE
TM
TM
TE
0.3
0.0
-0.12
-150
0
-300
TE/TM-absorption [1000/cm]
Energy -E0 [meV]